Genomic and Functional Studies of Uveal Melanoma

Genomic and Functional Studies of Uveal Melanoma

A dissertation presented

by

Chelsea Schwartz Place

to

The Division of Medical Sciences

In partial fulfillment of the requirements

for the degree of

Doctor of Philosophy

in the subject of

Biological Chemistry and Molecular Pharmacology

Harvard University

Cambridge, Massachusetts

April 2015

Dissertation Advisor: Dr. Levi A. Garraway Chelsea Schwartz Place

Genomic and Functional Studies of Uveal Melanoma

Abstract

Uveal melanoma (UM) is a rare form of melanoma that is lethal once metastatic. Primary tumors in the iris, ciliary body, and choroid of the eye metastasize in 50% of patients, despite effective treatment of the initial tumor. The majority of uveal melanomas harbor activating mutations in GNAQ or GNA11, which relay signaling to downstream effectors including protein kinase C (PKC) and the mitogen-activated protein kinase (MAPK) signaling pathway (RAF-MEK-ERK). Both PKC and MEK inhibitors are currently in clinical trials, however, MEK inhibition alone is insufficient to improve overall survival. These observations highlight a need to identify new drug targets for the design of novel therapies including combinations.

To uncover novel UM biology and nominate strategies for combination therapy, genomic and functional genomic approaches were applied. Whole exome sequencing of primary and metastatic tumors identified somatic genetic alterations that drive tumorigenesis. Recurrent mutations in *GNAQ*, *GNA11*, *BAP1*, *SF3B1*, and *EIF1AX* were confirmed. Mutations in potential drivers of metastasis, *SMARCA4* and *IQGAP1*, were also identified. Furthermore, the function of N-terminal tail mutations in the translation initiation factor EIF1AX was probed using loss of function studies to assess both viability and mRNA regulation at the level of translation. Upon EIF1AX knockdown, the efficiency of ribosomal protein translation was reduced in wild type, but not mutant cells. Deregulated translation may play an important role in UM tumorigenesis.

To identify putative co-targets of MEK and PKC inhibitors, genome-scale RNA interference drug enhancer screens were performed. These screens nominated several novel

genes and pathways for further study in UM. In particular, the mitochondrial folate pathway enzyme MTHFD2 was identified as a novel PKC inhibitor sensitizer. The strongest MEK inhibitor enhancer was the MAPK pathway member, BRAF. Indeed, targeting multiple nodes of the MAPK signaling pathway achieved stronger pathway suppression and synergistic effects. Co-inhibition of RAF/MEK or MEK/ERK may warrant clinical investigation in patients. Overall, these studies provide a foundation for our understanding of UM genomics and combination therapy opportunities. Several novel avenues for future study of UM biology and co-dependencies are uncovered. Translation of these findings into clinical studies will be of the utmost importance.

TABLE OF CONTENTS

Chapter 1. Introduction **1**
Clinical features of uveal melanoma **2**
Epidemiology 2
Risk factors 2
Diagnosis and standard of care 3
Uveal melanoma biology 4
Prognostics 4
The genetics of uveal melanoma **5**
Copy number alterations 5
Somatic and germline point mutations 6
Prognostic value of genetic features 10
Treatment strategies **10**
Targeting GNAQ/11-mutant tumors 11
Other targeted therapy approaches 14
Immunotherapy 15
Precision medicine for uveal melanoma **17**
Limitations to existing therapeutic strategies 17
Rationale for this work 18
Chapter 2. Systematic genomic characterization of primary and metastatic uveal melanoma **20**
Attributions **21**
Abstract **22**
Introduction **22**
Results **23**
Discussion **56**
Materials and Methods **58**
Chapter 3. Systematic identification of targets for co-inhibition with MEK and protein kinase C inhibitors in uveal melanoma **66**
Attributions **67**
Abstract **68**
Introduction **68**

Results **70**
Discussion **101**
Materials and Methods **104**
Chapter 4. Conclusion and future directions **109**
Summary **110**
Limitations of this study 111
Future directions for UM studies **113**
Genome characterization 113
Targeted therapy 114
Mechanisms of resistance 117
Concluding Remarks **118**
References **120**

List of Figures

Figure 1.1. Signaling downstream of mutated GNAQ or GNA11 ($\alpha_{Q/11}$) in UM 8

Figure 2.1. Somatic mutations in primary and metastatic uveal melanoma 24
Figure 2.2. Copy number profiles of 52 uveal melanomas 31
Figure 2.3. Trio 2 clinical timeline 33
Figure 2.4. EIF1AX-regulated growth and translation in uveal melanoma 36
Figure 2.5. EIF1AX sequence and protein expression across UM cell lines 37
Figure 2.6. *EIF1AX* sequence and expression levels from polysome profiling RNAseq 38
Figure 2.7. EIF1AX-dependency across 216 cell lines from Project Achilles 40
Figure 2.8. Decreased EIF1AX expression impairs translation of protein synthesis machinery in wildtype, but not mutated setting 41
Figure 2.9. Genes with significant changes in translational efficiency (TE) following EIF1AX knockdown cluster into 4 groups..... 55

Figure 3.1. RNA interference drug enhancer screens identify novel MEK and PKC inhibitor sensitizers in UM cells 71
Figure 3.2. Primary screen comparison and validation growth curves 77
Figure 3.3. Schematic of enhancer gene selection steps 84
Figure 3.4. MTHFD2 is a novel dependency in UM cells..... 87
Figure 3.5. Suppression of BRAF expression sensitizes UM cells to MEK inhibition 89
Figure 3.6. BRAF shRNAs further sensitize UM cells to MEK inhibition..... 90
Figure 3.7. Sensitivity of Omm2.3 cells to MEK inhibition following BRAF knockout 92
Figure 3.8. BRAF inhibition results in paradoxical pathway activation in *GNAQ/11*-mutant cells 93
Figure 3.9. Combined pan-RAF and MEK inhibition is synergistic in UM cells..... 95
Figure 3.10. MEKDD confers resistance to pan-RAF inhibition in UM cells 98
Figure 3.11. Combined MEK and ERK inhibition is synergistic in UM cells..... 99
Figure 3.12. ERK resistance alleles confer resistance to MAPK inhibitors in UM cells 100

List of Tables

Table 1.1. Summary of ongoing clinical trials for UM 16

Table 2.1. Clinical characteristics of analysis set 25
Table 2.2. Sequencing metrics of 52 uveal melanomas 26
Table 2.3. Extended clinical characteristics of 52 uveal melanomas 27
Table 2.4. Validation of selected mutations by targeted resequencing 32
Table 2.5. All somatic alterations identified in trio analysis 34
Table 2.6. Genes with a *z*-score < −2 in Omm2.3 cell line 43
Table 2.7. Genes with a *z*-score < −2 in Omm1 cell line 45
Table 2.8. Genes with a *z*-score < −2 in 92.1 cell line 49
Table 2.9. Genes from interaction analysis with significant changes in translational efficiency following EIF1AX knockdown. 53

Table 3.1. The top 100 genes from the MEK inhibitor screen ranked by 2nd best shRNA 73
Table 3.2. The top 100 genes from the PKC inhibitor screen ranked by 2nd best shRNA 75
Table 3.3. Genes that no longer score by 2nd best shRNA following removal of seed-nominated shRNAs 79
Table 3.4. Genes and corresponding shRNA sequences in the custom shRNA pool used for validation screens 80

Acknowledgements

There are many people who I need to thank for their support during graduate school and for their contributions to the work presented here. Levi Garraway has been an incredible mentor from the first day of my rotation through to today. I am grateful for the opportunity to work on exciting science using cutting edge approaches, but also for all of the conversations and guidance along the way. Levi challenged me to think independently, ask interesting and novel questions, and be skeptical. His ability to see the big picture has consistently grounded my perspective and motivated my science.

I also want to thank my dissertation advisory committee members Matthew Meyerson, Len Zon, and Pasi Jänne for their helpful insights, critiques, and guidance during the course of my project. I have looked forward to our meetings as an opportunity to gain the perspective of experts and engage in critical discussion. It was even during a DAC when I first learned about CRISPR technology. Thank you to my defense committee members too, Matthew Meyerson, Ben Ebert, David Fisher, and Gary Schwartz for taking the time to read and discuss my work.

The Garraway Lab is an enriching, positive, and energetic group of individuals brought together by Levi. I feel fortunate to have spent time in both the DFCI and Broad locations of the lab, allowing me to get to know and work with many members of the group. For our screening project, I had the opportunity to work closely with Steven Whittaker, who provided many helpful suggestions for both the screen design and analysis. Glenn Cowley in the Broad Genetic Perturbation Platform was also incredibly helpful with designing, executing, and analyzing our shRNA screens. I also want to thank other members of the platform, including Mudra Hegde, John Doench, and David Root for their analysis and insights.

I was fortunate to work with two extremely talented computational biologists. Eli Van Allen and Ali Amin-Mansour were fantastic collaborators on our uveal genomics project. Thank you to our external collaborators on this project too, Ivana Kim at MEEI and Scott Woodman

and Bita Esmaeli at MDACC. Thank you to Peter ‘t Hoen (LUMC) for help with polysome analysis as well. The Broad Genomics Platform also provided support; in particular, Sara Seepo was involved on the project management side. In addition, I need to thank Cailin Joyce in the Novina Lab for taking the time to teach us the polysome profiling technique and allow us to use her set-up. Dan Treacy provided immense help with the polysome profiling experiments and beyond. His expertise from prior experience and fantastic RNA handling skills were true assets to the project. He also executed several of the follow-up experiments for our drug enhancer project.

I want to thank each member of the Garraway Lab for his or her helpful conversations. Those at DFCI (Dan Treacy, Flora Luo, Ginevra Botta, Eva Goetz, Chengyin Min, Rajee Antony, Bokang Rabasha , Xuining Le, Ben Izar, and Lior Golomb) have been supportive through all of the ups and downs of graduate school. I am grateful to Flora and Dan for their advice on everything from data analysis to email writing and beyond. Eva is the person who I turn to first for experimental and analytical advice. I am thankful for her expertise as well as for her willingness to read and provide feedback on my thesis. At the Broad, Jason Ruth provided helpful input regarding *in vivo* experimental design. I also appreciated conversations and guidance from others (Terrence Wong, Rick Wilson, Cory Johannessen, Franklin Huang, David Konieczkowski, Judit Jane-Valbuena, and JP Theurillat). I worked closely with Judit during my rotation and have looked to her as a mentor since.

I also need to thank my family for their support from day less than 1. My brothers Skyler and Camden have been supporters, role models, and friends. They challenge me to exceed my own expectations, but remind me to enjoy every step along the way. My parents Erna and Bob have been there for me from my first beam routine in a competition to my college graduation and beyond. They provide unwavering support, push me to follow my interests, and challenge me to step outside of my comfort zone. Their combined strength, intellect, and creativity are inspiring. I am also incredibly lucky to have met my fiancé Chris during graduate school.

Together, we have struggled through the challenges and celebrated the successes that come with science. Chris also ensured that I made time for the activities that I enjoy: skiing, travel, cooking, and even golf.

Finally, I would like to thank my funding sources. This work was possible due to generous support from the National Institutes of Health (National Cancer Institute Award # F31CA171320 and the Harvard Clinical and Translational Science Center Training Grant Award # TL1 RR 025756) and CURE OM of the Melanoma Research Foundation.

CHAPTER 1

INTRODUCTION

Clinical features of uveal melanoma

Melanoma is a type of cancer that originates in melanocytes, which are pigment-producing cells. The most common form of melanoma is melanoma of the skin (cutaneous melanoma), however, melanoma arising in the eye (ocular melanoma) accounts for roughly 5% of cases (1). The most common form of intraocular cancer in adults is uveal melanoma (UM), which develops in the iris, ciliary body, and choroid of the eye. Posterior UM, which includes tumors of the ciliary body and/or choroid, is the subject of this thesis.

Epidemiology

Uveal melanoma is quite rare: the annual incidence is 5.1 per 1,000,000 in the United States (2). The majority of U.S. cases occur in Caucasian populations, and the corresponding 5-year survival rate is 81.6% (2). These statistics are similar to those reported worldwide (3). In the United Kingdom, 1 new patient per 100,000 individuals is diagnosed each year, and this rate has held constant for over a decade (4). Fortunately, these data demonstrate that the frequency of UM is not increasing over time. Most patients diagnosed with UM are elderly, with the median age at treatment being 62.8 years (5). This observation is consistent with the general trend of cancer occurring predominantly in aging populations.

Risk factors

Several factors influence the likelihood of developing UM. Light eye color, fair skin, and the ability to tan are statistically significant risk factors (6). Also, specific occupations render individuals more susceptible, such as welding (7, 8). An increased risk of UM is also associated with the presence of cutaneous nevi, nevi of the iris, and freckling (9).

The contribution of ultraviolet light (UV) to the development of UM has been a long-standing question. Although UV-induced DNA damage is a well-understood cause of cutaneous

melanoma, it does not appear to contribute to the development of UM (10). This observation is consistent with the location of most UM tumors in the posterior of the eye, away from direct UV exposure. Other environmental risk factors include the absence fluoridated water, which was recently associated with an increased rate of eye cancer (11). Overall, UM risk factors tend to be predominantly non-environmental.

Diagnosis and standard of care

Primary UM tumors can typically be detected by an ophthalmologist. At the time of diagnosis, the majority of patients notice symptoms ranging from visual disturbances to redness and pain, while other patients have no symptoms at all (12). Primary tumors are typically treated by either radiation therapy or enucleation. Radiation of UM tumors most often involves brachytherapy (13). By this method, implanted radioactive plaques deliver localized radiation to the tumor. Proton beams can also be used to effectively deliver radiation therapy to primary UM tumors (14). Tumor size is used to determine whether surgery should be performed, and enucleations often involve larger tumors. The Collaborative Ocular Melanoma Study (COMS) demonstrated no improved survival for patients with medium-sized tumors treated by either radiotherapy or enucleation (15). These results suggest that such patients could be treated effectively using strategies that preserve the eye.

Although radiation and enucleation can successfully treat primary UM, they do not prevent the onset of metastatic disease. Approximately 50% of UM patients will develop metastatic disease, which is uniformly fatal (16). The median survival time of metastatic patients is under 6 months (17). This diagnosis typically occurs years after the primary tumor was successfully treated (18). This observation suggests that UM cancer cells remain in the patient even after treatment. Targeting these cells is of the utmost importance to prevent the onset of metastatic disease. In the future, one could imagine developing strategies to treat high-risk patients with therapies in the adjuvant setting to prevent the growth of metastases.

Metastatic lesions are most often found in the liver (~90%), although less frequent sites include lung, bone, skin, and lymph nodes (18). The almost exclusive involvement of the liver is a metastatic pattern unique to UM. Currently, there are no effective therapies to treat metastatic UM. Both the prevalence and lethality of metastatic disease highlight an urgent need for novel strategies to treat these patients. Ongoing efforts to target metastatic UM, including current clinical trials, are highlighted in the treatment strategies section below.

Uveal melanoma biology

Initial studies of UM biology focused on tumorigenic phenotypes unique to UM. As discussed above, UM is highly metastatic to the liver (18). Thus, a key question in the UM field involves the extent to which liver-expressed growth factors, such as hepatocyte growth factor (HGF), might contribute to UM tumorigenesis and its metastatic potential.

HGF binds to the c-Met receptor tyrosine kinase to induce proliferation of liver cells (19). In one early study, c-Met expression was shown to correlate with the invasiveness of UM cell lines (20). Culture of UM cell lines in the presence of HGF results in c-Met activation and induces metastatic phenotypes, including invasion and migration *in vitro* (21, 22). In patients, over expression of c-Met in primary tumors may predict a worse outcome (23, 24). Together, these studies suggest that HGF/MET signaling may contribute to UM tumorigenesis. Based on these findings, MET has been postulated as a rational target for the treatment or prevention of metastatic UM. Recent preclinical efforts to characterize MET as a putative drug target are described in the treatment strategies section below.

Prognostics

Several clinical features of primary UM tumors are associated with poorer prognosis, including tumor diameter, extraocular growth, and involvement of the ciliary body (16). In a large study from the Liverpool Ocular Oncology Centre, tumor features that correlated with the

time between initial treatment and death due to metastatic UM also included sex, tumor stage (TNM classification), closed loops in the vasculature network, and the percentage of dividing cells (mitotic count) (5).

In addition to these clinical features, gene expression profiling has identified two molecular subtypes of UM that also correlate with outcome (25). So-called "Class 2" tumors express fewer melanocytic differentiation markers and typically metastasize, while "Class 1" tumors exhibit less aggressive phenotypes (26). More specifically, "Class 2" tumors exhibit higher expression of epithelial markers when compared to "Class 1" tumor profiles, while "Class 1" tumors express melanocyte lineage and neural crest genes more highly (26). The relevant gene signatures have been converted into a PCR-based 15-gene diagnostic test for clinical use (27, 28). This test has been extensively applied in the clinic and rapidly became the new standard for UM prognostic testing (29).

The genetics of uveal melanoma

The accumulation of somatic genetic changes that confer a proliferative advantage can result in aberrant cell growth and eventually tumorigenesis. In recent years, identification of oncogenic mutations that drive tumor growth has influenced the design of rational therapies to target specific genetic subtypes of cancer. For example, the majority of cutaneous melanoma tumors harboring activating mutations in BRAF ($BRAF^{V600E}$) are exquisitely sensitive to small molecule RAF inhibition (30). These and other examples highlight the importance of identifying driver mutations in cancer.

Copy number alterations

Aberrant chromosome copy number patterns are commonly observed in many different cancer types. These can exist as either arm-level or focal copy gains and losses (31).

Oncogenes (e.g., *MYC* and *CCND1*), are frequently amplified, while tumor suppressors (e.g., *CDKN2A*) are commonly deleted (31). Chromosomal copy number aberrations can also arise in the setting of resistance to targeted anticancer agents (32).

In UM, the most common somatic copy number alteration involves loss of a single copy of chromosome 3 (termed monosomy 3) (33, 34). Monosomy 3 is associated with a worse prognosis and metastatic disease (35). In addition to monosomy 3, UM tumors may also harbor recurrent gains of 8q and 6p as well as losses of 6q, 1p, and 16q (34, 36). 8q gain, 6q loss, and monosomy 3 correlate with the development of metastatic UM (37). The functional impact of many UM copy number alterations remains incompletely understood.

Somatic and germline point mutations

Several studies over the past few years have also sought to understand the nucleotide substitutions that may drive UM tumorigenesis. In contrast to cutaneous melanoma, UM tumors have low somatic mutation rates and no mutational signature due to UV irradiation-induced DNA damage (10). Thus, sun exposure *per se* does not appear to cause UM. In addition, although the mitogen-activated protein kinase (MAPK) pathway is active in both cutaneous and uveal melanomas, BRAF and NRAS are not mutated in uveal tumors (38), although these oncogenes are commonly mutated in cutaneous melanoma. These genetic data underscore the fact that uveal and cutaneous melanoma are entirely distinct from a molecular standpoint.

The majority of UM tumors (over 80%) harbor mutually exclusive oncogenic hotspot mutations in GNAQ and GNA11 (39, 40). These alterations almost always occur at residues R183 and Q209 and are likely to occur early on in UM progression (39-41). $GNAQ^{Q209L}$ is tumorigenic in 3T3 cells and renders the protein constitutively active due to the inability to hydrolyze GTP (42, 43). The GTP-bound protein is therefore able to continually signal to downstream effectors.

Mutations in GNAQ and GNA11 were initially implicated in melanocytes by a mutagenic screen for hyperpigmentation in mice (44). These proteins are members of the same family of α subunits of the heterotrimeric g-proteins. Heterotrimeric g-proteins transmit signals from G protein coupled receptors (GPCRs) at the cell surface to a variety of downstream signaling nodes. Several cellular pathways are activated by oncogenic GNAQ and GNA11; these pathways include protein kinase C and the MAPK signaling pathway (39, 45), the PI3K pathway (46) and small GTPase induction of YAP1 (47, 48) (**Figure 1.1**). Several of these downstream effectors may conceivably represent new targets for the development of *GNAQ/11*-mutant specific therapies (further detailed in treatment strategies section below).

In addition to GNAQ and GNA11, BRCA1 associated protein-1 (BAP1), is also recurrently mutated in UM (49). Inactivating mutations that include frameshift and nonsense mutations occur throughout the BAP1 coding region; this mutational distribution is consistent with the tumor suppressive function of BAP1 (50, 51). BAP1 is located on chromosome 3 and mutations typically occur in monosomy 3 tumors, resulting in functional loss of both copies of the gene (49). Mutations in BAP1 are associated with Class 2 gene expression profiles and metastasis (49).

BAP1 is a member of the Polycomb repressive deubiquitinase (PR-DUB) complex, which deubiquitinates histone H2A (52). BAP1 also deubiquitinates the cell cycle regulator HCF-1 (53, 54). In UM, loss of BAP1 expression results in conversion to a less differentiated

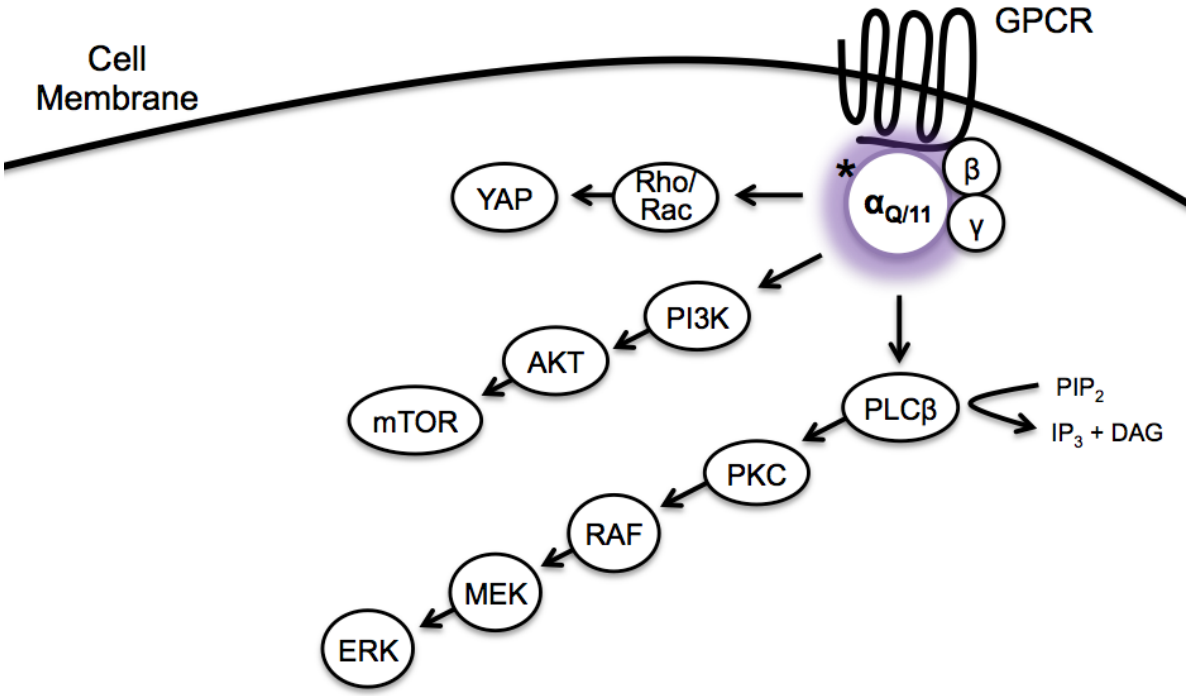

Figure 1.1. Signaling downstream of mutated GNAQ or GNA11 ($\alpha_{Q/11}$) in UM. Mutated protein is indicated by an asterix.

state, with no observed effect on cell proliferation (55). Efforts to target the functional impact of loss of BAP1 are underway and further discussed below in the treatment strategies section.

Germline mutations in BAP1 have also been described in individuals who develop UM, mesothelioma, and other cancer types (56-58). Mutations in the germline can be passed on through generations, indicating a hereditary component to UM. These observations further implicate BAP1 in UM tumorigenesis and suggest that germline mutations may be associated with a cancer syndrome phenotype. BAP1 is the only recurrent germline mutation currently identified to predispose individuals to UM.

Recently, more comprehensive genomic characterization of primary UM tumors led to the identification of recurrent mutations in the splicing factor SF3B1 (59). In UM, most SF3B1 mutations are located at residue 625 and correlate with good prognosis (59, 60). One key question was whether altered mRNA splicing occurs in mutated tumor cells. As anticipated, the splicing of specific mRNAs is impacted by SF3B1 R625 mutations (10). More specifically, SF3B1 mutations in CLL, breast cancer, and UM were recently shown to result in the use of cryptic 3' splice sites (61). The functional impact of differential splicing on UM biology and tumorigenesis remains to be further elucidated.

Recurrent mutations in the translation initiation factor EIF1AX occur in nearly 25% of primary UM tumors and may indicate a more favorable prognosis (60). EIF1AX mutations cluster at the N-terminus of the protein (60), and were also recently reported in thyroid carcinoma (62). Interestingly, EIF1AX is located on the x-chromosome, which results in expression of solely the mutant copy in tumor cells (60). This expression phenotype occurs in males because only one copy of the x chromosome is present, and in females due to inactivation of the non-mutant chromosome. The function of mutant EIF1AX in UM is further addressed in Chapter 2 of this thesis.

Prognostic value of genetic features

As discussed above, several recurrent somatic genetic alterations observed in UM may have prognostic importance. Monosomy 3 and BAP1 mutations are associated with Class 2 tumors and metastatic disease, while mutated SF3B1 and EIF1AX predict a better outcome (49, 59, 60). Loss of BAP1 protein expression in the nucleus also correlates well with metastatic potential (63). Given the many ways to down regulate gene expression, the assessment of protein levels may ultimately prove more meaningful than gene mutation status in the context of clinical prognostication. Indeed, reduced BAP1 protein levels were observed even in tumors with both copies of chromosome 3 (63). Expression of BAP1 protein may therefore be a more accurate predictor of metastatic potential than mutation or monosomy 3.

An emerging prognostic strategy may employ multiple genetic factors in combination to predict outcome. The combination of monosomy 3 with a BAP1 mutation and lack of EIF1AX mutation was significantly correlated with metastatic development (64). In principle, using multiple genetic events to predict outcome may offer a more robust approach than reliance on a single genetic feature. Now that the underlying genetic events of UM are better understood, the use of these features for clinical prognostics as well as treatment strategies can be further developed.

Treatment strategies

Developing strategies for more effective treatment of metastatic UM remains an unmet medical need. Conventional systemic chemotherapy is largely ineffective in this patient population (65). Several studies have sought to identify possible combination chemotherapy regimens that may improve outcomes. Combination therapy of gemcitabine and treosulfan resulted in a median progression free survival of 3 months in comparison to 2 months for treosulfan treatment alone (66). Treatment with the BOLD chemotherapy regimen (bleomycin,

vincristine, lomustine, and dacarbazine) combined with interferon alpha-2b did not elicit meaningful clinical responses (67). These data highlight the pressing need to identify novel treatment strategies for UM patients beyond chemotherapy.

Targeting GNAQ/11*-mutant tumors*

In recent years, efforts to develop targeted therapies to treat UM, and in particular, metastatic UM, have largely focused on understanding the underlying biology of UM pathogenesis. For example, several studies have demonstrated that *GNAQ* and *GNA11*-mutant UM cell lines depend on these g-proteins for growth (39, 45). However, designing small molecule inhibitors to block mutant GNAQ/11 function is challenged by their inability to hydrolyze GTP. Alternative therapeutic strategies are therefore necessary to selectively target *GNAQ/11*-mutant tumors.

Recent studies have focused on designing rationale approaches to inhibit pathways induced by oncogenic mutations in GNAQ and GNA11. The mitogen-activated protein kinase (MAPK) pathway, which signals from the protein kinase RAF to MEK and then to ERK, is perhaps the best-characterized pathway downstream of oncogenic GNAQ/11 (39, 40, 45). MEK emerged as a target for cancer therapy more than a decade ago (68). Small molecule inhibitors of MEK bind a pocket near the ATP site, rendering the protein catalytically inactive (69). This ATP non-competitive mechanism suggests that MEK inhibitors would be less prone to off-target inhibition of ATP-binding sites on other kinases.

Many MEK inhibitors have subsequently been developed and tested in several different cancer types and in combination with a variety of targeted and chemotherapy regimens (reviewed in 70). Thus far, MEK inhibition is most efficacious in *BRAF*-mutant cutaneous melanoma, although responses have also been observed in RAS driven cancers (71-73). Furthermore, two phase 3 trials in *BRA*F-mutant melanoma demonstrated that co-treatment with RAF and MEK inhibitors improved overall survival and reduced skin-related side effects when

compared to RAF inhibition alone (74, 75). The MEK inhibitor trametinib is now FDA approved for metastatic melanoma patients alone or in combination with the RAF inhibitor dabrafenib. In summary, these studies indicate that effective inhibition of MEK can be achieved in patients, and in some cases, result in clinical responses.

In UM, activation of the MAPK pathway occurs downstream of oncogenic GNAQ/11 and studies have demonstrated that *GNAQ/11*-mutant cells are sensitive to inhibition of MEK (39, 45). In addition, clinical trials using MEK inhibitors are underway and demonstrate improved progression free survival (76). However, no statistically significant improvement in overall survival was observed, suggesting that MEK inhibition is insufficient as a single agent. Combination strategies including MEK inhibition as a backbone may be necessary.

Several *in vitro* studies nominated combination therapies that build upon MEK inhibition. First, inhibition of the AKT pathway has been proposed. In UM cell lines, oncogenic GNAQ/11 induce the PI3K/AKT signaling pathway in parallel to MAPK activation (46). Indeed, combined inhibition of MEK and PI3K, AKT, or mTOR using small molecules enhances the anti-proliferative effect of MEK inhibition alone (45, 46, 77, 78). Subsequent clinical trials combining MEK and AKT inhibition are ongoing (NCT01979523). Inhibiting multiple pathways downstream of oncogenic GNAQ/11 will likely be more efficacious than single agent strategies.

In addition to MEK, protein kinase C (PKC) has also emerged as a novel therapeutic target downstream of mutant GNAQ/11 (79-81). There are 8 different PKC isoforms, many of which are activated across a wide variety of disease types, including cancer, diabetes, and heart disease (reviewed in 82). Based on this knowledge, developing isoform specific PKC inhibitors has been of great interest for some time. However, sequence similarity in the catalytic domain has made the generation of ATP-competitive inhibitors against specific isoforms difficult (82). Sotrastaurin (AEB071) is a pan-PKC inhibitor that was originally developed to block T-cell activation (83). However, minimal clinical activity as an immunosuppressant was observed in

transplant patients (84-86). In cancer, sotrastaurin shows promise in preclinical studies of diffuse large B-cell lymphomas (87).

In UM, *GNAQ/11*-mutant cells are sensitive to PKC inhibition *in vitro* (79-81). Furthermore, co-treatment with PKC and MEK inhibitors enhances the effect of either drug alone (79). Clinical trials using the pan-PKC inhibitor AEB071 (NCT01430416) as well as AEB071 plus the MEK inhibitor MEK162 (NCT01801358) are underway. Recent data also demonstrate enhanced sensitivity when combining a PKC inhibitor and the PI3Kα inhibitor BYL719 (88). This drug combination is the subject of a recent clinical trial (NCT02273219). These studies utilize a pan-PKC inhibitor, however, identifying which PKC isoforms are important for UM cell viability and subsequently designing isoform-specific inhibitors would be of interest for future therapies. This approach may increase the therapeutic window of PKC inhibitors if isoforms important for cancer growth differ from isoforms important for normal cell function.

Identifying additional pathways downstream of oncogenic GNAQ/11 is also of interest for the development of novel therapeutic strategies for UM. Most recently, YAP was nominated as a previously unappreciated dependency downstream of mutated GNAQ/11 (47, 48). YAP encodes Yes-associated protein 1, a transcriptional regulator downstream of Hippo signaling. YAP is a validated oncoprotein with important functions in growth, development, and more specifically, control of organ size (89). In *GNAQ/11*-mutant contexts, the small GTPases RhoA and Rac1 induced YAP1 activity (47). *GNAQ/11*-mutant cells were subsequently shown to be sensitive to YAP inhibition using both genetic and pharmacologic methods (47, 48). Given that activation of YAP likely occurs in parallel to induction of other pathways (some of which were described above), YAP inhibition may be most effective in combination with other targeted therapies.

In summary, several drug targets have been nominated downstream of oncogenic GNAQ and GNA11 in UM. In particular, the rationale for translating MEK and PKC inhibitors

into uveal melanoma clinical trials is well supported by preclinical data. However, the complex signaling induced by GNAQ/11 mutations suggests that co-inhibition of multiple downstream targets may be required to effectively treat patients harboring these mutations.

Other targeted therapy approaches

In addition to downstream effectors of mutant GNAQ/11, several other candidates for targeted therapy have emerged from mechanistic studies of UM biology. As discussed above, the almost exclusive involvement of the liver in UM metastasis prompted examination of a potential role for signaling via hepatocyte growth factor (HGF) and the HGF-receptor MET in UM cells. UM cells depend on activated MET for growth, although no genomic alterations in MET have been observed (90). In addition, MET inhibition using crizontinib minimized the development of metastasis in an orthotopic mouse model of UM (91). These data inspired clinical examination of MET inhibition in the adjuvant setting (NCT02223819). This ongoing clinical trial seeks to determine whether MET inhibition can prevent or postpone the development of metastatic disease in patients with Class 2 expression profiles who are likely to recur. Immunohistochemical analysis demonstrates expression of MET in the majority of UM tumors, with higher expression in metastatic samples (92). Together, these studies implicate MET as a putative therapeutic target in the adjuvant and/or metastatic setting.

Therapeutic targeting of tumors lacking functional BAP1 is also of interest. HDAC inhibitors have been demonstrated to induce the differentiation of UM cells (93). This phenotype effectively reverses the de-differentiation that occurs following BAP1 loss (93). A clinical trial using the HDAC inhibitor vorinostat is ongoing in metastatic UM patients (NCT01587352). A separate clinical study is investigating treatment with the HDAC inhibitor valproic acid in the adjuvant setting (NCT02068586). These studies will help to determine whether HDAC inhibition has a place in the treatment of metastatic UM. However, given that BAP1 mutations often occur in *GNAQ/11*-mutant tumors (49), targeting only BAP1-driven

phenotypes may be insufficient. Rather, co-targeting of both genetic lesions using some of the strategies described above may yield better outcomes.

In addition to the targeted therapies described above, several other drugs have been suggested for UM therapy. These agents include HSP90 inhibitors (94), for which there is also a clinical trial (NCT01200238), as well as p53 activators (95). A summary of the ongoing clinical trials for UM is displayed in **Table 1.1**. Forthcoming results from each of these trials should largely guide future treatment strategies for metastatic UM patients.

Immunotherapy

In recent years, immunotherapy has emerged as a novel approach to target several different cancer types by reactivating the immune system. For example, the CTLA-4 checkpoint inhibitor, ipilumumab, is currently FDA approved to treat metastatic cutaneous melanoma patients (96). In UM, ipilumumab shows moderate efficacy, with partial responses or stable disease achieved in approximately 30% of patients (97, 98). Additional clinical trials are ongoing to expand these studies of ipilumumab in the metastatic and adjuvant settings (**Table 1.1**). One additional clinical trial is seeking to treat UM with tumor infiltrating lymphocytes (TILs) (NCT01814046). This approach involves isolating TILs from a patient's tumor, expanding them considerably *in vitro*, and then re-delivering them to the patient. The hope is then that these immune cells will target and attack the cancer cells. Immunotherapy provides a promising new avenue for cancer therapy, although its relevance to UM treatment remains to be entirely elucidated.

Table 1.1 Summary of ongoing clinical trials for UM. The cellular target of each drug is indicated in parentheses underneath the category of therapy.

ClinicalTrials.gov Identifier	Drug(s)	Setting	Phase	Category
NCT02363283	Glembatumumab Vedotin	Metastasis	II	Antibody-Drug Conjugate
NCT01100528	Decarbzome + Interferon Alpha-2b	Adjuvent	II	Chemotherapy
NCT01785316	Hepatic Perfusion	Metastasis	III	Chemotherapy
NCT00929019	mRNA transfected dendritic cell vaccine	Adjuvent	I/II	Immunotherapy
NCT01983748	Dendritic cell with autologous tumor RNA	Adjuvent	III	Immunotherapy
NCT01961115	INCB024360 and Vaccine Therapy	Metastasis	II	Immunotherapy
NCT01585194	Ipilimumab	Adjuvent, Metastasis	I/II	Immunotherapy (CTLA4)
NCT01730157	Radioembolization and Ipilimumab	Metastasis	0	Immunotherapy (CTLA4)
NCT02359851	Pembrolizumab	Metastasis	II	Immunotherapy (PD-1)
NCT01814046	Young TIL	Metastasis	II	Immunotherapy
NCT01143402	Temozolomide or Selumetinib	Metastasis	II	Targeted therapy (Chemo or MEK)
NCT01587352	Vorinostat	Metastasis	II	Targeted therapy (HDAC)
NCT01200238	Ganetespib	Metastasis	II	Targeted therapy (HSP90)
NCT01377025	Sorafenib	Metastasis	II	Targeted therapy (Kinases)
NCT01974752	Selumetinib	Metastasis	III	Targeted therapy (MEK)
NCT01979523	Trametinib +/- GSK2141795	Metastasis	II	Targeted therapy (MEK + AKT)
NCT02223819	Crizotinib	Adjuvent	II	Targeted therapy (MET)
NCT01252251	Everolimus + Pasireotide	Metastasis	II	Targeted therapy (mTOR + SSTR)
NCT01430416	AEB071	Metastasis	I	Targeted therapy (PKC)
NCT01801358	AEB071 + MEK162	Metastasis	I/II	Targeted therapy (PKC + MEK)
NCT02273219	AEB071 + BYL719	Metastasis	I	Targeted therapy (PKC + PI3K)
NCT02068586	Sunitinib or Valproic Acid	Adjuvent	II	Targeted therapy (RTK or HDAC)
NCT01533948	Axitinib	Metastasis	II	Targeted therapy (RTK)

Understanding the underlying genetic and biological basis of cancer is incredibly important for the design of rational therapeutic strategies. This concept has been born out by studies that demonstrate dramatic clinical response to inhibition of oncogenic driver mutations. However, resistance to targeted therapies frequently emerges. Also, some tumors are intrinsically resistant to targeted agents, regardless of the presence of oncogene alterations predicted to confer a therapeutic vulnerability. Moreover, many cancer types harbor low frequency driver events that may require large sample cohorts for adequately powered clinical trials. These challenges highlight a need to understand the full genetic underpinnings of each cancer type as well as the landscape of resistance mechanisms to targeted therapies.

Limitations to existing therapeutic strategies

As noted above, recent studies in UM suggest that PKC and MEK inhibitors may target dependencies linked to mutant GNAQ/11 signaling. However, both *in vitro* and clinical studies suggest that single agent treatment strategies will be insufficient (76, 79). As discussed above, hypothesis driven approaches to inhibit multiple downstream pathways of oncogenic GNAQ/11 were subsequently applied (45, 46, 77, 78). These combination therapy strategies are limited by both existing knowledge of GNAQ/11 biology and available therapeutics. Systematic and unbiased approaches to identify novel co-targets are therefore needed. Drug enhancer screening approaches could be applied to test putative targets for combination therapy with drugs currently in UM clinical trials. These studies could help to identify novel genes and pathways for the development of combination therapies to treat patients.

Our understanding of the somatic genetic events that drive UM tumorigenesis also remains incomplete. Recent studies focused on comprehensive sequencing of small cohorts of samples (<20 tumors) (59, 60), which limits the ability to identify lower frequency recurrently

mutated genes. Studies of cutaneous melanoma, for example, nominated driver genes that are mutated at frequencies as low as 5-10% of samples (99, 100). Larger sample cohorts need to be characterized in order to identify putative rare driver mutations in UM.

In addition, more extensive functional analyses of recurrently mutated genes are needed to understand the therapeutic potential of these alterations. Little is known about the contributions of SF3B1 and EIF1AX mutations to UM tumorigenesis. By understanding the biology of these mutant proteins, one can begin to decipher whether they represent a targetable opportunity for drug development.

Finally, comprehensive studies of genomic events that drive progression from primary to metastatic UM are lacking. Several genetic features that are associated with metastatic potential are understood, however, focused examination of metastatic tumor samples has been only occasionally performed. One recent study reported genetic profiling of just over 400 genes using targeted sequencing of 5 liver metastases (101). This study is limited by the lack of primary tumor analysis; enrichment or depletion of genetic alterations in the metastatic sample in comparison to the primary is therefore impossible to determine. Future analyses using trios of samples, including normal, primary, and metastatic tumor DNA, will be necessary to further detail the genetic changes that contribute to UM progression and understand whether they are therapeutically targetable.

Rationale for this work

As discussed above, metastatic UM remains a deadly disease with poor outcome and no effective treatment strategies. Recent studies have identified several possible targeted therapy approaches for UM treatment, however, new therapeutic combinations will likely be required to achieve profound and durable clinical responses. This work has leveraged two parallel approaches to identify novel therapeutic strategies to treat metastatic UM. First, comprehensive genomic characterization of primary and metastatic UM has been performed to identify novel

recurrently mutated genes and begin to understand their cellular effects. Second, systematic RNAi-based drug enhancer screening was performed to identify novel targets for combination therapy using MEK and PKC inhibitors as a backbone. Together, these studies aim to improve our understanding of UM biology and nominate strategies for combination therapy.

CHAPTER 2

SYSTEMATIC GENOMIC CHARACTERIZATION OF PRIMARY AND METASTATIC UVEAL MELANOMA

Attributions

This chapter is reprinted from a manuscript in preparation with the following authorship:

Ivana K. Kim[1]*, Chelsea S. Place[2,3]*, Bita Esmaeli[4]*, Ali Amin-Mansour[3], Daniel J. Treacy[2], Scott L. Carter[2,3], Eran Hodis[3], Nikhil Wagle[2,3], Sara Seepo[3], Xiaoxing Yu[4], Anne Marie Lane[1], Evangelos S. Gragoudas[1], Francisca Vazquez[3], Elizabeth Nickerson[3], Kristian Cibulskis[3], Aaron McKenna[3,5], Stacey B. Gabriel[3], Gad Getz[3], Eliezer M. Van Allen[2,3], Levi A. Garraway[2,3]**, Scott E. Woodman[4]**

1) Massachusetts Eye and Ear Infirmary, Harvard Medical School, Boston, MA, 02114
2) Dana-Farber Cancer Institute, Harvard Medical School, Boston, MA 02115
3) The Broad Institute of Harvard and MIT, Cambridge, MA 02142
4) The University of Texas MD Anderson Cancer Center, Houston, TX 77030
5) University of Washington, Seattle, WA 98195

*These authors contributed equally to this work; **These authors contributed equally to this work

All of the experiments and analysis were performed by Chelsea Place except as follows:

Ivana Kim, Bita Esmaeli, and Scott Woodman provided patient tumor samples, clinical information, and analysis. Analysis of whole exome sequencing of primary tumors was performed with Eli Van Allen (**Figure 2.1A-C**). Analysis of trios of samples was performed by Ali Amin-Mansour using ABSOLUTE, which was reviewed by Scott Carter (**Figure 2.1D and E**). Polysome profiling experiments were performed with the assistance of Daniel Treacy (**Figure 2.4D**). Daniel Treacy performed RNA extractions from input and polysome fractions. RNA sequencing analysis was performed collaboratively with Eliezer Van Allen (**Figure 2.8**). The polysome interaction analysis was performed by Ali Amin-Mansour under the advisement of Peter ‘t Hoen (**Table 2.9; Figure 2.9**). Sequencing was performed at the Broad Institute.

Abstract

To further our understanding of the somatic genetic basis of uveal melanoma, we sequenced the protein-coding regions of 61 primary tumors and 3 liver metastases together with paired normal DNA. Known recurrent mutations were identified in *GNAQ, GNA11, BAP1, EIF1AX*, and *SF3B1*. Putative driver gene mutations found exclusively in metastatic tumor samples included *SMARCA4* and *IQGAP1*. Knockdown of both wild type and mutant EIF1AX was lethal to uveal melanoma cells. We probed the function of N-terminal tail EIF1AX mutations by performing RNA sequencing of polysome-associated transcripts in cells expressing endogenous wild type or mutant EIF1AX. Ribosome occupancy of the global translational apparatus was sensitive to suppression of wild type but not mutant EIF1AX. Together, these studies suggest that cells expressing mutant EIF1AX may exhibit aberrant translational regulation, which may promote tumorigenesis in uveal melanoma and other cancer types.

Introduction

Uveal melanoma (UM), which accounts for 5% of all melanomas, occurs in the iris, ciliary body, and choroid of the eye. Approximately 50% of UM patients develop metastatic disease, most often to the liver (102). Primary UM is treated by either enucleation or radiation, while metastatic UM has no effective therapies and a survival rate of less than 6 months (17). Thus, improved treatment of metastatic UM represents an unmet medical need.

Over 80% of UM tumors harbor activating hotspot mutations in *GNAQ* or *GNA11*, which encode alpha subunits of guanine nucleotide binding (G) proteins (39, 40). Mutations at residues 183 and 209 of these proteins result in activation of downstream signaling including the protein kinase C, mitogen-activated protein kinase (MAPK), and YAP1 pathways (45, 47, 48,

79). Frequently observed copy number alterations in UM tumors include loss of a single copy of chromosome 3 (monosomy 3), amplification of 8q or 6p, and less frequently 1p or 16q loss (34, 36). Monosomy 3 is predictive of worse prognosis (35) and often co-occurs with loss of function mutations in the tumor suppressor BAP1, which is located on chromosome 3 (49). In addition to *GNAQ*, *GNA11*, and *BAP1*, recurrent mutations in the splicing factor, *SF3B1*, as well as the translation initiation factor, *EIF1AX*, have been recently characterized in primary UM tumors (59, 60).

Despite these advances, large-scale genome characterization efforts in UM have been limited by sample size and restricted to primary tumors. To expand knowledge of the somatic genetics of primary and metastatic UM, we sequenced the protein-coding exons of 61 primary tumors and 3 liver metastases. We also pursued systematic functional studies of EIF1AX, a translation factor recurrently mutated in UM.

Results

Somatic mutations in primary uveal melanoma

Solution-phase hybrid capture and whole exome sequencing were performed on paired primary tumor and normal genomic DNA from 61 patients with uveal melanoma (UM). Primary tumor samples were obtained following enucleation. Germline DNA was isolated from peripheral blood (N=26) or adjacent normal choroidal tissue (N=35). 101-fold mean target coverage was achieved, with an average of 90% of exonic bases covered per sample.

A subset of 52 tumor/normal pairs passed standard quality control metrics, including screening for tumor DNA in normal samples or normal DNA in tumor samples, and were included in our analysis set (**Tables 2.1-2.3**). The mean nonsynonymous somatic mutation rate was 0.35 mutations per megabase (range: 0.031 to 3.02), with an average of 25 nonsynonymous coding mutations per patient (**Figure 2.1A; Table 2.2**). As expected and in

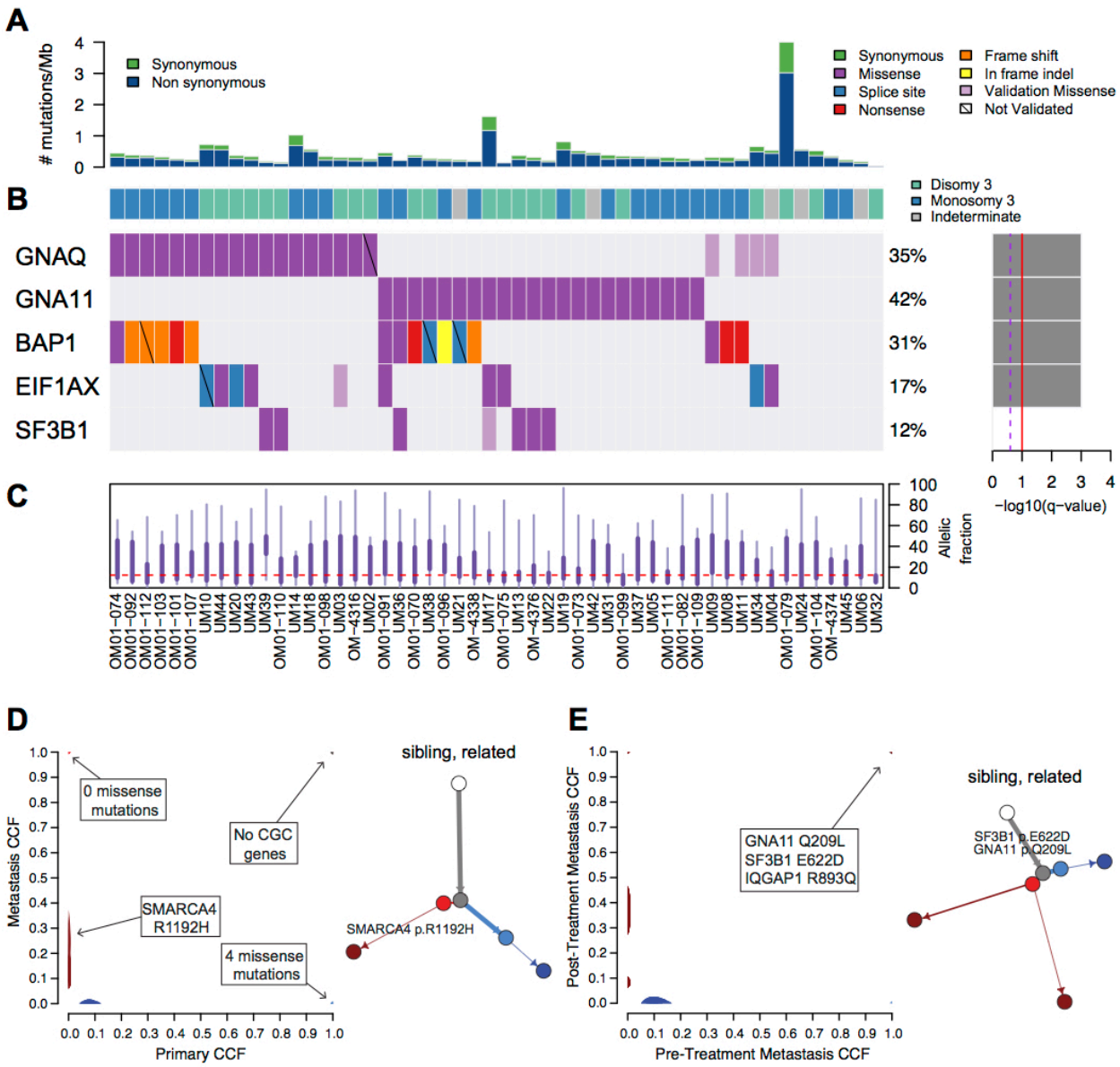

Figure 2.1. Somatic mutations in primary and metastatic uveal melanoma. (A) The number of synonymous and nonsynonymous mutations per megabase of DNA sequence for 52 samples, arranged in columns. **(B)** Mutations in recurrently mutated genes are color-coded and ordered by significance. Percentages on right indicate mutation frequency observed in exome sequencing. **(C)** Boxplots represent the distributions of allelic fractions observed per sample. **(D)** The percentage of tumor cells (CCF) harboring a given mutation in the primary tumor in comparison to a metastatic liver sample from the same patient (UM45; left). Cancer gene census is indicated by CGC. Phylogenetic analysis of primary and metastatic tumor samples indicates sibling relationship (right). **(E)** As in (D), but comparing a pre-treatment metastatic tumor sample to a post-treatment metastasis (Trio 2).

Table 2.1. Clinical characteristics of analysis set.

Patients	MEEI (N=23)	MDACC (N=29)
Age at diagnosis (Median; range)	65 (34-89)	62 (23-83)
Normal DNA source	Blood	Adjacent choroid
Gender		
Male	14	17
Female	9	12
Anatomic Site		
Choroid	10	22
Choroid/CB	12	6
CB/Iris	1	1
Tumor Stage		
I	0	2
II	4	14
III	17	12
IV	0	1
N/A	2	0

Table 2.2. Sequencing metrics of 52 uveal melanomas.

Patient ID	Normal Type	% Cross-Contamination		Mean Target Coverage (X)		Fraction PF Reads		Fraction Selected Bases		Fraction Zero Coverage Targets		Synonymous mutation rate	Nonsynoymous mutation rate	Mutations/Mb	# of coding mutations
		Tumor	Normal	Tumor	Normal	Tumor	Normal	Tumor	Normal	Tumor	Normal				
UVEAL-OM-01-110	Whole Blood	2.5	2	76.86	106.67	0.95	0.94	0.91	0.91	0.02	0.01	3.05E-08	1.22E-07	0.15	10
UVEAL-OM-01-111	Whole Blood	2	1.9	119.10	151.38	0.94	0.94	0.91	0.91	0.01	0.01	1.22E-07	1.83E-07	0.31	21
UVEAL-OM-01-112	Whole Blood	2.5	2.7	146.00	84.00	0.94	0.93	0.91	0.90	0.02	0.02	6.11E-08	3.05E-07	0.37	28
UVEAL-OM-4316	Whole Blood	2.4	2.9	138.53	109.84	0.94	0.92	0.91	0.90	0.02	0.02	1.07E-07	1.98E-07	0.31	21
UVEAL-OM-4338	Whole Blood	2.4	2.3	117.90	115.82	0.94	0.92	0.91	0.91	0.01	0.02	1.53E-08	1.83E-07	0.20	14
UVEAL-OM-4374	Whole Blood	3.1	1.5	89.34	164.07	0.95	0.95	0.91	0.91	0.02	0.01	4.58E-08	3.05E-07	0.35	24
UVEAL-OM-4376	Whole Blood	1.6	2.1	124.60	105.25	0.94	0.92	0.91	0.91	0.02	0.02	9.16E-08	2.14E-07	0.31	22
UVEAL-OM01-070	Whole Blood	0.6	0.3	97.70	106.83	0.91	0.90	0.90	0.89	0.02	0.02	6.11E-08	3.21E-07	0.38	25
UVEAL-OM01-073	Whole Blood	0.2	0.3	94.30	90.57	0.91	0.91	0.90	0.90	0.02	0.02	7.63E-08	4.43E-07	0.52	35
UVEAL-OM01-074	Whole Blood	0.2	0.2	93.29	101.34	0.91	0.90	0.90	0.90	0.02	0.02	1.22E-07	3.21E-07	0.44	32
UVEAL-OM01-075	Whole Blood	0.3	0.5	99.33	94.54	0.91	0.91	0.90	0.90	0.02	0.02	0.00E+00	1.37E-07	0.14	9
UVEAL-OM01-079	Whole Blood	0.5	0.3	94.27	94.30	0.91	0.91	0.90	0.90	0.02	0.02	9.77E-07	3.02E-06	4.00	287
UVEAL-OM01-082	Whole Blood	0.4	0.3	92.47	93.16	0.91	0.91	0.90	0.90	0.02	0.02	9.16E-08	1.83E-07	0.27	19
UVEAL-OM01-091	Whole Blood	0.4	0.2	100.33	94.78	0.91	0.91	0.90	0.90	0.02	0.02	1.07E-07	3.51E-07	0.46	30
UVEAL-OM01-092	Whole Blood	0.2	0.3	102.83	93.51	0.91	0.91	0.90	0.90	0.02	0.02	9.16E-08	2.90E-07	0.38	27
UVEAL-OM01-096	Whole Blood	0.3	0.1	96.91	100.05	0.90	0.91	0.90	0.90	0.02	0.02	6.11E-08	1.98E-07	0.26	18
UVEAL-OM01-098	Whole Blood	0.3	0.4	101.12	94.53	0.90	0.91	0.90	0.90	0.02	0.02	1.07E-07	2.29E-07	0.34	25
UVEAL-OM01-099	Whole Blood	0.6	0.8	100.91	97.58	0.91	0.90	0.90	0.90	0.02	0.02	7.63E-08	2.75E-07	0.35	23
UVEAL-OM01-101	Whole Blood	1.1	1.1	102.45	82.66	0.91	0.91	0.90	0.90	0.02	0.02	3.05E-08	2.29E-07	0.26	18
UVEAL-OM01-103	Whole Blood	0.4	0.7	98.66	96.81	0.91	0.90	0.90	0.90	0.02	0.02	7.63E-08	2.44E-07	0.32	25
UVEAL-OM01-104	Whole Blood	0.6	0.2	93.76	101.47	0.91	0.91	0.90	0.90	0.02	0.02	1.53E-07	3.66E-07	0.52	35
UVEAL-OM01-107	Whole Blood	1.4	0.3	94.71	99.20	0.91	0.90	0.90	0.90	0.02	0.02	4.58E-08	1.83E-07	0.23	16
UVEAL-OM01-109	Whole Blood	0.8	0.4	101.06	93.91	0.91	0.91	0.90	0.90	0.02	0.02	3.05E-08	2.14E-07	0.24	17
UVEAL-UM2	Adjacent Normal Tissue	1.8	6.1	128.32	60.70	0.95	0.93	0.91	0.86	0.02	0.02	6.11E-08	1.98E-07	0.26	50
UVEAL-UM3	Adjacent Normal Tissue	2.4	4.3	95.68	80.21	0.95	0.93	0.91	0.82	0.02	0.01	7.63E-08	2.29E-07	0.31	17
UVEAL-UM4	Adjacent Normal Tissue	2.1	6	123.71	81.38	0.94	0.93	0.93	0.87	0.04	0.02	9.16E-08	4.43E-07	0.53	25
UVEAL-UM5	Adjacent Normal Tissue	2	2.4	109.92	91.57	0.95	0.95	0.91	0.91	0.02	0.02	4.58E-08	2.75E-07	0.32	80
UVEAL-UM6	Adjacent Normal Tissue	0.1	0.1	84.98	97.26	0.93	0.94	0.91	0.91	0.02	0.01	4.58E-08	1.22E-07	0.17	111
UVEAL-UM8	Adjacent Normal Tissue	1.3	2.5	102.79	111.32	0.95	0.95	0.91	0.91	0.03	0.02	1.37E-07	1.68E-07	0.31	40
UVEAL-UM9	Adjacent Normal Tissue	2.5	2.6	97.66	110.68	0.95	0.95	0.91	0.91	0.03	0.02	9.16E-08	2.14E-07	0.31	63
UVEAL-UM10	Adjacent Normal Tissue	2.4	2.8	100.60	98.00	0.95	0.95	0.91	0.91	0.02	0.02	1.53E-07	5.65E-07	0.72	20
UVEAL-UM11	Adjacent Normal Tissue	1.8	2.4	91.84	97.06	0.95	0.93	0.91	0.93	0.02	0.02	4.58E-08	2.14E-07	0.26	24
UVEAL-UM13	Adjacent Normal Tissue	2.5	2.3	86.94	108.43	0.95	0.95	0.91	0.91	0.02	0.02	1.22E-07	2.44E-07	0.37	16
UVEAL-UM14	Adjacent Normal Tissue	1.4	2.5	125.68	111.54	0.95	0.95	0.91	0.91	0.02	0.02	3.36E-07	6.87E-07	1.02	17
UVEAL-UM17	Adjacent Normal Tissue	5.5	1.7	70.02	110.23	0.94	0.95	0.87	0.91	0.02	0.03	4.43E-07	1.18E-06	1.62	45
UVEAL-UM18	Adjacent Normal Tissue	8.2	1.3	73.19	163.95	0.94	0.95	0.89	0.91	0.02	0.01	6.11E-08	5.04E-07	0.56	22
UVEAL-UM19	Adjacent Normal Tissue	6.5	2.3	34.53	90.19	0.94	0.95	0.81	0.91	0.02	0.02	2.60E-07	5.50E-07	0.81	26
UVEAL-UM20	Adjacent Normal Tissue	1.4	2.9	98.69	111.04	0.95	0.95	0.91	0.91	0.02	0.01	9.16E-08	2.75E-07	0.37	2
UVEAL-UM21	Adjacent Normal Tissue	2.4	1.5	117.37	122.91	0.95	0.95	0.92	0.92	0.02	0.04	4.58E-08	1.83E-07	0.23	46
UVEAL-UM22	Adjacent Normal Tissue	2.3	1	119.32	251.30	0.95	0.92	0.91	0.91	0.02	0.02	4.58E-08	1.68E-07	0.21	16
UVEAL-UM24	Adjacent Normal Tissue	7.9	1.6	66.40	94.47	0.93	0.95	0.80	0.91	0.02	0.02	3.05E-08	5.34E-07	0.56	24
UVEAL-UM31	Adjacent Normal Tissue	3.2	3.3	93.85	68.22	0.95	0.95	0.91	0.90	0.02	0.02	1.22E-07	2.60E-07	0.38	18
UVEAL-UM32	Adjacent Normal Tissue	3.3	6.8	94.59	58.42	0.95	0.92	0.91	0.85	0.02	0.02	0.00E+00	3.05E-08	0.03	13
UVEAL-UM34	Adjacent Normal Tissue	1.8	2.1	112.33	94.20	0.95	0.95	0.91	0.91	0.03	0.02	1.68E-07	4.89E-07	0.66	38
UVEAL-UM36	Adjacent Normal Tissue	0.1	0.1	83.08	96.37	0.94	0.94	0.91	0.91	0.02	0.02	1.53E-08	2.14E-07	0.23	31
UVEAL-UM37	Adjacent Normal Tissue	0.1	0.1	78.57	82.55	0.93	0.93	0.91	0.91	0.02	0.02	4.58E-08	2.90E-07	0.34	24
UVEAL-UM38	Adjacent Normal Tissue	0.1	0.1	93.28	75.52	0.93	0.92	0.91	0.91	0.02	0.02	4.58E-08	2.29E-07	0.27	47
UVEAL-UM39	Adjacent Normal Tissue	0.1	0.1	86.60	90.54	0.92	0.93	0.91	0.90	0.02	0.02	3.05E-08	1.53E-07	0.18	16
UVEAL-UM42	Adjacent Normal Tissue	0.1	0.2	113.48	93.68	0.94	0.93	0.91	0.91	0.06	0.02	6.11E-08	3.97E-07	0.46	21
UVEAL-UM43	Adjacent Normal Tissue	0.1	0.1	85.32	96.18	0.94	0.93	0.91	0.91	0.02	0.02	1.07E-07	2.29E-07	0.34	11
UVEAL-UM44	Adjacent Normal Tissue	0.2	0.1	120.59	83.73	0.93	0.92	0.92	0.91	0.02	0.02	1.53E-07	5.50E-07	0.70	20
UVEAL-UM45	Adjacent Normal Tissue	0.1	0.1	91.11	102.17	0.93	0.93	0.91	0.91	0.02	0.02	6.11E-08	1.68E-07	0.23	21

Table 2.3. Extended clinical characteristics of 52 uveal melanomas.

Patient Information			Medical Information			Genetic Information					Prognostic Information
						Somatic Mutations				Copy Number	
UM / ID	Age at Dx	Gender	Anatomic Site	AJCC Stage	Metastatic UM	GNAQ/11	BAP1	EIF1AX	SF3B1	Chr 3 status	Gene Expression Profile
OM-4316	78	Female	Choroid	IIIA	No	GNAQ				D3	
OM-4338	56	Male	Choroid	IIB	No	GNA11	BAP1			M3	
OM-4374	56	Female	Choroid/CB	IIIB	Yes					M3	2
OM-4376	61	Female	Choroid	IIIA	No	GNA11			SF3B1	D3	
OM01-070	77	Male	Choroid	N/A	No	GNA11	BAP1			D3	
OM01-073	69	Male	Choroid	IIA	Yes*	GNA11				D3	
OM01-074	66	Male	Choroid/CB	IIIA	Yes*	GNAQ	BAP1			M3	
OM01-075	50	Male	Choroid	IIIA	No	GNA11		EIF1AX		D3	
OM01-079	68	Male	Choroid/CB	IIIB	No					D3	
OM01-082	69	Female	Choroid/CB	IIIB	Yes*	GNA11				M3	
OM01-091	66	Male	Choroid/CB	IIB/IIIA^	Yes*	GNA11	BAP1	EIF1AX		M3	
OM01-092	51	Male	Choroid/CB	IIIA	Yes*	GNAQ	BAP1			M3	
OM01-096	70	Female	Choroid/CB	IIIB	Yes*	GNA11	BAP1			M3	
OM01-098	84	Male	Choroid/CB	IIIB	No#	GNAQ				M3	
OM01-099	65	Female	Choroid	IIB	No	GNA11				D3	
OM01-101	53	Female	Choroid/CB	IIIA	No#	GNAQ	BAP1			M3	
OM01-103	89	Female	Choroid/CB	IIIA	No#	GNAQ	BAP1			M3	
OM01-104	57	Male	Choroid/CB	IIIB	No					D3	
OM01-107	55	Male	Choroid/CB	IIIB	No	GNAQ	BAP1			M3	
OM01-109	55	Male	CB/Iris	IIIA	No	GNA11				M3	
OM01-110	34	Male	Choroid	IIB	No	GNAQ			SF3B1	D3	
OM01-111	59	Male	Choroid	IIIA	No	GNA11				M3	
OM01-112	84	Female	Choroid	IIIA	No	GNAQ	BAP1[nv]			M3	
UM02	64	Male	Choroid	IIB	No	GNAQ[nv]				D3	1B
UM03	73	Male	Choroid/CB	IIIA	No#	GNAQ		EIF1AX[d]		D3	
UM04	64	Female	Choroid	IIA	No	GNAQ[d]		EIF1AX		indeterminate	
UM05	52	Female	Choroid	IIIB	No	GNA11				M3	
UM06	23	Male	Choroid/CB	IIIB	No					indeterminate	
UM08	48	Female	Choroid	IIA	No		BAP1			M3	2
UM09	27	Female	Choroid/CB	IIIA	Yes*	GNAQ[d]	BAP1			M3	
UM10	40	Male	Choroid	IIB	No	GNAQ		EIF1AX[nv]		D3	1B
UM11	N/A	Male	Choroid	IIA	No	GNAQ[d]	BAP1			M3	1A
UM13	57	Female	Choroid	IIA	No	GNA11			SF3B1	D3	1
UM14	81	Female	Choroid	IIIA	No	GNAQ				M3	1A
UM17	53	Female	Choroid	IIA	No	GNA11		EIF1AX	SF3B1[d]	D3	
UM18	64	Male	Choroid	I	No	GNAQ				M3	1A
UM19	33	Male	Choroid	IIIC	No	GNA11				M3	2
UM20	63	Male	Choroid	IIIA	No	GNAQ		EIF1AX		D3	1B
UM21	56	Male	Choroid	IIB	No	GNA11	BAP1[nv]			indeterminate	2
UM22	75	Male	Choroid	IIB	No	GNA11			SF3B1	D3	1A
UM24	64	Male	Choroid/CB	IIIA	No#					indeterminate	
UM31	70	Female	Choroid/CB	IIIB	Yes*	GNA11				M3	
UM32	68	Male	Choroid	IIIA	Yes*					D3	
UM34	83	Male	Choroid	IIB	No#	GNAQ[d]		EIF1AX		D3	
UM36	70	Female	Choroid	IIA	Yes*	GNA11	BAP1		SF3B1	M3	
UM37	69	Female	Choroid	IIB	Yes	GNA11				M3	2
UM38	54	Male	CB/Iris	IIIA	No	GNA11	BAP1[nv]			D3	2
UM39	53	Female	Choroid	I	No	GNAQ			SF3B1	D3	2
UM42	54	Male	Choroid	IIIA	No	GNA11				indeterminate	1B
UM43	50	Female	Choroid	IIA	No	GNAQ		EIF1AX		D3	1B
UM44	61	Male	Choroid	IIA	No	GNAQ		EIF1AX		D3	1B
UM45	78	Male	Choroid/CB	IV	Yes*					M3	2

*Deceased from metastatic uveal melanoma
#Deceased of other causes
^Complete tumor dimensions not available
N/A: Not available

d: mutation discovered by targeted resequencing
nv: mutation not validated by targeted resequencing

contrast to cutaneous melanoma sequencing studies (99, 100), no UV signature of DNA damage was observed in this cohort of UM samples.

Chromosomal copy number profiles were also generated using the CapSeg algorithm. Monosomy 3 was observed in 53% of analyzed patients (**Figure 2.2**). Consistent with prior studies (35), the majority of patients who had or went on to develop metastatic disease (11/13) harbored detectable monosomy 3 (**Table 2.3**). Also consistent with previous studies (37, 103), chromosome 8q copy number gains tended to co-occur with monosomy 3, while chromosome 6p copy number gains tended to be associated with the disomy 3 state. Other frequent chromosomal changes (e.g., chromosome 1p or 16q deletions) were also observed.

To identify significantly mutated genes in UM, we used the MutSigCV algorithm, which accounts for patient and gene-specific mutation frequency, gene size, and the ratio of synonymous to nonsynonymous mutations per gene (104). We found 4 genes (*GNAQ, GNA11, BAP1*, and *EIF1AX*) that were mutated more frequently than would be expected by chance (**Figure 2.1B**). All of these genes have been previously implicated in UM (39, 40, 49, 60). We observed 5 mutations in *SF3B1* by exome sequencing at residues 625, 662, and 666. Although *SF3B1* did not meet the significance threshold in this cohort, it is a known cancer gene that is also recurrently mutated in UM (59).

Targeted re-sequencing in all 52 tumor/normal pairs independently validated the somatic mutations identified in these 5 genes. In total, 98.4% of missense/nonsense mutations and 42.9% of small insertions/deletions were validated (**Table 2.4**). Re-sequencing also identified several additional hotspot mutations in *GNAQ* (Q209), *EIF1AX* (G15), and *SF3B1* (R625) (**Figure 2.1B**). Most of these mutations occurred in regions of low WES sequence coverage, which may explain why they were not called initially by standard analysis algorithms.

The majority of patients harbored mutually exclusive mutations at residues 209 or 183 of *GNAQ* and *GNA11* (**Figure 2.1B**). One sample (OM-01-110) contained a novel *GNAQ* mutation, which harbored two mutations at the same codon (GGA>CTA) resulting in a G48L substitution.

Sequencing reads spanning codon 48 confirmed that these mutations occur in cis. Residue 48 lies within a putative GTP-binding region of GNAQ (www.uniprot.org), although its functional effect is unknown.

Mutations in *BAP1, EIF1AX*, and *SF3B1* were almost entirely mutually exclusive, with only 2 out of 29 mutant samples harboring alterations in more than one gene. This observation suggests 3 predominant genetic classes of UM and is supported by data indicating mutant *BAP1* is associated with a worse prognosis while *EIF1AX* and *SF3B1* mutations indicate a better prognosis (49, 59, 60). Interestingly, patient OM-091 harbored missense mutations in both EIF1AX (R13C) and BAP1 (N102K); however, mutant *EIF1AX* was present at a low allelic fraction (0.051), suggesting a subclonal event. Sample UM36 contained missense mutations in both BAP1 (G185R; with an allelic fraction of 0.83) and SF3B1 (K666T; with an allelic fraction of 0.48). The majority of SF3B1 mutations in UM occur at residue 625, however, lysine 666 is recurrently mutated in CLL (105). Of note, both OM-091 and UM36 patients died of metastatic UM (**Table 2.3**), consistent with previous studies linking BAP1 with metastasis (49).

Somatic mutations in metastatic uveal melanoma

To search for mutated genes in the metastatic setting, we sequenced multiple tumors from two UM patients with metastatic disease (UM45 and Trio 2). We utilized the ABSOLUTE algorithm to assign each somatic mutation a cancer cell fraction (CCF), which corresponds to the percentage of tumor cells harboring the genetic event (106). We then utilized cancer cell fractions to identify and compare clonal and subclonal events across distinct tumor samples from the same patient (107).

For patient UM45, the paired primary enucleated tumor and a single metastatic sample from a liver biopsy were sequenced. Only 4 clonal missense mutations were present in both samples (**Figure 2.1D**, top right). Phylogenetic analysis using CCFs suggests these tumors are siblings, which indicates that both the primary and metastatic cells evolved from a common

ancestor. In this tumor, *SMARCA4* R1192H mutation was enriched in the metastatic sample in comparison to the primary tumor (**Figure 2.1D;** primary CCF 0, metastatic CCF 0.12). SMARCA4 (or BRG1) is a catalytic subunit of the SWI/SNF chromatin remodeling complex, which undergoes somatic mutation in multiple cancers (108, 109). Although the functional consequence of this mutation is unknown, codon 1192 resides within the conserved C-terminal helicase domain and is recurrently mutated in the COSMIC database.

For Trio 2, pre- and post-treatment liver metastases were sequenced, in addition to a normal sample (no primary tumor sample was available in this case; see **Figure 2.3** for clinical timeline). Therapies included an HSP90 inhibitor, temozolamide plus sorafenib, as well as a MEK inhibitor. Interestingly, the pre-treatment tumor harbored only 4 unique missense mutations (1 clonal and 3 subclonal), while the post-treatment sample harbored 25 (1 clonal and 24 subclonal), suggestive of a treatment-induced induction in mutation rate (**Figure 2.1E; Table 2.5**). Phylogenetic analysis suggests that these samples also are siblings. Seven clonal missense mutations were present in both samples, including GNA11 Q209L, SF3B1 E622D, and IQGAP1 R893Q (**Figure 2.1E; Table 2.5**). IQGAP1 encodes Ras GTPase-activating-like protein, however, it does not harbor Ras-GAP activity and instead functions as a scaffold protein in several signaling pathways that contribute to tumorigenic phenotypes including invasion and metastasis (110). IQGAP1 is not significantly mutated in any cancer type (111), but rather is frequently over expressed (110). All somatic mutations and CCF values determined by ABSOLUTE are available in **Table 2.5**.

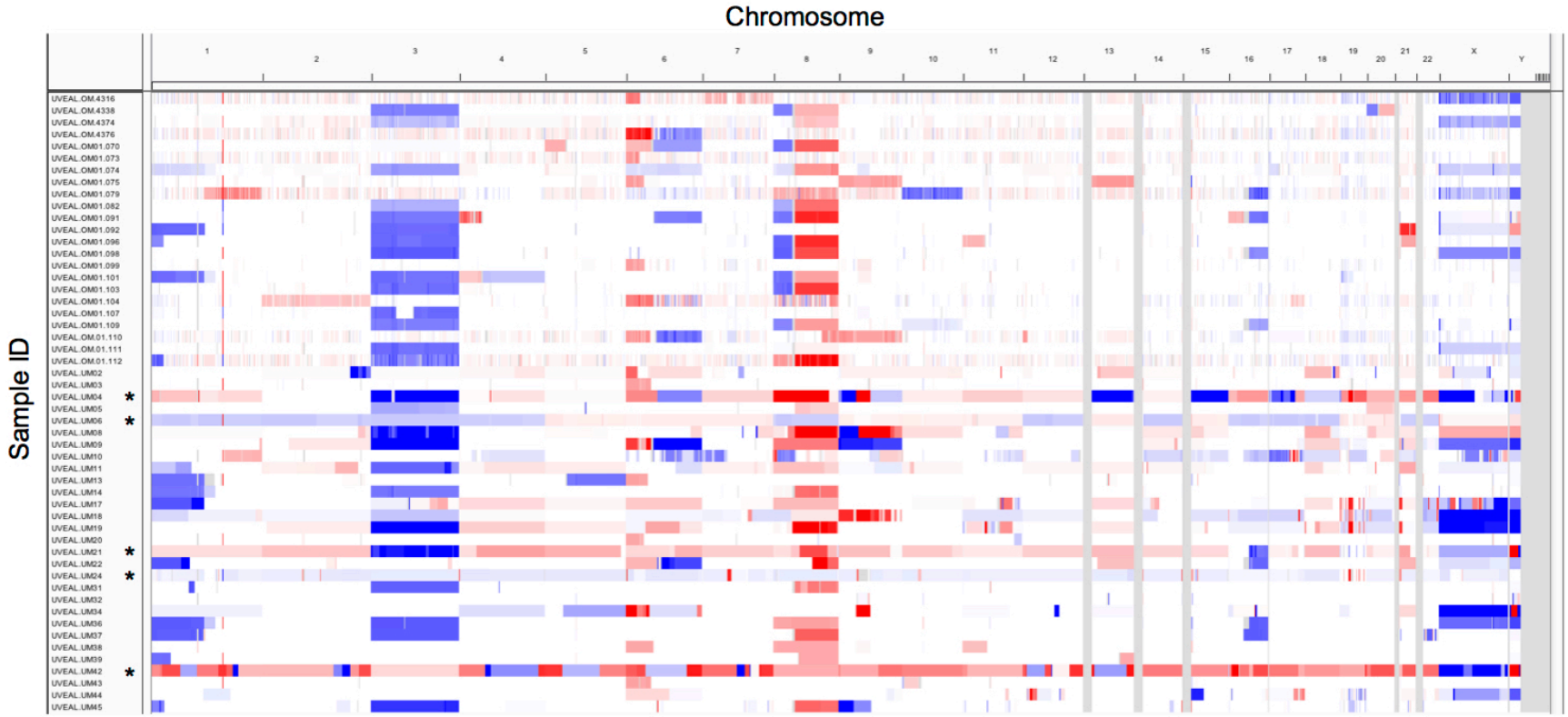

Figure 2.2. Copy number profiles of 52 uveal melanomas. Coverage values from whole exome sequencing were converted into segmentation files and visualized using IGV. *Indicates samples for which chromosome 3 status was indeterminate due to noise across the genome.

Table 2.4. Validation of selected mutations by targeted resequencing.

Patient ID	Hugo Symbol	Chr.	Start Position	End Position	Variant Classification	Ref. allele	Tumor Allele	Protein Change	Detected by Exome Sequencing	Independent Deep Sequencing
OM-4316	GNAQ	9	80409488	80409488	Missense	T	G	Q209P	yes	Validated
OM-4338	BAP1	3	52437159	52437162	Frame_Shift_Del	GTGA	-	S628fs	yes	Validated
OM-4338	GNA11	19	3118942	3118942	Missense	A	T	Q209L	yes	Validated
OM-4376	SF3B1	2	198267483	198267483	Missense	C	T	R625H	yes	Validated
OM-4376	GNA11	19	3118942	3118942	Missense	A	T	Q209L	yes	Validated
OM01-070	BAP1	3	52440916	52440916	Nonsense	C	T	W196*	yes	Validated
OM01-070	GNA11	19	3118942	3118942	Missense	A	T	Q209L	yes	Validated
OM01-073	GNA11	19	3118942	3118942	Missense	A	T	Q209L	yes	Validated
OM01-074	BAP1	3	52442068	52442068	Missense	T	C	H94R	yes	Validated
OM01-074	GNAQ	9	80409488	80409488	Missense	T	G	Q209P	yes	Validated
OM01-075	EIF1AX	X	20156729	20156729	Missense	T	C	K10E	yes	Validated
OM01-075	GNA11	19	3118942	3118942	Missense	A	T	Q209L	yes	Validated
OM01-082	GNA11	19	3118942	3118942	Missense	A	T	Q209L	yes	Validated
OM01-091	BAP1	3	52442043	52442043	Missense	G	C	N102K	yes	Validated
OM01-091	EIF1AX	X	20156720	20156720	Missense	G	A	R13C	yes	Validated
OM01-091	GNA11	19	3118942	3118942	Missense	A	T	Q209L	yes	Validated
OM01-092	BAP1	3	52438516	52438516	Frame_Shift_Del	A	-	Y401fs	yes	Assay Failed
OM01-092	GNAQ	9	80409488	80409488	Missense	T	A	Q209L	yes	Assay Failed
OM01-096	BAP1	3	52443599	52443601	In_Frame_Del	CTC	-	E31del	yes	Validated
OM01-096	GNA11	19	3118942	3118942	Missense	A	T	Q209L	yes	Validated
OM01-098	GNAQ	9	80409488	80409488	Missense	T	G	Q209P	yes	Validated
OM01-099	GNA11	19	3118942	3118942	Missense	A	T	Q209L	yes	Validated
OM01-101	BAP1	3	52440383	52440383	Nonsense	G	T	Y223*	yes	Validated
OM01-101	GNAQ	9	80409488	80409488	Missense	T	G	Q209P	yes	Validated
OM01-103	BAP1	3	52442539	52442540	Frame_Shift_Ins	-	T	T69fs	yes	Validated
OM01-103	GNAQ	9	80409488	80409488	Missense	T	A	Q209L	yes	Validated
OM01-107	BAP1	3	52439211	52439211	Frame_Shift_Del	T	-	N344fs	yes	Assay Failed
OM01-107	GNAQ	9	80409488	80409488	Missense	T	A	Q209L	yes	Assay Failed
OM01-109	GNA11	19	3118942	3118942	Missense	A	T	Q209L	yes	Validated
OM01-110	SF3B1	2	198267484	198267484	Missense	G	A	R625C	yes	Validated
OM01-110	GNAQ	9	80537256	80537256	Missense	C	G	G48R	yes	Validated
OM01-110	GNAQ	9	80537255	80537255	Missense	C	A	G48V	yes	Validated
OM01-111	GNA11	19	3118942	3118942	Missense	A	T	Q209L	yes	Validated
OM01-112	BAP1	3	52436645	52436655	Frame_Shift_Del	CAGATGA	-	E673fs	yes	Not Validated
OM01-112	GNAQ	9	80409488	80409488	Missense	T	A	Q209L	yes	Validated
UM02	GNAQ	9	80409488	80409488	Missense	T	G	Q209P	yes	Not Validated
UM03	EIF1AX	X	20156713	20156713	Missense	C	T	G15D	no	Discovered
UM03	GNAQ	9	80409488	80409488	Missense	T	G	Q209P	yes	Validated
UM04	EIF1AX	X	20156735	20156735	Missense	C	T	G8R	yes	Validated
UM04	GNAQ	9	80409488	80409488	Missense	T	G	Q209P	no	Discovered
UM05	GNA11	19	3118942	3118942	Missense	A	T	Q209L	yes	Validated
UM08	BAP1	3	52437296	52437296	Nonsense	G	T	S583*	yes	Validated
UM09	BAP1	3	52441261	52441261	Missense	A	G	F170S	yes	Validated
UM09	GNAQ	9	80409488	80409488	Missense	T	G	Q209P	no	Discovered
UM10	EIF1AX	X	20156742	20156754	Splice_Site	ATGGTTTAA	-	G6_splice	yes	Not Validated
UM10	GNAQ	9	80409488	80409488	Missense	T	G	Q209P	yes	Validated
UM11	BAP1	3	52438491	52438491	Nonsense	G	A	Q410*	yes	Validated
UM11	GNAQ	9	80409488	80409488	Missense	T	A	Q209L	no	Discovered
UM13	SF3B1	2	198267483	198267483	Missense	C	T	R625H	yes	Validated
UM13	GNA11	19	3118942	3118942	Missense	A	T	Q209L	yes	Validated
UM14	GNAQ	9	80412494	80412494	Missense	G	C	R183G	yes	Validated
UM17	SF3B1	2	198267483	198267483	Missense	C	T	R625H	no	Discovered
UM17	EIF1AX	X	20156713	20156713	Missense	C	T	G15D	yes	Validated
UM17	GNA11	19	3118942	3118942	Missense	A	T	Q209L	yes	Validated
UM18	GNAQ	9	80409488	80409488	Missense	T	G	Q209P	yes	Validated
UM19	GNA11	19	3118942	3118942	Missense	A	T	Q209L	yes	Validated
UM20	EIF1AX	X	20156740	20156740	Splice_Site	C	T	G6_splice	yes	Validated
UM20	GNAQ	9	80409488	80409488	Missense	T	A	Q209L	yes	Validated
UM21	BAP1	3	52441460	52441477	Splice_Site	ATATCCTT	-	S126_splice	yes	Not Validated
UM21	GNA11	19	3118942	3118942	Missense	A	T	Q209L	yes	Validated
UM22	SF3B1	2	198267372	198267372	Missense	T	C	H662R	yes	Validated
UM22	GNA11	19	3118942	3118942	Missense	A	T	Q209L	yes	Validated
UM31	GNA11	19	3118942	3118942	Missense	A	T	Q209L	yes	Validated
UM34	EIF1AX	X	20156740	20156740	Splice_Site	C	A	G6_splice	yes	Validated
UM34	GNAQ	9	80409488	80409488	Missense	T	A	Q209L	no	Discovered
UM36	SF3B1	2	198267360	198267360	Missense	T	G	K666T	yes	Validated
UM36	BAP1	3	52441217	52441217	Missense	C	G	G185R	yes	Validated
UM36	GNA11	19	3118942	3118942	Missense	A	T	Q209L	yes	Validated
UM37	GNA11	19	3118942	3118942	Missense	A	T	Q209L	yes	Validated
UM38	BAP1	3	52438464	52438498	Splice_Site	AGAGTTGG	-	R417_splice	yes	Not Validated
UM38	GNA11	19	3118942	3118942	Missense	A	T	Q209L	yes	Validated
UM39	SF3B1	2	198267483	198267483	Missense	C	T	R625H	yes	Validated
UM39	GNAQ	9	80409488	80409488	Missense	T	A	Q209L	yes	Validated
UM42	GNA11	19	3118942	3118942	Missense	A	T	Q209L	yes	Validated
UM43	EIF1AX	X	20156734	20156734	Missense	C	T	G8E	yes	Validated
UM43	GNAQ	9	80409488	80409488	Missense	T	A	Q209L	yes	Validated
UM44	EIF1AX	X	20156731	20156731	Missense	C	T	G9D	yes	Validated
UM44	GNAQ	9	80409488	80409488	Missense	T	A	Q209L	yes	Validated

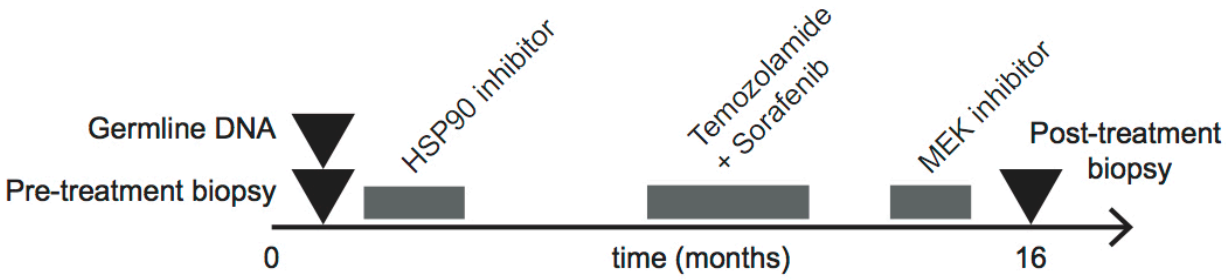

Figure 2.3. Trio 2 clinical timeline. Biopsy and treatment are indicated across time course.

Table 2.5. All somatic alterations identified in trio analysis.

								X-Axis (Primary/Pre-Treatment Metastatic)					Y-Axis (Metastatic/Post-Treatment Metastatic)				
Patient ID	Hugo Symbol	Chr.	Position	Variant Classification	Ref. Allele	Tumor Allele	Protein Change	Total num. of reads	Num. of alt. reads	Num. of ref. reads	CCF	Class	Total num. of reads	Num. of alt. reads	Num. of ref. reads	CCF	Class
Trio 2	ASIC5	4	156763488	Missense_Mutation	G	G	p.P294T	74	27	47	1	Clonal	51	16	35	0.96	Clonal
Trio 2	C9	5	39341760	Missense_Mutation	T	T	p.K76E	257	0	257	0	Not Detected	137	5	132	0.08	Subclonal
Trio 2	CABIN1	22	24481002	Missense_Mutation	T	T	p.V1054A	351	0	351	0	Not Detected	262	14	248	0.08	Subclonal
Trio 2	CHD6	20	40043833	Missense_Mutation	C	C	p.G2311V	259	0	259	0	Not Detected	178	3	175	0.08	Subclonal
Trio 2	COL22A1	8	139691889	Missense_Mutation	T	T	p.N1015H	339	0	339	0	Not Detected	262	20	242	0.37	Subclonal
Trio 2	COL9A1	6	70980045	Missense_Mutation	G	G	p.P390L	82	0	82	0	Not Detected	41	6	35	0.37	Subclonal
Trio 2	DBC1	9	121929586	Missense_Mutation	A	A	p.S688P	437	0	437	0	Not Detected	247	5	242	0.08	Subclonal
Trio 2	DNAH7	2	196771666	Missense_Mutation	G	G	p.S1391C	94	36	58	1	Clonal	67	0	67	0	Not Detected
Trio 2	DTNA	18	32400842	Missense_Mutation	G	G	p.D322N	53	0	53	0	Not Detected	25	10	15	0.37	Subclonal
Trio 2	EPYC	12	91366716	Missense_Mutation	C	C	p.V128M	49	14	35	1	Clonal	27	10	17	0.96	Clonal
Trio 2	ETFDH	4	159627912	Missense_Mutation	C	C	p.P534T	216	0	216	0	Not Detected	142	3	139	0.08	Subclonal
Trio 2	F2	11	46750378	Missense_Mutation	C	C	p.T488M	120	0	120	0	Not Detected	99	3	96	0.08	Subclonal
Trio 2	GLYAT	11	58491925	Missense_Mutation	C	C	p.E15D	285	91	194	1	Clonal	205	55	150	0.96	Clonal
Trio 2	GNA11	19	3118942	Missense_Mutation	A	A	p.Q209L	19	9	10	1	Clonal	10	7	3	0.96	Clonal
Trio 2	IQGAP1	15	91017819	Missense_Mutation	G	G	p.R893Q	148	49	99	1	Clonal	70	29	41	0.96	Clonal
Trio 2	KIAA0408	6	127775099	Missense_Mutation	T	T	p.T10A	226	0	226	0	Not Detected	143	4	139	0.08	Subclonal
Trio 2	KPNA1	3	122186267	Missense_Mutation	G	G	p.R47W	64	28	36	1	Clonal	32	12	20	0.96	Clonal
Trio 2	LATS2	13	21557371	Missense_Mutation	T	T	p.Y825C	142	0	142	0	Not Detected	81	7	74	0.08	Subclonal
Trio 2	LOC401010	2	132200496	Missense_Mutation	C	C	p.R502S	27	0	27	0	Not Detected	27	3	24	0.37	Subclonal
Trio 2	LOXL2	8	23217716	Missense_Mutation	A	A	p.S140P	61	0	61	0	Not Detected	49	3	46	0.08	Subclonal
Trio 2	LRP1B	2	141946087	Missense_Mutation	G	G	p.R306W	89	0	89	0	Not Detected	56	16	40	0.72	Clonal
Trio 2	MACC1	7	20198840	Missense_Mutation	G	G	p.P382S	110	5	105	0.1	Subclonal	72	0	72	0	Not Detected
Trio 2	MCM6	2	136605755	Nonsense_Mutation	G	G	p.Q641*	89	0	89	0	Not Detected	60	7	53	0.37	Subclonal
Trio 2	NOTCH4	6	32178560	Missense_Mutation	C	C	p.C945F	152	3	149	0.1	Subclonal	147	0	147	0	Not Detected
Trio 2	NUP153	6	17637398	Missense_Mutation	A	A	p.M817T	149	0	149	0	Not Detected	97	11	86	0.37	Subclonal
Trio 2	OR8A1	11	124440614	Missense_Mutation	T	T	p.F217S	249	0	249	0	Not Detected	160	9	151	0.08	Subclonal
Trio 2	PCDHAC2	5	140248908	Missense_Mutation	C	C	p.L74I	130	0	130	0	Not Detected	80	3	77	0.08	Subclonal
Trio 2	PCMT1	6	150092352	Missense_Mutation	G	G	p.R95H	55	0	55	0	Not Detected	32	8	24	0.37	Subclonal
Trio 2	PHF3	6	64423233	Missense_Mutation	A	A	p.K1917E	91	0	91	0	Not Detected	74	5	69	0.08	Subclonal
Trio 2	PTK2	8	141669602	Missense_Mutation	G	G	p.A1041V	106	0	106	0	Not Detected	106	12	94	0.37	Subclonal
Trio 2	RHPN2	19	33535242	Missense_Mutation	C	C	p.R33Q	23	0	23	0	Not Detected	11	4	7	0.37	Subclonal
Trio 2	RSF1	11	77409725	Missense_Mutation	C	C	p.G841V	133	3	130	0.1	Subclonal	78	0	78	0	Not Detected
Trio 2	SF3B1	2	198267491	Missense_Mutation	C	C	p.E622D	98	32	66	1	Clonal	83	34	49	0.96	Clonal
Trio 2	TAF13	1	109608831	Missense_Mutation	C	C	p.G44W	113	0	113	0	Not Detected	65	3	62	0.08	Subclonal
Trio 2	TAS2R19	12	11175070	Missense_Mutation	T	T	p.D34G	143	0	143	0	Not Detected	114	4	110	0.08	Subclonal
Trio 2	ZNF323	6	28295250	Missense_Mutation	C	C	p.V148L	236	0	236	0	Not Detected	163	5	158	0.08	Subclonal
UM 45	DAG1	3	49568814	Frame_Shift_Del	CTGTGGT	-	SYPVVGWH2	24	14	10	0.68	Subclonal	44	7	37	0.38	Subclonal
UM 45	FAM86DP	3	75475709	Missense_Mutation	T	C	p.I177V	53	3	50	0.08	Subclonal	63	0	63	0	Not Detected
UM 45	GOLGB1	3	121416107	Missense_Mutation	T	A	p.K1088M	22	15	7	0.9	Clonal	97	0	97	0	Not Detected
UM 45	AFAP1	4	7774605	Missense_Mutation	G	A	p.A732V	65	22	43	0.9	Clonal	62	0	62	0	Not Detected
UM 45	MAN2A1	5	109155558	Missense_Mutation	A	C	p.L766F	66	30	36	1	Clonal	180	45	135	0.89	Clonal
UM 45	CXXC5	5	139060428	Missense_Mutation	C	T	p.A107V	252	0	252	0	Not Detected	187	5	182	0.12	Subclonal
UM 45	HNRNPA2B1	7	26240196	Missense_Mutation	A	G	p.M1T	228	0	228	0	Not Detected	210	24	186	0.38	Subclonal
UM 45	MGAM	7	141799428	Missense_Mutation	G	T	p.A1693S	83	0	83	0	Not Detected	104	4	100	0.12	Subclonal
UM 45	TMEM2	9	74365231	Missense_Mutation	T	C	p.N20S	76	0	76	0	Not Detected	66	4	62	0.12	Subclonal
UM 45	UNC5B	10	73050857	Missense_Mutation	G	A	p.A429T	415	0	415	0	Not Detected	310	5	305	0.12	Subclonal
UM 45	FAT3	11	92086051	Missense_Mutation	G	A	p.R258H	78	0	78	0	Not Detected	201	4	197	0.12	Subclonal
UM 45	UHRF1BP1L	12	100452122	Missense_Mutation	T	C	p.D978G	21	5	16	1	Clonal	73	24	49	0.89	Clonal
UM 45	HCFC2	12	104496981	Missense_Mutation	A	G	p.E770G	22	7	15	1	Clonal	112	34	78	0.89	Clonal
UM 45	TUBA3C	13	19751479	Missense_Mutation	C	T	p.R215H	304	0	304	0	Not Detected	217	9	208	0.12	Subclonal
UM 45	CYSLTR2	13	49281339	Missense_Mutation	T	A	p.L129Q	106	47	59	1	Clonal	139	32	107	0.89	Clonal
UM 45	PSME2	14	24613443	Missense_Mutation	G	A	p.A152V	289	0	289	0	Not Detected	221	4	217	0.12	Subclonal
UM 45	DUOX2	15	45387733	Missense_Mutation	C	T	p.V1381M	123	51	72	0.9	Clonal	58	0	58	0	Not Detected
UM 45	FBN1	15	48704920	Missense_Mutation	C	T	p.G2691D	138	0	138	0	Not Detected	136	4	132	0.12	Subclonal
UM 45	SDK2	17	71418438	Missense_Mutation	T	G	p.K678T	87	10	77	0.08	Subclonal	37	0	37	0	Not Detected
UM 45	SMARCA4	19	11143994	Missense_Mutation	G	A	p.R1192H	132	0	132	0	Not Detected	99	8	91	0.12	Subclonal
UM 45	PEPD	19	34003620	Missense_Mutation	C	T	p.R27Q	62	0	62	0	Not Detected	60	3	57	0.12	Subclonal
UM 45	BTBD3	20	11903707	Missense_Mutation	G	A	p.R321H	170	4	166	0.08	Subclonal	143	0	143	0	Not Detected
UM 45	FRG1B	20	29628236	Missense_Mutation	G	C	p.A50P	64	0	64	0	Not Detected	195	5	190	0.12	Subclonal
UM 45	RLF	1	40705305	Nonsense_Mutation	C	G	p.S1644*	39	17	22	0.9	Clonal	79	0	79	0	Not Detected

Mutant and wild type EIF1AX play essential roles in uveal melanoma cells

Consistent with prior studies (60), we observed recurrent mutations within the N-terminal 15 amino acids of the x-linked translation initiation factor, EIF1AX (**Figure 2.4A**). This clustering pattern stands in contrast to pan-cancer analyses in which synonymous and non-synonymous mutations were observed throughout the *EIF1AX* coding region (111). We also identified a homozygous G→A mutation at the start of exon 2 in a single established UM cell line (92.1) out of 7 tested lines (**Figure 2.5**). Transcriptome analysis (RNAseq) of this cell line demonstrated faithful transcription of the G6D missense mutation, without evidence for altered mRNA splicing (**Figure 2.6A**). All mutations in our UM cohort were non-synonymous and situated within the unstructured EIF1AX N-terminal tail (NTT) (112), raising the possibility of a gain of function event.

EIF1AX encodes an essential component of translation initiation (113). Binding of EIF1AX to the small ribosomal subunit aids in assembly of the pre-initiation complex (PIC) as well as mRNA scanning (114-116). More specifically, the EIF1AX-NTT stimulates PIC formation, interacts with eIF2 and eIF3, and regulates start codon recognition (117-119). Therefore, somatic mutations in the *EIF1AX*-NTT may result in changes in translational regulation—either global or mRNA-specific effects.

In an attempt to gain preliminary insights into the function of mutant EIF1AX in UM cells, we used lentiviral shRNA knockdown to suppress EIF1AX expression in a panel of UM cell lines, including the 92.1 line (*EIF1AX* G6D mutant). Expression of *EIF1AX* shRNAs both decreased *EIF1AX* gene expression and impaired UM cell viability (**Figure 2.4B and C**)**.** Notably, both *EIF1AX*-mutant and *EIF1AX*-wildtype UM cell lines exhibited suppressed viability following knockdown, suggesting that EIF1AX may be uniformly essential in UM cells.

We next sought to determine if *EIF1AX* might represent a pan-essential gene across multiple contexts. To assess this, we leveraged Project Achilles data set 2.4.3 (www.broadinstitute.org/achilles) that scores the effect of gene knockdown on cell proliferation

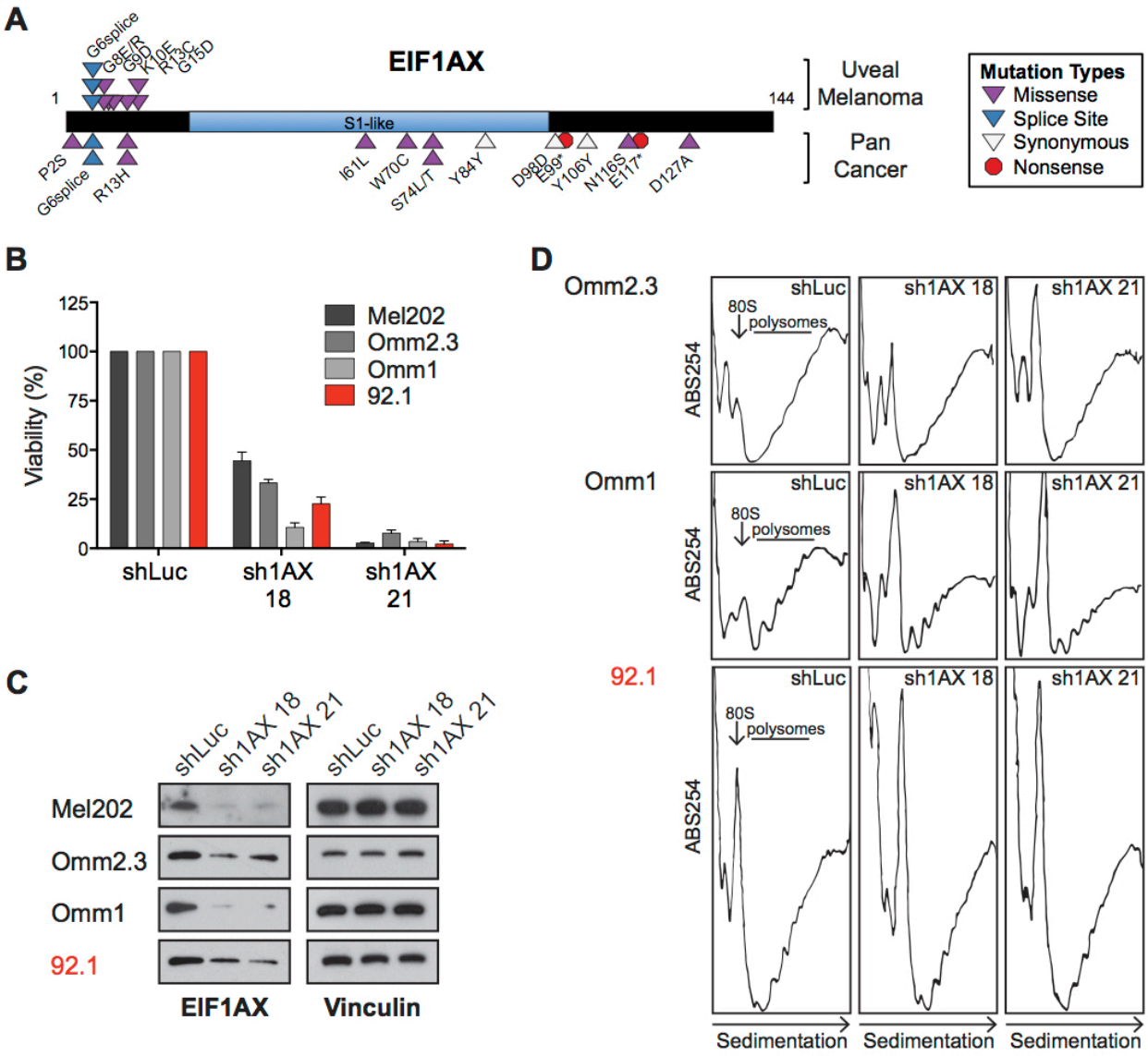

Figure 2.4. EIF1AX-regulated growth and translation in uveal melanoma. (A) Top, distribution of EIF1AX mutations observed in cohort of 52 uveal melanomas in comparison to other cancer types (as reported by www.tumorportal.org). **(B)** Uveal melanoma cells were infected with EIF1AX or control shRNAs and cell viability was determined after 6 days using MTS. Percent growth is relative to shLuc-expressing cells. Error bars represent SD of mean from 3 independent experiments. **(C)** Immunoblot analysis of EIF1AX protein levels in shRNA-expressing cells. **(D)** Polysome profiles of UM cell lines expressing shRNAs against EIF1AX and Luciferase.

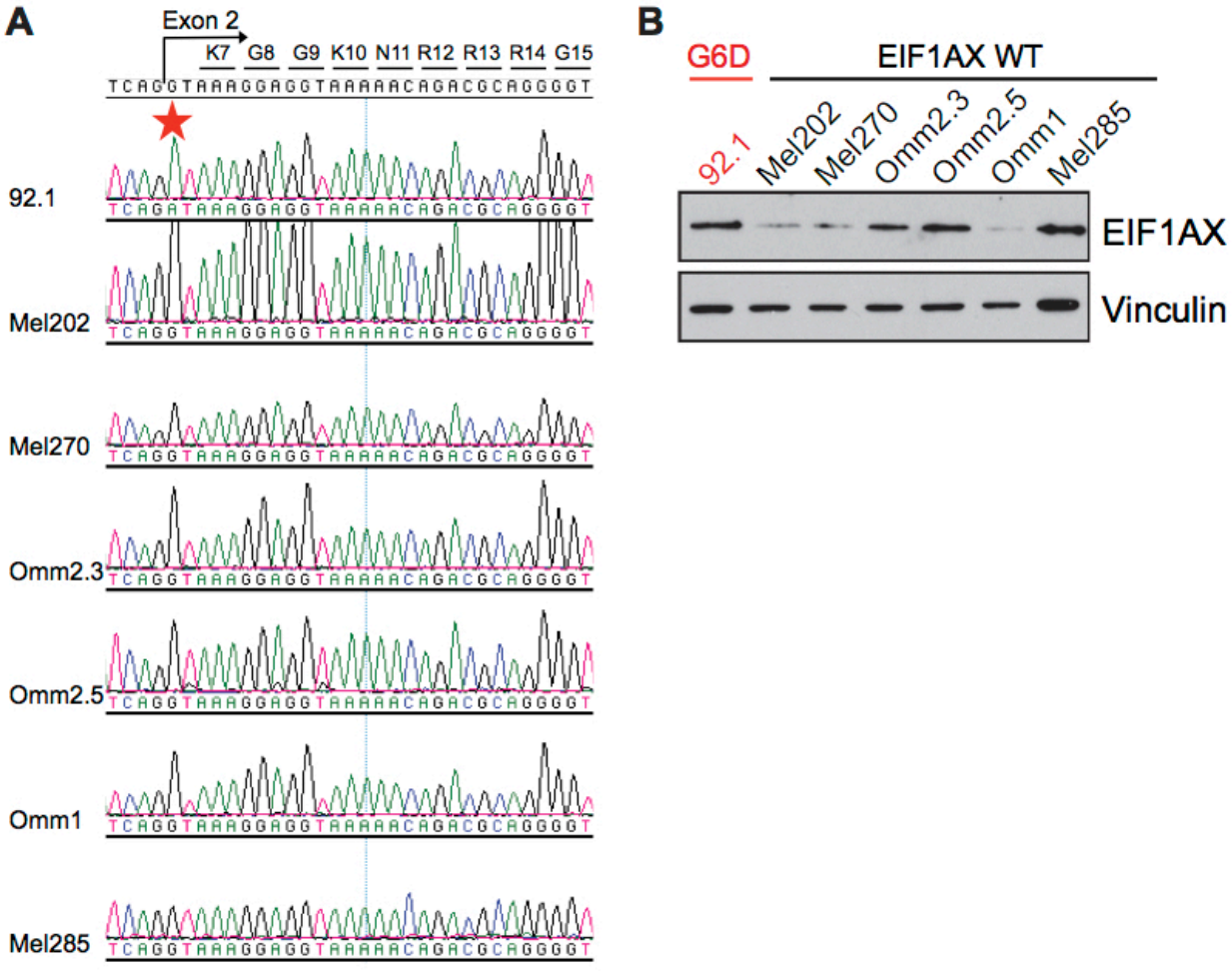

Figure 2.5. EIF1AX sequence and protein expression across UM cell lines. (A) Exon 2 sequencing trace displays putative EIF1AX G6D mutation in 92.1 cell line. **(B)** Immunoblot analysis of EIF1AX protein levels.

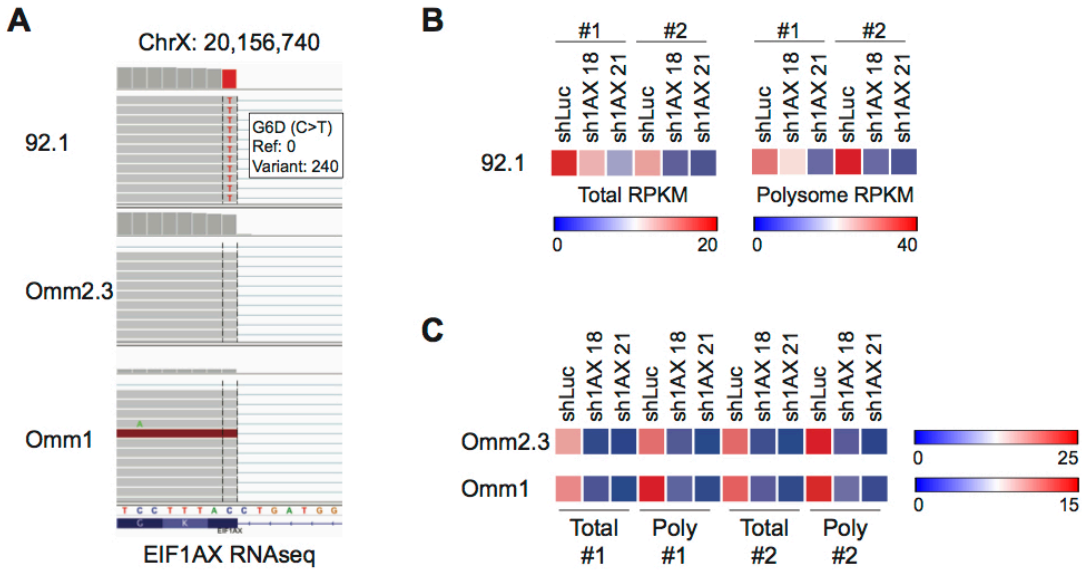

Figure 2.6. *EIF1AX* sequence and expression levels from polysome profiling RNAseq. **(A)** IGV screenshot of *EIF1AX* exon 2 start indicates exclusive mRNA expression of the G6D variant in the 92.1 cell line. **(B)** Heatmap displays *EIF1AX* expression levels in RPKM for total and polysome-associated mRNA in 92.1 cells expressing indicated shRNAs. **(C)** As in (B), but for Omm2.3 and Omm1 *EIF1AX*-wildtype cells.

using pooled shRNA screening across 216 cell lines of various lineages, but not including UM (120). Cells are infected with a pool of shRNAs and the relative levels of shRNA present at 16 population doublings is compared to the initial plasmid pool (120). Of the shRNAs targeting *EIF1AX*, 2 out of 5 were strongly depleted across all 216 cell lines (**Figure 2.7A**, top). Although off-target effects cannot be entirely ruled out, these 2 shRNAs were most potent at suppressing EIF1AX protein levels (**Figure 2.7B**). The magnitude of shRNA depletion was similar to the known essential gene, ribosomal protein S6 (RPS6) (**Figure 2.7A**, bottom). Taken together, these data suggest that *EIF1AX* may represent a pan-essential gene. Therefore, *EIF1AX*-NTT mutations in UM likely do not confer a simple loss of function phenotype.

Mutant EIF1AX regulated translation

We next sought to test the hypothesis that EIF1AX-NTT mutations might regulate translation of a distinct set of transcripts compared to wild type EIF1AX. To investigate this possibility, we performed polysome profiling of mutant and wild type UM cell lines expressing shRNAs targeting *EIF1AX* or Luciferase (shLuc; control). Interestingly, the 80S peak in our *EIF1AX* mutant cell line (92.1) showed a greater amplitude than that seen in *EIF1AX* wild type cells (Omm2.3 and Omm1), raising the possibility that mutant EIF1AX might be associated with altered protein translation. RNAi-mediated suppression of EIF1AX expression also augmented the 80S peak in all contexts tested, suggestive of reduced polysome formation and impaired translation initiation (**Figure 2.4D**).

EIF1AX-regulated translation was further probed by massively parallel sequencing of mRNAs from polysome fractions. Sequencing of polysome-associated transcripts provides a means to identify those mRNAs that undergo active translation in the cells (121, 122). We defined the “translational efficiency” of each expressed transcript (RPKM≥1 in input lysate) by normalizing polysome-associated mRNA levels to total mRNA levels from input lysate (123). To identify transcripts regulated by EIF1AX, the difference in translational efficiency between

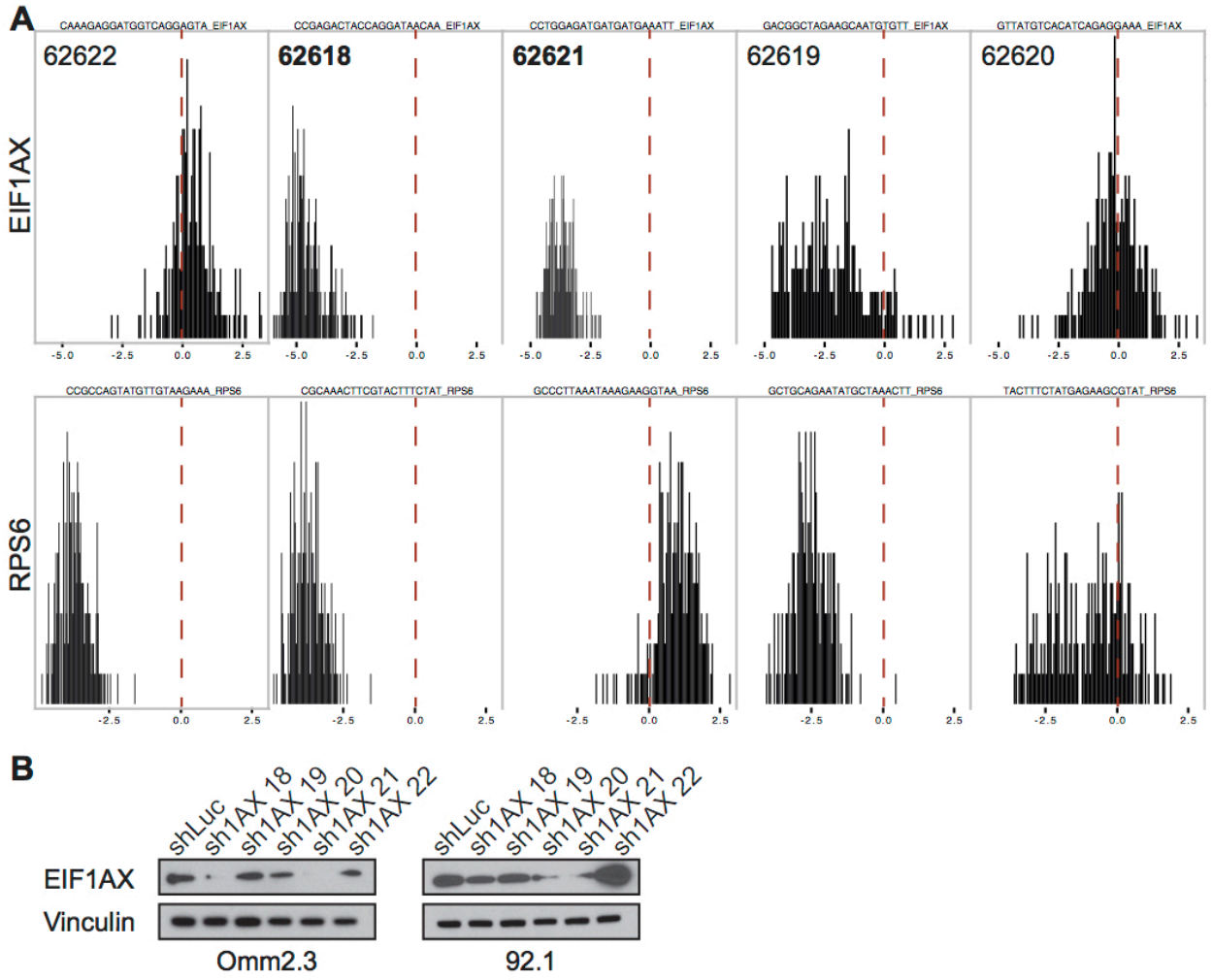

Figure 2.7. EIF1AX-dependency across 216 cell lines from Project Achilles. (A) Histograms represent shRNA level scores (normalized log fold change) for 5 EIF1AX (top) and 5 RPS6 (bottom) shRNAs from 216 cell lines in Achilles v2.4.3. Lower values represent more depletion indicating more dependency. EIF1AX shRNAs used in this study are bolded. **(B)** Immunoblot analysis of EIF1AX protein levels in 2 uveal melanoma cell lines expressing indicated shRNAs.

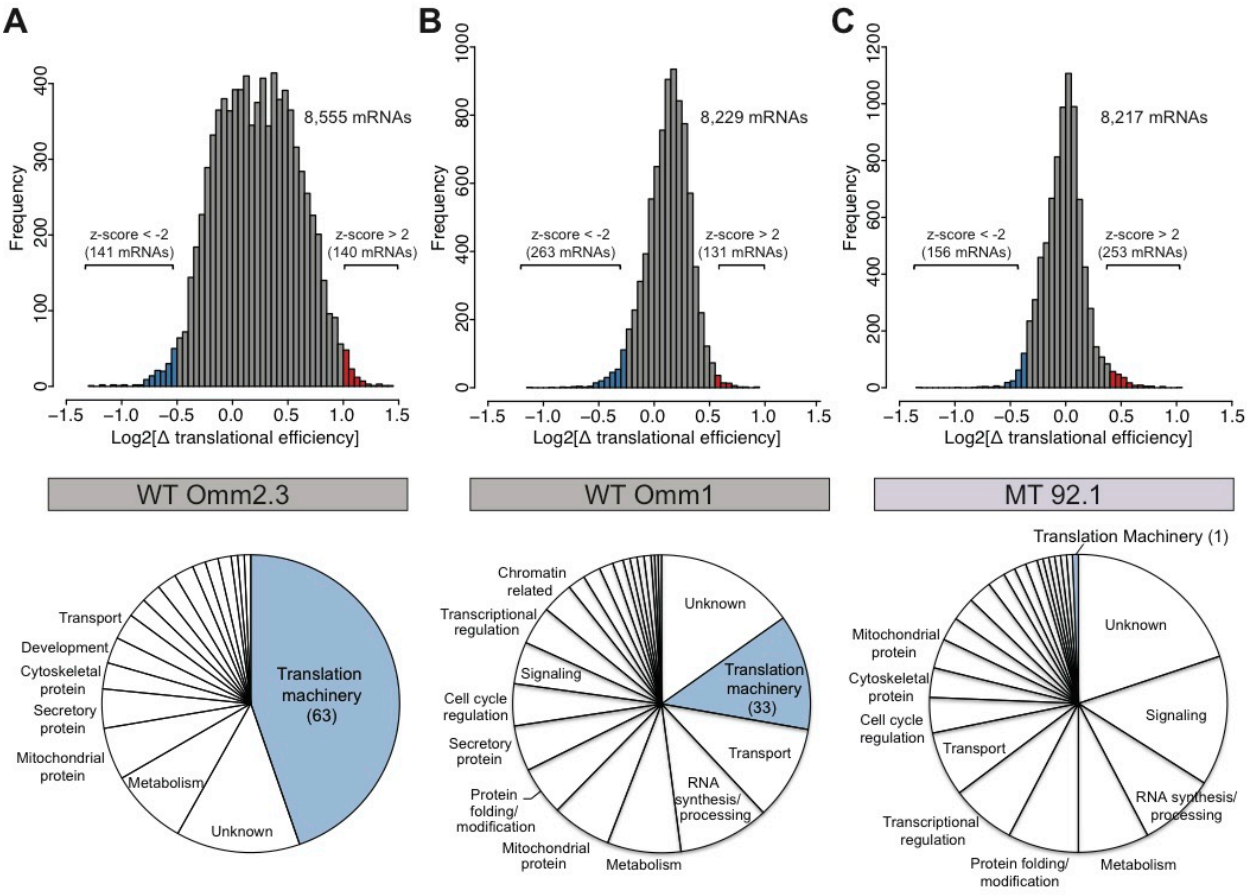

Figure 2.8. Decreased EIF1AX expression impairs translation of protein synthesis machinery in wildtype, but not mutated setting. Histogram at top represents changes in translational efficiency following EIF1AX knockdown in Omm2.3 **(A)**, Omm1 **(B)**, and 92.1 **(C)** cells**.** Translational efficiency was calculated by dividing polysome RPKM by total RPKM from input lysate. Cells expressing EIF1AX shRNAs were compared to shLuc-expressing cells. Genes with *z* score < −2 were nominated as sensitive to EIF1AX knockdown. Data represent mean of two biological replicates per shRNA and 2 unique EIF1AX shRNAs. 3 cell lines are presented, as labeled in center. Pie chart below represents functional classification of genes with *z* score < −2.

control (shLuc) and sh1AX expressing cells was determined; a *z*-score threshold of 2 was then used to nominate candidate EIF1AX-regulated transcripts (**Figure 2.8A-C**, top). These studies identified transcripts with altered translational efficiency following EIF1AX knockdown. The magnitude of log2 fold change between control and knockdown cells ranged from −1.34 to 1.05 in mutant cells (92.1), −1.27 to 1.4 and −1.14 to 0.95 in wild type cells (Omm2.3 and Omm1, respectively).

Next, we examined the predicted functional classes of putative EIF1AX-regulated transcripts. We found that a large fraction of mRNAs that showed significantly reduced translational efficiency following knockdown of wild type EIF1AX (*z*-score < −2) encode factors known to govern protein synthesis, such as ribosomal proteins and translation initiation factors (**Figure 2.8A and B**, bottom; **Table 2.6 and 2.7**). In the Omm2.3 and Omm1 (EIF1AX wild type) cell lines, 59 and 22 ribosomal proteins were suppressed, respectively, of 82 total ribosomal proteins detected by our RNA sequencing approach ($p<0.0001$). This indicates that knockdown of wild type EIF1AX expression results in significantly suppressed translation of ribosomal proteins. Ribosomal protein translation is regulated in a coordinated manner by a 5' terminal oligopyrimidine tract (5' TOP) within the mRNA sequence (124). These data demonstrate that a significant portion of EIF1AX-sensitive transcripts encode 5'TOP recognition proteins.

RNAi knockdown of EIF1AX in the 92.1 cell line (*EIF1AX* G6D mutant) resulted in significant reduction in the translational efficiency of 156 genes (*z*-score < −2) (**Figure 2.8C; Table 2.8**). Of these genes, only one encoded a member of the translation machinery (mitochondrial ribosomal protein L1). This result is in stark contrast to the phenotype observed in wild type cells and raises the possibility that wild type and mutant EIF1AX exert a differential impact on protein translation in UM cells.

Table 2.6. Genes with a z-score < −2 in Omm2.3 cell line. Gene name, functional class, and log fold change in translational efficiency between control and EIF1AX knockdown is indicated.

	Hugo Symbol	Name	Functional Class	Change in TE
1	GFER	growth factor, augmenter of liver regeneration	mitochondrial protein	-1.266
2	C20orf24	chromosome 20 open reading frame 24	Apoptosis	-1.197
3	TMEM160	transmembrane protein 160	unknown	-1.182
4	C4orf48	chromosome 4 open reading frame 48	secretory protein	-1.066
5	DBNDD2	dysbindin (dystrobrevin binding protein 1) domain containing 2	unknown	-1.062
6	PGP	phosphoglycolate phosphatase	metabolism	-1.011
7	C9orf116	chromosome 9 open reading frame 116	unknown	-0.970
8	C19orf24	chromosome 19 open reading frame 24	unknown	-0.961
9	C19orf81	chromosome 19 open reading frame 81	unknown	-0.883
10	RPL39	ribosomal protein L39	Translation machinery	-0.853
11	RPLP2	ribosomal protein, large, P2	Translation machinery	-0.817
12	TMEM238	transmembrane protein 238	unknown	-0.808
13	RPL30	ribosomal protein L30	Translation machinery	-0.797
14	ZNF90	zinc finger protein 90	unknown	-0.788
15	RPL36	ribosomal protein L36	Translation machinery	-0.768
16	RPL34	ribosomal protein L34	Translation machinery	-0.763
17	RPS15A	ribosomal protein S15a	Translation machinery	-0.760
18	RPS28	ribosomal protein S28	Translation machinery	-0.759
19	RPS19	ribosomal protein S19	Translation machinery	-0.753
20	RPL28	ribosomal protein L28	Translation machinery	-0.753
21	RPS17L	ribosomal protein S17-like	Translation machinery	-0.750
22	PDF	peptide deformylase (mitochondrial); component of oligomeric golgi complex 8	mitochondrial protein	-0.746
23	RPL27A	ribosomal protein L27a	Translation machinery	-0.739
24	SAC3D1	SAC3 domain containing 1	Cell cycle regulation	-0.734
25	RPL37A	ribosomal protein L37a	Translation machinery	-0.728
26	MYEOV2	myeloma overexpressed 2	unknown	-0.722
27	RPS16	ribosomal protein S16	Translation machinery	-0.719
28	RPS13	ribosomal protein S13	Translation machinery	-0.717
29	RPS27	ribosomal protein S27	Translation machinery	-0.717
30	CLEC11A	C-type lectin domain family 11, member A	secretory protein	-0.716
31	RPL38	ribosomal protein L38	Translation machinery	-0.709
32	SCGB1D2	secretoglobin, family 1D, member 2	secretory protein	-0.704
33	RPS17	ribosomal protein S17	Translation machinery	-0.704
34	RPL35	ribosomal protein L35	Translation machinery	-0.704
35	RPS21	ribosomal protein S21	Translation machinery	-0.702
36	RPL21	ribosomal protein L2	Translation machinery	-0.699
37	RPL35A	ribosomal protein L35a	Translation machinery	-0.697
38	RPL26	ribosomal protein L26	Translation machinery	-0.696
39	RGS10	regulator of G-protein signaling 10	signaling	-0.695
40	RPL29	ribosomal protein L29	Translation machinery	-0.692
41	ANKRD9	ankyrin repeat domain 9	unknown	-0.687
42	HES4	hairy and enhancer of split 4 (Drosophila)	development	-0.686
43	PDXP	pyridoxal (pyridoxine, vitamin B6) phosphatase	metabolism	-0.684
44	RPS14	ribosomal protein S14	Translation machinery	-0.682
45	RPS25	ribosomal protein S25	Translation machinery	-0.681
46	RPS29	ribosomal protein S29	Translation machinery	-0.679
47	RPL18A	ribosomal protein L18a	Translation machinery	-0.671
48	RPS18	ribosomal protein S18	Translation machinery	-0.670
49	RPS23	ribosomal protein S23	Translation machinery	-0.667
50	RPL32	ribosomal protein L32	Translation machinery	-0.663
51	RPS15	ribosomal protein S15	Translation machinery	-0.662
52	FAM173A	family with sequence similarity 173, member A	unknown	-0.655
53	HIST3H2A	histone cluster 3, H2a	chromatin related	-0.655
54	HOXD3	homeobox D3	development	-0.655
55	RPL37	ribosomal protein L37	Translation machinery	-0.654
56	UBA52	ubiquitin A-52 residue ribosomal protein fusion product 1	Translation machinery	-0.651
57	GET4	chromosome 7 open reading frame 20	Transport	-0.649
58	RPL23	ribosomal protein L23	Translation machinery	-0.644
59	APOC1	apolipoprotein C-I	secretory protein	-0.642
60	LSMD1	LSM domain containing 1	protein modification	-0.638
61	ATP5D	ATP synthase, H+ transporting, mitochondrial F1 complex, delta subunit	metabolism	-0.636
62	RPL12	ribosomal protein L12	Translation machinery	-0.635
63	RPS8	ribosomal protein S8	Translation machinery	-0.633
64	MAL	mal, T-cell differentiation protein	immunity	-0.627
65	C16orf74	chromosome 16 open reading frame 74	unknown	-0.627
66	MZT2B	mitotic spindle organizing protein 2B	cytoskeletal protein	-0.626
67	RPS27A	ribosomal protein S27a	Translation machinery	-0.624
68	RPL22L1	ribosomal protein L22-like 1	Translation machinery	-0.620
69	RPL13	ribosomal protein L13	Translation machinery	-0.620
70	RPL10A	ribosomal protein L10a	Translation machinery	-0.615

Table 2.6 (Continued).

71	MESP1	mesoderm posterior 1 homolog (mouse)	development	-0.611
72	RPS11	ribosomal protein S11	Translation machinery	-0.611
73	RPS9	ribosomal protein S9	Translation machinery	-0.610
74	RHOF	ras homolog gene family, member F (in filopodia)	signaling	-0.606
75	MZT2A	mitotic spindle organizing protein 2A	cytoskeletal protein	-0.603
76	RPS10	ribosomal protein S10	Translation machinery	-0.602
77	ZNF580	zinc finger protein 580	Cell cycle regulation	-0.599
78	TRAPPC5	trafficking protein particle complex 5	Transport	-0.599
79	RPL18	ribosomal protein L18	Translation machinery	-0.595
80	RPL31	ribosomal protein L31	Translation machinery	-0.595
81	RPL11	ribosomal protein L11	Translation machinery	-0.592
82	RPL27	ribosomal protein L27	Translation machinery	-0.591
83	RPL13A	ribosomal protein L13a	Translation machinery	-0.590
84	METRN	meteorin, glial cell differentiation regulator	secretory protein	-0.588
85	RPS5	ribosomal protein S5	Translation machinery	-0.586
86	CST3	cystatin C	secretory protein	-0.585
87	PPDPF	pancreatic progenitor cell differentiation and proliferation factor homolog (zebrafish)	unknown	-0.584
88	CTU1	ATP binding domain 3	RNA synthesis/process	-0.584
89	PCBD2	pterin-4 alpha-carbinolamine dehydratase/dimerization cofactor of hepatocyte nuclear factor 1 alpha (TCF1) 2	metabolism	-0.581
90	MAP1LC3A	microtubule-associated protein 1 light chain 3 alpha	cytoskeletal protein	-0.577
91	C11orf73	chromosome 11 open reading frame 73	Transport	-0.575
92	CHURC1	churchill domain containing 1	development	-0.575
93	FTH1	ferritin, heavy polypeptide 1	iron storage	-0.574
94	PRELID1	PRELI domain containing 1; similar to Px19-like protein	mitochondrial protein	-0.573
95	COMMD6	COMM domain containing 6	signaling	-0.573
96	RPL14	ribosomal protein L14	Translation machinery	-0.572
97	HINT1	histidine triad nucleotide binding protein 1	Transcriptional regulati	-0.569
98	CHCHD10	coiled-coil-helix-coiled-coil-helix domain containing 10	mitochondrial protein	-0.566
99	HIGD2A	HIG1 hypoxia inducible domain family, member 2A	metabolism	-0.565
100	RPS7	ribosomal protein S7	Translation machinery	-0.562
101	ENDOG	endonuclease G	mitochondrial protein	-0.561
102	ZNF688	zinc finger protein 688; zinc finger protein 785	unknown	-0.561
103	RPL10	ribosomal protein L10	Translation machinery	-0.560
104	TLCD1	TLC domain containing 1	Transport	-0.558
105	POLR2I	polymerase (RNA) II (DNA directed) polypeptide I, 14.5kDa	RNA synthesis/process	-0.558
106	DNLZ	DNL-type zinc finger	mitochondrial protein	-0.552
107	MRPL23	mitochondrial ribosomal protein L23	Translation machinery	-0.548
108	PHLDA2	pleckstrin homology-like domain, family A, member 2	unknown	-0.546
109	RPS3	ribosomal protein S3 pseudogene 3; ribosomal protein S3	Translation machinery	-0.546
110	TXNDC17	thioredoxin domain containing 17	oxidation/reduction	-0.544
111	SEPW1	selenoprotein W, 1	oxidation/reduction	-0.544
112	GADD45GIP1	growth arrest and DNA-damage-inducible, gamma interacting protein 1	Cell cycle regulation	-0.542
113	ZNF524	zinc finger protein 524	unknown	-0.541
114	C15orf61	chromosome 15 open reading frame 61	unknown	-0.541
115	ATP5G2	ATP synthase, H+ transporting, mitochondrial F0 complex, subunit C2 (subunit 9)	metabolism	-0.540
116	NDUFB1	NADH dehydrogenase (ubiquinone) 1 beta subcomplex, 1, 7kDa	metabolism	-0.540
117	TOMM7	translocase of outer mitochondrial membrane 7 homolog (yeast)	mitochondrial protein	-0.539
118	RPS24	ribosomal protein S24	Translation machinery	-0.539
119	RPL17	ribosomal protein L17	Translation machinery	-0.539
120	RPL24	ribosomal protein L24	Translation machinery	-0.537
121	HIST1H4K	histone cluster 1, H4	chromatin related	-0.537
122	RPS12	ribosomal protein S12	Translation machinery	-0.535
123	SLC2A4RG	SLC2A4 regulator	Transcriptional regulati	-0.533
124	C1orf86	chromosome 1 open reading frame 86	protein modification	-0.533
125	RPL22	ribosomal protein L22	Translation machinery	-0.532
126	RPS3A	ribosomal protein S3A	Translation machinery	-0.530
127	RPL23A	ribosomal protein L23a	Translation machinery	-0.529
128	POLR1D	polymerase (RNA) I polypeptide D, 16kDa	RNA synthesis/process	-0.529
129	COX7C	cytochrome c oxidase subunit VIIc	metabolism	-0.529
130	PGLS	6-phosphogluconolactonase	metabolism	-0.528
131	ATP5I	ATP synthase, H+ transporting, mitochondrial F0 complex, subunit E	metabolism	-0.526
132	ATP5E	ATP synthase, H+ transporting, mitochondrial F1 complex, epsilon subunit	metabolism	-0.525
133	LYRM4	LYR motif containing 4	Translation machinery	-0.525
134	ATP5L	ATP synthase, H+ transporting, mitochondrial F0 complex, subunit G	metabolism	-0.523
135	C12orf57	chromosome 12 open reading frame 57	unknown	-0.520
136	C9orf16	chromosome 9 open reading frame 16	unknown	-0.520
137	RBX1	ring-box 1	protein modification	-0.519
138	FAM195A	chromosome 16 open reading frame 14	unknown	-0.518
139	MRPL33	mitochondrial ribosomal protein L33	Translation machinery	-0.517
140	BRK1	BRICK1, SCAR/WAVE actin-nucleating complex subunit	cytoskeletal protein	-0.516
141	CHCHD5	coiled-coil-helix-coiled-coil-helix domain containing 5	mitochondrial protein	-0.516

Table 2.7. Genes with a z-score < −2 in Omm1 cell line. Gene name, functional class, and log fold change in translational efficiency (TE) between control and EIF1AX knockdown cells is indicated.

	Hugo Symbol	Name	Functional Class	Change in TE
1	C20orf24	chromosome 20 open reading frame 24	Apoptosis	-1.140
2	ZC3HAV1L	zinc finger CCCH-type, antiviral 1-like	unknown	-0.915
3	SMAGP	small trans-membrane and glycosylated protein	Cell-cell interaction	-0.845
4	PDF	peptide deformylase (mitochondrial); component of oligomeric golgi complex 8	Mitochondrial protein	-0.840
5	BBIP1	BBSome-interacting protein 1	Transport	-0.754
6	C4orf48	chromosome 4 open reading frame 48	Secretory protein	-0.747
7	TMEM160	transmembrane protein 160	unknown	-0.739
8	NRGN	neurogranin (protein kinase C substrate, RC3)	Signaling	-0.707
9	C19orf24	chromosome 19 open reading frame 24	Secretory protein	-0.696
10	GET4	chromosome 7 open reading frame 20	Transport	-0.681
11	SNRPF	small nuclear ribonucleoprotein polypeptide F	RNA synthesis and processing	-0.659
12	RPL36AL	ribosomal protein L36a-like	Translation machinery	-0.652
13	PRELID1	PRELI domain containing 1; similar to Px19-like protein	Mitochondrial protein	-0.629
14	MGP	matrix Gla protein	Secretory protein	-0.626
15	ZNF695	zinc finger protein 695	unknown	-0.596
16	KIF20A	kinesin family member 20A	Transport	-0.596
17	TXNDC5	thioredoxin domain containing 5 (endoplasmic reticulum); muted homolog (mouse)	Protein folding/modification	-0.581
18	C19orf77	similar to HSPC323	unknown	-0.573
19	PCSK1N	proprotein convertase subtilisin/kexin type 1 inhibitor	Secretory protein	-0.548
20	RPL26	ribosomal protein L26	Translation machinery	-0.540
21	VN1R1	vomeronasal 1 receptor 1	Signaling	-0.539
22	TNNC1	troponin C type 1 (slow)	Muscle contraction	-0.537
23	GFER	growth factor, augmenter of liver regeneration	Mitochondrial protein	-0.531
24	TIMM23B	translocase of inner mitochondrial membrane 23 homolog (yeast)	Mitochondrial protein	-0.529
25	RDH14	retinol dehydrogenase 14 (all-trans/9-cis/11-cis); 5'-nucleotidase, cytosolic IB	Metabolism	-0.528
26	UCN2	urocortin 2	Secretory protein	-0.522
27	C8orf59	chromosome 8 open reading frame 59	unknown	-0.517
28	HIST1H2BL	histone cluster 1, H2bl	Chromatin related	-0.515
29	PSMA1	proteasome (prosome, macropain) subunit, alpha type, 1	Protein cleavage/degradation	-0.515
30	PGP	phosphoglycolate phosphatase	Metabolism	-0.511
31	CGB7	chorionic gonadotropin, beta polypeptide 7	Secretory protein	-0.503
32	TMEM126A	transmembrane protein 126A	Mitochondrial protein	-0.501
33	MRPL51	mitochondrial ribosomal protein L51	Translation machinery	-0.499
34	FAM103A1	family with sequence similarity 103, member A1	RNA synthesis and processing	-0.498
35	CHIC2	cysteine-rich hydrophobic domain 2	Transport	-0.497
36	ENDOG	endonuclease G	Mitochondrial protein	-0.494
37	FAM173A	family with sequence similarity 173, member A	unknown	-0.489
38	GTF2A2	general transcription factor IIA, 2, 12kDa	RNA synthesis and processing	-0.488
39	EEF1B2	eukaryotic translation elongation factor 1 beta 2	Translation machinery	-0.474
40	MT2A	metallothionein 2A	metal binding/storage	-0.474
41	TPRKB	TP53RK binding protein	RNA synthesis and processing	-0.469
42	CCDC153	coiled-coil domain containing 153	unknown	-0.469
43	HSPA8	heat shock 70kDa protein 8	Protein folding/modification	-0.469
44	ACOT13	acyl-CoA thioesterase 13	Cytoskeletal protein	-0.463
45	INTS12	integrator complex subunit 12	RNA synthesis and processing	-0.463
46	AGPAT1	1-acylglycerol-3-phosphate O-acyltransferase 1 (lysophosphatidic acid acyltransferase, alpha)	Metabolism	-0.462
47	DYNLL1	dynein, light chain, LC8-type 1	Transport	-0.458
48	PRAF2	PRA1 domain family, member 2	Transport	-0.453
49	SSBP1	single-stranded DNA binding protein 1	Mitochondrial protein	-0.453
50	RPL5	ribosomal protein L5	Translation machinery	-0.451
51	SHFM1	split hand/foot malformation (ectrodactyly) type 1	DNA repair	-0.450
52	CBLN3	cerebellin 3 precursor	Secretory protein	-0.450
53	TMEM50A	transmembrane protein 50A	unknown	-0.449
54	NACA	nascent polypeptide-associated complex alpha subunit	Transport	-0.449
55	RPL17	ribosomal protein L17	Translation machinery	-0.446
56	ATP5S	ATP synthase, H+ transporting, mitochondrial F0 complex, subunit s (factor B)	Metabolism	-0.443
57	MTHFS	5,10-methenyltetrahydrofolate synthetase (5-formyltetrahydrofolate cyclo-ligase)	Metabolism	-0.441
58	COX6C	cytochrome c oxidase subunit VIc	Metabolism	-0.439
59	MRPS36	mitochondrial ribosomal protein S36	Translation machinery	-0.438
60	SEC11C	SEC11 homolog C (S. cerevisiae)	unknown	-0.437
61	FABP6	fatty acid binding protein 6, ileal	Transport	-0.436
62	TLCD1	TLC domain containing 1	Transport	-0.432
63	OIP5	Opa interacting protein 5	Cell cycle regulation	-0.431
64	ENY2	enhancer of yellow 2 homolog (Drosophila)	Transport	-0.430
65	NPTN	neuroplastin	Cell-cell interaction	-0.430
66	CMC1	COX assembly mitochondrial protein homolog (S. cerevisiae)	Mitochondrial protein	-0.428
67	MARS	methionyl-tRNA synthetase	Translation machinery	-0.428
68	RAB1A	RAB1A, member RAS oncogene family	Transport	-0.427

Table 2.7 (Continued).

69	MED30	mediator complex subunit 30	RNA synthesis and processing	-0.426
70	DNAJC9	DnaJ (Hsp40) homolog, subfamily C, member 9	Protein folding/modification	-0.425
71	C20orf201	chromosome 20 open reading frame 201	unknown	-0.424
72	RAB4A	RAB4A, member RAS oncogene family	Transport	-0.419
73	IK	similar to CG18005; IK cytokine, down-regulator of HLA II	unknown	-0.412
74	ACTN4	actinin, alpha 4	Cytoskeletal protein	-0.411
75	C19orf81		unknown	-0.408
76	HIST1H2BD	histone cluster 1, H2bd	Chromatin related	-0.408
77	PIGH	phosphatidylinositol glycan anchor biosynthesis, class H	Protein folding/modification	-0.405
78	TBCA	tubulin folding cofactor A	Cytoskeletal protein	-0.405
79	RHOF	ras homolog gene family, member F (in filopodia)	Signaling	-0.403
80	DBI	diazepam binding inhibitor (GABA receptor modulator, acyl-Coenzyme A binding protein)	Signaling	-0.403
81	NDUFB3	NADH dehydrogenase (ubiquinone) 1 beta subcomplex, 3, 12kDa	Metabolism	-0.401
82	PDCD5	programmed cell death 5	Apoptosis	-0.401
83	AMN	amnionless homolog (mouse)	unknown	-0.400
84	MTRNR2L8		Secretory protein	-0.399
85	EWSR1	Ewing sarcoma breakpoint region 1	Transcriptional regulation	-0.398
86	MYBBP1A	MYB binding protein (P160) 1a	Transcriptional regulation	-0.396
87	TFB1M	transcription factor B1, mitochondrial	Mitochondrial protein	-0.395
88	PTPMT1	protein tyrosine phosphatase, mitochondrial 1	Metabolism	-0.395
89	CACYBP	similar to calcyclin binding protein; calcyclin binding protein	Protein folding/modification	-0.393
90	RPL30	ribosomal protein L30	Translation machinery	-0.390
91	RPS27A	ribosomal protein S27a	Translation machinery	-0.390
92	PDIA3	protein disulfide isomerase family A, member 3	Protein folding/modification	-0.389
93	DBP	D site of albumin promoter (albumin D-box) binding protein	Transcriptional regulation	-0.387
94	CYFIP1	cytoplasmic FMR1 interacting protein 1	Cytoskeletal protein	-0.387
95	JTB	jumping translocation breakpoint	Cell cycle regulation	-0.386
96	CGB1	chorionic gonadotropin, beta polypeptide 1	Secretory protein	-0.385
97	PLA2G16	phospholipase A2, group XVI	Metabolism	-0.383
98	EBNA1BP2	EBNA1 binding protein 2	Cell cycle regulation	-0.381
99	SAC3D1	SAC3 domain containing 1	Cell cycle regulation	-0.378
100	ATPIF1	ATPase inhibitory factor 1	Mitochondrial protein	-0.378
101	HCST	hematopoietic cell signal transducer	Signaling	-0.377
102	RGS10	regulator of G-protein signaling 10	Signaling	-0.375
103	CLN5	ceroid-lipofuscinosis, neuronal 5	unknown	-0.371
104	SNRPE	small nuclear ribonucleoprotein polypeptide E	RNA synthesis and processing	-0.371
105	VTI1B	vesicle transport through interaction with t-SNAREs homolog 1B (yeast)	Transport	-0.371
106	GOLGA7B	golgi autoantigen, golgin subfamily a, 7B	unknown	-0.371
107	HP	haptoglobin-related protein; haptoglobin	Secretory protein	-0.370
108	HNRNPM	heterogeneous nuclear ribonucleoprotein M	RNA synthesis and processing	-0.370
109	SNRPD1	small nuclear ribonucleoprotein D1 polypeptide 16kDa	RNA synthesis and processing	-0.370
110	ZNF749	zinc finger protein 749	unknown	-0.369
111	MED31	mediator complex subunit 31	RNA synthesis and processing	-0.367
112	FTSJ3	FtsJ homolog 3 (E. coli)	RNA synthesis and processing	-0.365
113	RPS27L	ribosomal protein S27-like	Translation machinery	-0.364
114	LONP2	lon peptidase 2, peroxisomal	Protein cleavage/degradation	-0.363
115	CAND2	cullin-associated and neddylation-dissociated 2 (putative)	Protein folding/modification	-0.362
116	SYNJ2BP	synaptojanin 2 binding protein	unknown	-0.361
117	RAB13	RAB13, member RAS oncogene family; similar to hCG24991	Transport	-0.360
118	RPL38	ribosomal protein L38	Translation machinery	-0.358
119	ATP5E	ATP synthase, H+ transporting, mitochondrial F1 complex, epsilon subunit	Metabolism	-0.358
120	PDIA6	protein disulfide isomerase family A, member 6	Protein folding/modification	-0.357
121	TIMM9	translocase of inner mitochondrial membrane 9 homolog (yeast)	Mitochondrial protein	-0.356
122	RPL35A	ribosomal protein L35a	Translation machinery	-0.356
123	PRR7	proline rich 7 (synaptic)	Signaling	-0.355
124	RPS24	ribosomal protein S24	Translation machinery	-0.354
125	TMEM18	transmembrane protein 18	Transcriptional regulation	-0.354
126	LDHB	lactate dehydrogenase B	Metabolism	-0.352
127	HOXD3	homeobox D3	Development	-0.351
128	MPG	N-methylpurine-DNA glycosylase	DNA repair	-0.348
129	RPL31	ribosomal protein L31	Translation machinery	-0.348
130	NIPA2	non imprinted in Prader-Willi/Angelman syndrome 2	Transport	-0.347
131	SNRPD2	small nuclear ribonucleoprotein D2 polypeptide 16.5kDa	RNA synthesis and processing	-0.347
132	TMEM223	transmembrane protein 223	unknown	-0.346
133	TYMS	thymidylate synthetase	Metabolism	-0.346
134	DPY30	dpy-30 homolog (C. elegans)	Chromatin related	-0.344
135	DLL3	delta-like 3 (Drosophila)	Development	-0.344
136	SKIV2L2	superkiller viralicidic activity 2-like 2 (S. cerevisiae)	RNA synthesis and processing	-0.342
137	CCDC109B	coiled-coil domain containing 109B	Mitochondrial protein	-0.341
138	CDC26	cell division cycle 26 homolog (S. cerevisiae)	Cell cycle regulation	-0.341
139	CLN3	ceroid-lipofuscinosis, neuronal 3	Transport	-0.341

Table 2.7 (Continued).

140	CTU1	ATP binding domain 3	RNA synthesis and processing	-0.341
141	MRPS18C	mitochondrial ribosomal protein S18C	Translation machinery	-0.339
142	CENPW	centromere protein w	Cell cycle regulation	-0.337
143	GTPBP4	GTP binding protein 4	Signaling	-0.336
144	HINT1	histidine triad nucleotide binding protein 1	Transcriptional regulation	-0.334
145	PDHA1	pyruvate dehydrogenase (lipoamide) alpha 1	Metabolism	-0.330
146	HIST3H2A	histone cluster 3, H2a	Chromatin related	-0.327
147	FTH1	ferritin, heavy polypeptide 1	metal binding/storage	-0.326
148	TMEM238		unknown	-0.326
149	C11orf74	chromosome 11 open reading frame 74	unknown	-0.326
150	UQCRB	ubiquinol-cytochrome c reductase binding protein	Metabolism	-0.326
151	ABRACL	ABRA C-terminal protein	unknown	-0.324
152	FAM213B	prostamide/prostaglandin F synthase	Metabolism	-0.322
153	FAM64A	family with sequence similarity 64, member A	Cell cycle regulation	-0.321
154	C15orf61	chromosome 15 open reading frame 61	unknown	-0.319
155	C11orf73	chromosome 11 open reading frame 73	Transport	-0.319
156	CASP6	caspase 6, apoptosis-related cysteine peptidase	Apoptosis	-0.319
157	ZNHIT3	zinc finger, HIT type 3	unknown	-0.318
158	RPL34	ribosomal protein L34	Translation machinery	-0.318
159	EIF3H	eukaryotic translation initiation factor 3, subunit H	Translation machinery	-0.318
160	EIF3E	eukaryotic translation initiation factor 3, subunit E	Translation machinery	-0.316
161	LSM6	LSM6 homolog, U6 small nuclear RNA associated (S. cerevisiae)	RNA synthesis and processing	-0.316
162	GNPTG	N-acetylglucosamine-1-phosphate transferase, gamma subunit	Protein folding/modification	-0.316
163	NUDT5	nudix (nucleoside diphosphate linked moiety X)-type motif 5	Metabolism	-0.316
164	H2AFY	H2A histone family, member Y	Chromatin related	-0.316
165	GTF2H5	general transcription factor IIH, polypeptide 5	RNA synthesis and processing	-0.315
166	EXOSC10	exosome component 10	RNA synthesis and processing	-0.313
167	ATP5G2	ATP synthase, H+ transporting, mitochondrial F0 complex, subunit C2 (subunit 9)	Metabolism	-0.313
168	COPG2	coatomer protein complex, subunit gamma 2	Transport	-0.313
169	C12orf45	chromosome 12 open reading frame 45	unknown	-0.308
170	ANAPC13	anaphase promoting complex subunit 13	Cell cycle regulation	-0.307
171	GTF2IRD2	GTF2I repeat domain containing 2	Transcriptional regulation	-0.306
172	RPL23	ribosomal protein L23	Translation machinery	-0.305
173	CSTB	cystatin B (stefin B)	Protein cleavage/degradation	-0.305
174	RPS25	ribosomal protein S25	Translation machinery	-0.304
175	EIF3J	eukaryotic translation initiation factor 3, subunit J	Translation machinery	-0.304
176	ZCRB1	zinc finger CCHC-type and RNA binding motif 1	RNA synthesis and processing	-0.302
177	DRAM2	DNA-damage regulated autophagy modulator 2	Apoptosis	-0.302
178	MRPL33	mitochondrial ribosomal protein L33	Translation machinery	-0.301
179	PIR	pirin (iron-binding nuclear protein)	Transcriptional regulation	-0.301
180	PWP2	PWP2 periodic tryptophan protein homolog (yeast)	unknown	-0.301
181	DDX27	DEAD (Asp-Glu-Ala-Asp) box polypeptide 27	RNA synthesis and processing	-0.301
182	EIF1B	eukaryotic translation initiation factor 1B	Translation machinery	-0.300
183	CCNH	cyclin H	Transcriptional regulation	-0.299
184	MDP1	magnesium-dependent phosphatase 1	unknown	-0.298
185	FAM162A	family with sequence similarity 162, member A	Apoptosis	-0.298
186	PITPNC1	phosphatidylinositol transfer protein, cytoplasmic 1	Transport	-0.296
187	CDKN2D	cyclin-dependent kinase inhibitor 2D (p19, inhibits CDK4)	Cell cycle regulation	-0.296
188	MRPS15	mitochondrial ribosomal protein S15	Translation machinery	-0.295
189	GPRC5B	G protein-coupled receptor, family C, group 5, member B	Signaling	-0.295
190	DYNC1H1	dynein, cytoplasmic 1, heavy chain 1	Transport	-0.294
191	ATF4	activating transcription factor 4 (tax-responsive enhancer element B67)	Transcriptional regulation	-0.294
192	SEC61B	Sec61 beta subunit	Transport	-0.293
193	HIST1H2BN	histone cluster 1, H2bn	Chromatin related	-0.292
194	NSA2	TGF beta-inducible nuclear protein 1	Cell cycle regulation	-0.292
195	PPDPF	pancreatic progenitor cell differentiation and proliferation factor homolog (zebrafish)	unknown	-0.291
196	NCAPG	non-SMC condensin I complex, subunit G	Cell cycle regulation	-0.291
197	MTERFD2	MTERF domain containing 2	Mitochondrial protein	-0.290
198	NAA38	LSM8 homolog, U6 small nuclear RNA associated (S. cerevisiae)	Protein folding/modification	-0.290
199	CCT8	chaperonin containing TCP1, subunit 8 (theta)	Protein folding/modification	-0.290
200	C1QBP	complement component 1, q subcomponent binding protein	immunity	-0.290
201	TOMM7	translocase of outer mitochondrial membrane 7 homolog (yeast)	Mitochondrial protein	-0.289
202	RBBP4	hypothetical LOC642954; retinoblastoma binding protein 4	Chromatin related	-0.289
203	TROAP	trophinin associated protein (tastin)	Cell-cell interaction	-0.288
204	METTL5	methyltransferase like 5	unknown	-0.288
205	RPL14	ribosomal protein L14	Translation machinery	-0.288
206	FH	fumarate hydratase	Metabolism	-0.287
207	TIMM21	Mitochondrial import inner membrane translocase subunit Tim21	Mitochondrial protein	-0.287
208	MAP1LC3B2	microtubule-associated protein 1 light chain 3 beta 2	Protein folding/modification	-0.287
209	CDKN3	cyclin-dependent kinase inhibitor 3	Cell cycle regulation	-0.287
210	LSM5	LSM5 homolog, U6 small nuclear RNA associated (S. cerevisiae)	RNA synthesis and processing	-0.286

Table 2.7 (Continued).

211	FAM195A	chromosome 16 open reading frame 14	unknown	-0.286
212	RNASEH1	ribonuclease H1	RNA degradation	-0.285
213	FCGR2A	Fc fragment of IgG, low affinity IIa, receptor (CD32)	immunity	-0.283
214	METTL12	methyltransferase like 12	unknown	-0.283
215	RBBP7	retinoblastoma binding protein 7	Chromatin related	-0.283
216	SDF4	stromal cell derived factor 4	unknown	-0.283
217	RPL7	ribosomal protein L7	Translation machinery	-0.283
218	RPL22	ribosomal protein L22 pseudogene 11; ribosomal protein L22	Translation machinery	-0.282
219	ARMC7	armadillo repeat containing 7	unknown	-0.281
220	COX6B1	cytochrome c oxidase subunit Vib polypeptide 1 (ubiquitous)	Metabolism	-0.280
221	RPS7	ribosomal protein S7	Translation machinery	-0.280
222	PPP1R11	protein phosphatase 1, regulatory (inhibitor) subunit 11	Signaling	-0.280
223	PPIL3	peptidylprolyl isomerase (cyclophilin)-like 3	Protein folding/modification	-0.280
224	TRAPPC5	trafficking protein particle complex 5	Transport	-0.279
225	S100A13	S100 calcium binding protein A13	Transport	-0.279
226	SNRPG	small nuclear ribonucleoprotein polypeptide G	unknown	-0.279
227	CHCHD10	coiled-coil-helix-coiled-coil-helix domain containing 10	Mitochondrial protein	-0.278
228	COG8	peptide deformylase (mitochondrial); component of oligomeric golgi complex 8	Transport	-0.278
229	RPS28	ribosomal protein S28	Translation machinery	-0.277
230	S100B	S100 calcium binding protein B	Signaling	-0.277
231	PRELID2	PRELI domain containing 2	Mitochondrial protein	-0.277
232	PSMA3	proteasome (prosome, macropain) subunit, alpha type, 3	Protein cleavage/degradation	-0.275
233	PNP	nucleoside phosphorylase	Metabolism	-0.274
234	TEP1	telomerase-associated protein 1	telomerase component	-0.274
235	KIAA1429	Protein virilizer homolog	RNA synthesis and processing	-0.274
236	EFCAB10	EF-hand calcium binding domain 10	unknown	-0.272
237	MEMO1	mediator of cell motility 1; similar to mediator of cell motility 1	Signaling	-0.272
238	RPL24	ribosomal protein L24; ribosomal protein L24 pseudogene 6	Translation machinery	-0.272
239	RBFA		unknown	-0.272
240	NENF	neuron derived neurotrophic factor	Secretory protein	-0.271
241	SPATA24	hypothetical protein LOC202051	Transcriptional regulation	-0.270
242	C1orf54	chromosome 1 open reading frame 54	unknown	-0.269
243	LSMD1	LSM domain containing 1	Protein folding/modification	-0.269
244	NOC2L	nucleolar complex associated 2 homolog (S. cerevisiae)	Chromatin related	-0.269
245	CEBPG	CCAAT/enhancer binding protein (C/EBP), gamma	Transcriptional regulation	-0.269
246	RPL37A	ribosomal protein L37a	Translation machinery	-0.269
247	CSTF2	cleavage stimulation factor, 3' pre-RNA, subunit 2, 64kDa	RNA synthesis and processing	-0.268
248	RPS15A	ribosomal protein S15a	Translation machinery	-0.268
249	ATP6V0E2	ATPase, H+ transporting V0 subunit e2	Transport	-0.268
250	CCDC107	coiled-coil domain containing 107	unknown	-0.267
251	BEST1	bestrophin 1	Transport	-0.267
252	FLT3LG	fms-related tyrosine kinase 3 ligand	Secretory protein	-0.267
253	U2AF1	U2 small nuclear RNA auxiliary factor 1	RNA synthesis and processing	-0.266
254	TYMP	thymidine phosphorylase	Metabolism	-0.266
255	METRN	meteorin, glial cell differentiation regulator	Secretory protein	-0.266
256	SEC61G	Sec61 gamma subunit	Transport	-0.266
257	ANKRD39	ankyrin repeat domain 39	unknown	-0.265
258	TOM1L1	target of myb1 (chicken)-like 1	unknown	-0.265
259	IER3IP1	immediate early response 3 interacting protein 1	unknown	-0.265
260	NHP2L1	NHP2 non-histone chromosome protein 2-like 1 (S. cerevisiae)	RNA synthesis and processing	-0.265
261	FLII	flightless I homolog (Drosophila)	Cytoskeletal protein	-0.264
262	RBM8A	RNA binding motif protein 8A	RNA synthesis and processing	-0.264
263	DDX1	DEAD (Asp-Glu-Ala-Asp) box polypeptide 1	RNA synthesis and processing	-0.263

Table 2.8. Genes with a z-score < −2 in 92.1 cell line. Gene name, functional class, and log fold change in translational efficiency (TE) between control and EIF1AX knockdown cells is indicated.

	Hugo Symbol	Name	Functional Class	Change in TE
	GPRIN1	G protein regulated inducer of neurite outgrowth 1	Signaling	-1.339
1	ZC3HAV1L	zinc finger CCCH-type, antiviral 1-like	unknown	-0.979
2	GFER	growth factor, augmenter of liver regeneration	mitochondrial protein	-0.816
3	GATC	glutamyl-tRNA(Gln) amidotransferase, subunit C homolog (bacterial)	RNA synthesis and processing	-0.771
4	GET4	golgo to ER traffic protein 4 homolog	Transport	-0.762
5	NEURL2	neuralized homolog 2 (Drosophila)	Protein folding/modification	-0.756
6	EIF4EBP3	eukaryotic translation initiation factor 4E binding protein 3	translation inhibitor	-0.748
7	DNAJC3	DnaJ (Hsp40) homolog, subfamily C, member 3	Protein folding/modification	-0.729
8	CDCA4	cell division cycle associated 4	transcriptional regulation	-0.709
9	SAC3D1	SAC3 domain containing 1	Cell cycle regulation	-0.705
10	C20orf24	chromosome 20 open reading frame 24	Apoptosis/autophagy	-0.664
11	PRKG1	protein kinase, cGMP-dependent, type I	Signaling	-0.658
12	PAG1	phosphoprotein associated with glycosphingolipid microdomains 1	immunity	-0.641
13	MRPL1	mitochondrial ribosomal protein L1	translation machinery	-0.632
14	TAF2	TAF2 RNA polymerase II, TATA box binding protein (TBP)-associated factor, 150kDa	RNA synthesis and processing	-0.629
15	EFNA3	ephrin-A3	Signaling	-0.627
16	CASP6	caspase 6, apoptosis-related cysteine peptidase	Apoptosis/autophagy	-0.621
17	RDH14	retinol dehydrogenase 14 (all-trans/9-cis/11-cis); 5'-nucleotidase, cytosolic IB	Metabolism	-0.619
18	C5orf30	chromosome 5 open reading frame 30	unknown	-0.576
19	ASAP2	ArfGAP with SH3 domain, ankyrin repeat and PH domain 2	Signaling	-0.575
20	MTPN	myotrophin; leucine zipper protein 6	cytoskeletal protein	-0.562
21	ZC2HC1A		unknown	-0.549
22	TMEM160	transmembrane protein 160	unknown	-0.545
23	GPAM	glycerol-3-phosphate acyltransferase, mitochondrial	Metabolism	-0.544
24	DBT	dihydrolipoamide branched chain transacylase E2	Metabolism	-0.544
25	MAK16	MAK16 homolog (S. cerevisiae)	unknown	-0.538
26	C18orf25	chromosome 18 open reading frame 25	unknown	-0.532
27	NRGN	neurogranin (protein kinase C substrate, RC3)	Signaling	-0.531
28	PPIP5K2	histidine acid phosphatase domain containing 1	Signaling	-0.528
29	RBL2	retinoblastoma-like 2 (p130)	chromatin related	-0.526
30	MLXIP	MLX interacting protein	transcriptional regulation	-0.526
31	ZFP90	zinc finger protein 90 homolog (mouse)	unknown	-0.526
32	SCFD1	sec1 family domain containing 1	Transport	-0.519
33	PRKD3	protein kinase D3	Signaling	-0.518
34	GPD1L	glycerol-3-phosphate dehydrogenase 1-like	Metabolism	-0.513
35	NAA30	N-acetyltransferase 12 (GCN5-related, putative)	Protein folding/modification	-0.513
36	NUBPL	nucleotide binding protein-like	Metabolism	-0.506
37	SLC38A1	solute carrier family 38, member 1	Transport	-0.505
38	SETD7	SET domain containing (lysine methyltransferase) 7	Protein folding/modification	-0.503
39	CLN5	ceroid-lipofuscinosis, neuronal 5	unknown	-0.497
40	CMTM6	CKLF-like MARVEL transmembrane domain containing 6	unknown	-0.497
41	RAB43	RAB43, member RAS oncogene family	Signaling	-0.497
42	BACH1	BTB and CNC homology 1, basic leucine zipper transcription factor 1	transcriptional regulation	-0.496
43	PDF	peptide deformylase (mitochondrial); component of oligomeric golgi complex 8	mitochondrial protein	-0.496
44	SEL1L	sel-1 suppressor of lin-12-like (C. elegans)	Protein cleavage/degradation	-0.495
45	CYP7B1	cytochrome P450, family 7, subfamily B, polypeptide 1	Metabolism	-0.494
46	ALS2	amyotrophic lateral sclerosis 2 (juvenile)	Signaling	-0.489
47	GOPC	golgi associated PDZ and coiled-coil motif containing	Transport	-0.488
48	ZZZ3	zinc finger, ZZ-type containing 3	chromatin related	-0.485
49	SLC35E2	solute carrier family 35, member E2	unknown	-0.483
50	OTUD6B	OTU domain containing 6B	Protein folding/modification	-0.480
51	MTUS1	mitochondrial tumor suppressor 1	Cell cycle regulation	-0.476
52	SREK1IP1		RNA synthesis and processing	-0.475
53	UVRAG	UV radiation resistance associated gene	Apoptosis/autophagy	-0.474
54	FBXL4	F-box and leucine-rich repeat protein 4	Protein folding/modification	-0.474
55	MOB1A	MOB kinase activator 1A	Signaling	-0.473
56	CCDC85C	coiled-coil domain containing 85C	cell-cell interaction	-0.465
57	CDCA7L	cell division cycle associated 7-like	transcriptional regulation	-0.463
58	ARHGAP12	Rho GTPase activating protein 12	Signaling	-0.461
59	ADCY7	adenylate cyclase 7	Signaling	-0.461
60	RNF150	ring finger protein 150	unknown	-0.455
61	CCDC125	coiled-coil domain containing 125	unknown	-0.455
62	USP32	similar to TBC1 domain family, member 3; ubiquitin specific peptidase 32	Protein folding/modification	-0.454
63	HEATR5A	HEAT repeat containing 5A	unknown	-0.448
64	KCTD6	potassium channel tetramerisation domain containing 6	Protein folding/modification	-0.448
65	ZNF322		transcriptional regulation	-0.448
66	MSANTD4	Myb/SANT-like DNA-binding domain containing 4 with coiled-coils	unknown	-0.447
67	ZEB2	zinc finger E-box binding homeobox 2	transcriptional regulation	-0.447
68	GRPEL2	GrpE-like 2, mitochondrial (E. coli)	mitochondrial protein	-0.444
69	KIF2A	kinesin heavy chain member 2A	cytoskeletal protein	-0.443
70	GLCE	glucuronic acid epimerase	Metabolism	-0.442
71	RPE	ribulose-5-phosphate-3-epimerase	Metabolism	-0.442
72	GBAS	glioblastoma amplified sequence	Metabolism	-0.442
73	HP	haptoglobin-related protein; haptoglobin	Secretory protein	-0.442
74	ETNK1	ethanolamine kinase 1	Metabolism	-0.440
75	SLC25A24	solute carrier family 25 (mitochondrial carrier; phosphate carrier), member 24	mitochondrial protein	-0.439
76	PUS7	pseudouridylate synthase 7 homolog (S. cerevisiae)	RNA synthesis and processing	-0.439

Table 2.8 (Continued).

77	PRR11	proline rich 11	unknown	-0.433
78	GATSL2	GATS protein-like 2	unknown	-0.433
79	CLIC4	chloride intracellular channel 4	Transport	-0.432
80	RBM45	RNA binding motif protein 45	development	-0.431
81	FAM208B	family with sequence similarity 208, member B	unknown	-0.430
82	LYRM2	LYR motif containing 2	unknown	-0.430
83	PSD3	pleckstrin and Sec7 domain containing 3	Signaling	-0.429
84	ZC3H12C	zinc finger CCCH-type containing 12C	unknown	-0.429
85	GOLIM4	golgi integral membrane protein 4	Transport	-0.428
86	HES7	hairy and enhancer of split 7 (Drosophila)	transcriptional regulation	-0.427
87	KLHL24	kelch-like 24 (Drosophila)	unknown	-0.425
88	PPWD1	peptidylprolyl isomerase domain and WD repeat containing 1	RNA synthesis and processing	-0.425
89	KLF6	Kruppel-like factor 6	transcriptional regulation	-0.425
90	C17orf80	chromosome 17 open reading frame 80	unknown	-0.423
91	EYA4	eyes absent homolog 4 (Drosophila)	DNA synthesis and repair	-0.422
92	CAST	calpastatin	Protein cleavage/degradation	-0.422
93	ZNF227	zinc finger protein 227	unknown	-0.421
94	FBXL3	F-box and leucine-rich repeat protein 3	Protein folding/modification	-0.420
95	ATP13A3	ATPase type 13A3	Transport	-0.420
96	UCN	urocortin	Secretory protein	-0.420
97	AFF4	AF4/FMR2 family, member 4	RNA synthesis and processing	-0.420
98	FAM126A	family with sequence similarity 126, member A	unknown	-0.420
99	NIPAL2	NIPA-like domain containing 2	unknown	-0.417
100	SRXN1	sulfiredoxin 1 homolog (S. cerevisiae)	Oxidation/reduction	-0.417
101	GXYLT1	glycosyltransferase 8 domain containing 3	Protein folding/modification	-0.415
102	DDX52	DEAD (Asp-Glu-Ala-Asp) box polypeptide 52	RNA synthesis and processing	-0.415
103	RSL24D1	ribosomal L24 domain containing 1; similar to ribosomal protein L24-like	ribosome biogenesis	-0.414
104	NUDT6	nudix (nucleoside diphosphate linked moiety X)-type motif 6	Cell cycle regulation	-0.414
105	NCOR1	nuclear receptor co-repressor 1	chromatin related	-0.413
106	ZNF77	zinc finger protein 77	unknown	-0.413
107	TAF1B	TATA box binding protein (TBP)-associated factor, RNA polymerase I, B, 63kDa	RNA synthesis and processing	-0.413
108	MYO5A	myosin VA (heavy chain 12, myoxin)	Transport	-0.412
109	CD46	CD46 molecule, complement regulatory protein	immunity	-0.411
110	PRIM1	primase, DNA, polypeptide 1 (49kDa)	DNA synthesis and repair	-0.410
111	EXO1	exonuclease 1	DNA synthesis and repair	-0.409
112	QTRTD1	queuine tRNA-ribosyltransferase domain containing 1	RNA synthesis and processing	-0.408
113	RRM2B	ribonucleotide reductase M2 B (TP53 inducible)	DNA synthesis and repair	-0.407
114	SWAP70	SWAP switching B-cell complex 70kDa subunit	Signaling	-0.406
115	RHOBTB3	Rho-related BTB domain containing 3	Transport	-0.405
116	ETV1	ets variant 1	transcriptional regulation	-0.405
117	ITGB3BP	integrin beta 3 binding protein (beta3-endonexin)	transcriptional regulation	-0.405
118	ADAM17	ADAM metallopeptidase domain 17	Protein cleavage/degradation	-0.405
119	INTS5	integrator complex subunit 5	RNA synthesis and processing	-0.404
120	TRIM44	tripartite motif-containing 44	unknown	-0.403
121	LYAR	Ly1 antibody reactive homolog (mouse)	Cell cycle regulation	-0.403
122	SPATA2L	spermatogenesis associated 2-like	unknown	-0.402
123	TACC1	transforming, acidic coiled-coil containing protein 1	Cell cycle regulation	-0.401
124	ANKRD52	ankyrin repeat domain 52	unknown	-0.401
125	FZD6	frizzled homolog 6 (Drosophila)	Signaling	-0.399
126	MED13	mediator complex subunit 13	RNA synthesis and processing	-0.398
127	SLC25A40	solute carrier family 25, member 40	mitochondrial protein	-0.398
128	SETD6	SET domain containing 6	Protein folding/modification	-0.397
129	MFAP3	microfibrillar-associated protein 3	extracellular matrix protein	-0.395
130	SGCZ	sarcoglycan zeta	glycoprotein	-0.395
131	UBE2G2	ubiquitin-conjugating enzyme E2G 2 (UBC7 homolog, yeast)	Protein folding/modification	-0.395
132	GPRC5B	G protein-coupled receptor, family C, group 5, member B	Signaling	-0.394
133	TMOD3	tropomodulin 3 (ubiquitous)	cytoskeletal protein	-0.394
134	SRPK1	SFRS protein kinase 1	Signaling	-0.393
135	PRKAA1	protein kinase, AMP-activated, alpha 1 catalytic subunit	Signaling	-0.392
136	PHKB	phosphorylase kinase, beta	Signaling	-0.391
137	WDSUB1	WD repeat, sterile alpha motif and U-box domain containing 1	unknown	-0.390
138	HIST3H2A	histone cluster 3, H2a	chromatin related	-0.390
139	PAN3	PAN3 poly(A) specific ribonuclease subunit homolog (S. cerevisiae)	RNA synthesis and processing	-0.390
140	CAB39L	calcium binding protein 39-like	Apoptosis/autophagy	-0.390
141	ENOX2	ecto-NOX disulfide-thiol exchanger 2	Metabolism	-0.390
142	ABLIM1	actin binding LIM protein 1	cytoskeletal protein	-0.389
143	CENPL	centromere protein L	Cell cycle regulation	-0.388
144	NFYA	nuclear transcription factor Y, alpha	transcriptional regulation	-0.387
145	GPR124	G protein-coupled receptor 124	Signaling	-0.386
146	IDH3A	isocitrate dehydrogenase 3 (NAD+) alpha	Metabolism	-0.386
147	DSG2	desmoglein 2	cell-cell interaction	-0.386
148	KIF3B	kinesin family member 3B	cytoskeletal protein	-0.386
149	ZBTB43	zinc finger and BTB domain containing 43	unknown	-0.386
150	IPPK	inositol 1,3,4,5,6-pentakisphosphate 2-kinase	Signaling	-0.385
151	PEX13	peroxisomal biogenesis factor 13	Transport	-0.385
152	LRP6	low density lipoprotein receptor-related protein 6	Signaling	-0.385
153	INTS8	integrator complex subunit 8	RNA synthesis and processing	-0.385
154	ZNF559	zinc finger protein 559	unknown	-0.384
155	FYTTD1	forty-two-three domain containing 1	Transport	-0.383

EIF1AX-regulated translation: interaction analysis

As an additional means to assess the role of EIF1AX in protein translation, we utilized a contrast matrix based approach to identify genes with differential translational efficiency in the setting of EIF1AX knockdown (125). The expression levels for each gene (read counts) were first normalized using the trimmed mean of M values (TMM) method (126). This approach assumes that most genes are not differentially expressed between samples and identifies a sample-specific scaling factor to allow for more accurate comparisons. Next, we identified genes whose translational efficiency was affected by the knockdown of EIF1AX. To this end, we determined the interaction effect of control – knockdown and polysome – total. This analysis identifies genes for which the ratio between polysome and total mRNA (translational efficiency) is shifted upon knockdown of EIF1AX.

By this method, 896 genes achieved significance (p-value < 0.05). Next, we computed CPM (counts per million) values. We filtered for significantly expressed genes, which were defined as those for which at least 50% of the samples achieved a CPM > 2. There were 142 genes that passed this filter (**Table 2.9**). These genes include many that were previously identified by the results described above. For example, the translational efficiencies of *C20orf24*, *GET4*, *GFER*, *PDF*, *SAC3D1*, and *TMEM160* were significantly reduced following EIF1AX knockdown in all three lines (**Figure 2.8 and Table 2.6-2.8**). These 6 genes also achieved significance by our interaction modeling. These genes therefore represent those commonly regulated by wild type and mutant EIF1AX. Of these 142 genes, only 7 show an increased translational efficiency following EIF1AX knockdown (**Table 3.9**). These data support the function of EIF1AX as an initiation factor essential for translation.

To understand common trends across the results, we categorized the genes based on their translational efficiency profile. The 142 genes grouped into 4 clusters (**Figure 2.9A**). Overall, the genes within a cluster display a common change in translational efficiency following EIF1AX knockdown (**Figure 2.9B**). Clusters 1, 2, and 3 exhibit reduced translational

efficiencies following EIF1AX knockdown predominately in the wild type cell lines (Omm2.3 and Omm1), while Cluster 4 includes genes with increased translational efficiencies across the cell lines (**Figure 2.9B**). Cluster 2 exhibits the least change in translational efficiency in the mutant cell line (92.1). This cluster includes 26 ribosomal proteins (**Figure 2.9B**, red). Three ribosomal proteins in other clusters (1 and 3) also demonstrate similar trends across the cell lines as the 26 ribosomal proteins in cluster 2. These data indicate that knockdown of wild type EIF1AX results in reduced efficiency of ribosomal protein translation, while knockdown of mutant EIF1AX levels does not. These findings provide orthogonal analytical support for the results described above.

We next sought to further examine the efficiency of ribosomal protein translation across all 78 RSP/RPL genes in these UM cells. The median translational efficiency of ribosomal proteins was reduced following EIF1AX knockdown in wild type, but not mutant cells (**Figure 2.9C**). Interestingly, the mutant cells (92.1) exhibited lower translational efficiency values in control cells when compared to control wild type cells (**Figure 2.9C)**. These data are consistent with our polysome profiling results and suggest that cells expressing mutant EIF1AX exhibit aberrant translation.

Table 2.9. Genes from interaction analysis with significant changes in translational efficiency following EIF1AX knockdown. P-value and cluster is indicated for each gene.

Gene	logFC	logCPM	LR	PValue	Rank	FDR	Cluster
PDF	-0.796	3.299	12.091	0.0005	1	1	1
GFER	-1.059	2.353	10.343	0.0013	2	1	1
RGS10	-0.502	4.503	9.542	0.0020	3	1	2
C20orf24	-1.100	4.889	8.795	0.0030	4	1	1
PGP	-0.755	5.256	8.671	0.0032	5	1	1
GET4	-0.773	1.982	8.211	0.0042	6	1	1
NKX2-4	-0.535	2.309	8.068	0.0045	7	1	3
SAC3D1	-0.741	3.467	8.054	0.0045	8	1	1
RP11-154J22.1	-0.978	2.169	7.996	0.0047	9	1	3
RPL36AL	-0.446	8.266	7.996	0.0047	10	1	1
TMEM160	-1.097	5.549	7.978	0.0047	11	1	2
ZC3HAV1L	-0.845	2.410	7.739	0.0054	12	1	3
RPL26	-0.515	9.475	7.374	0.0066	13	1	2
C19orf24	-0.795	3.834	7.302	0.0069	14	1	1
SNRPF	-0.485	6.294	7.108	0.0077	15	1	1
RP11-641D5.1	-0.449	7.519	7.094	0.0077	16	1	2
RPL35A	-0.506	9.795	6.807	0.0091	17	1	2
RP11-592N21.1	-0.483	6.295	6.627	0.0100	18	1	2
RPL22	-0.374	8.579	6.464	0.0110	19	1	2
CHCHD10	-0.588	6.513	6.449	0.0111	20	1	3
PRELID1	-0.556	7.337	6.395	0.0114	21	1	1
AC007036.5	-0.500	1.342	6.201	0.0128	22	1	3
AC022431.1	-0.497	6.114	6.103	0.0135	23	1	2
RP1-241P17.4	-0.333	4.993	6.066	0.0138	24	1	1
UQCRFS1P1	-0.536	4.669	6.007	0.0143	25	1	2
PCF11	0.405	3.661	5.998	0.0143	26	1	4
SERPINA1	-0.569	1.674	5.982	0.0145	27	1	3
RP4-706A16.3	-0.441	7.809	5.840	0.0157	28	1	2
RPL30	-0.529	10.858	5.756	0.0164	29	1	2
AC005000.1	-0.340	4.381	5.742	0.0166	30	1	1
FAM176B	-0.765	2.969	5.589	0.0181	31	1	1
MRPL51	-0.392	7.198	5.429	0.0198	32	1	1
H1FX-AS1	-0.492	3.868	5.395	0.0202	33	1	1
RP11-587D21.1	-0.487	5.810	5.319	0.0211	34	1	2
RP11-734J24.1	-0.511	2.001	5.304	0.0213	35	1	2
PDXP	-0.560	2.518	5.298	0.0213	36	1	3
RP11-51O6.1	-0.486	6.334	5.275	0.0216	37	1	2
RPS27A	-0.463	10.894	5.265	0.0218	38	1	2
MRPS15	-0.386	7.209	5.260	0.0218	39	1	1
MRPS36	-0.356	5.134	5.249	0.0220	40	1	1
RPL34	-0.470	9.433	5.239	0.0221	41	1	2
RPS25	-0.457	8.334	5.233	0.0222	42	1	2
RPL17	-0.453	9.130	5.232	0.0222	43	1	3
RP11-359H18.1	-0.686	2.626	5.231	0.0222	44	1	2
TLCD1	-0.489	4.498	5.231	0.0222	45	1	1
UBA52	-0.477	10.764	5.127	0.0236	46	1	2
FAM173A	-0.648	4.715	5.117	0.0237	47	1	1
TMEM126A	-0.429	5.042	5.085	0.0241	48	1	1
CTD-2287O16.1	-0.454	7.065	5.062	0.0245	49	1	2
RPL31	-0.398	10.116	5.051	0.0246	50	1	2
C11orf73	-0.433	5.672	5.028	0.0249	51	1	1
SNRPE	-0.392	6.929	4.983	0.0256	52	1	1
RP11-572P18.1	-0.438	7.993	4.960	0.0259	53	1	2
AC093106.7	-0.458	5.515	4.949	0.0261	54	1	2
GTF2IRD2B	-0.408	2.112	4.938	0.0263	55	1	3
RP11-526L22.1	-0.355	5.406	4.890	0.0270	56	1	3
RPS15	-0.467	10.396	4.864	0.0274	57	1	2
XKR6	-0.518	2.3684	4.8361	0.0279	58	1	NA
KBTBD3	-0.463	1.278	4.817	0.0282	59	1	3
COX6C	-0.333	8.742	4.800	0.0285	60	1	1
RP11-430L17.1	-0.481	1.728	4.790	0.0286	61	1	2
RPL23	-0.424	10.394	4.761	0.0291	62	1	2
SNRPD2	-0.439	8.595	4.752	0.0293	63	1	1
RPS7	-0.413	10.222	4.747	0.0293	64	1	2
RPS15A	-0.470	8.995	4.746	0.0294	65	1	2
ZNF280D	-0.366	4.045	4.740	0.0295	66	1	1
C12orf45	-0.413	4.422	4.729	0.0297	67	1	3
RP11-50D9.1	-0.436	6.170	4.714	0.0299	68	1	2
ZNF526	0.319	3.870	4.686	0.0304	69	1	4
RPL29	-0.465	9.874	4.673	0.0306	70	1	2
RPL38	-0.476	9.698	4.665	0.0308	71	1	2

Table 2.9 (Continued).

CTD-2292P10.2	-0.608	2.667	4.665	0.0308	72	1	3
RPL21P119	-0.431	6.691	4.655	0.0310	73	1	2
RPLP2	-0.494	10.166	4.641	0.0312	74	1	2
ATP5G2	-0.401	9.237	4.585	0.0322	75	1	1
RPL21	-0.413	5.701	4.569	0.0326	76	1	2
AC011816.4	-0.480	6.177	4.559	0.0327	77	1	2
RPL35	-0.471	9.499	4.533	0.0332	78	1	2
RP11-463M16.4	-0.317	2.766	4.530	0.0333	79	1	1
SEC61B	-0.354	6.980	4.529	0.0333	80	1	1
ABCA11P	-0.381	2.856	4.488	0.0341	81	1	1
UQCRB	-0.326	8.449	4.467	0.0345	82	1	3
RP11-11N9.4	-0.400	5.236	4.426	0.0354	83	1	1
RPAIN	-0.321	4.325	4.425	0.0354	84	1	1
DYNLL1	-0.389	8.610	4.407	0.0358	85	1	1
RP11-20O24.4	-0.411	7.087	4.403	0.0359	86	1	3
RP11-466H18.1	-0.396	9.092	4.356	0.0369	87	1	2
RPS19	-0.513	11.209	4.339	0.0373	88	1	2
TMF1	0.556	2.998	4.318	0.0377	89	1	4
C4orf48	-0.788	6.379	4.316	0.0377	90	1	1
SAA2	-0.502	1.294	4.298	0.0382	91	1	3
HINT1	-0.449	9.023	4.298	0.0382	92	1	1
CTU1	-0.530	3.447	4.295	0.0382	93	1	1
ANKRD9	-0.498	5.521	4.293	0.0383	94	1	1
RP11-203F10.6	-0.447	3.497	4.286	0.0384	95	1	2
RPL5	-0.354	9.702	4.284	0.0385	96	1	3
RPL36	-0.486	9.715	4.270	0.0388	97	1	2
RP11-15B17.1	-0.413	6.688	4.257	0.0391	98	1	3
MRPS33	-0.329	6.132	4.255	0.0391	99	1	2
ENDOG	-0.565	3.400	4.253	0.0392	100	1	1
NDUFB3	-0.368	6.216	4.247	0.0393	101	1	1
MAT2A	0.359	6.531	4.244	0.0394	102	1	4
RP11-822E23.1	-0.450	2.072	4.236	0.0396	103	1	2
RPS28	-0.524	6.309	4.229	0.0397	104	1	2
RP11-56D16.2	-0.508	1.399	4.221	0.0399	105	1	1
DBP	-0.389	3.809	4.219	0.0400	106	1	1
AC079250.1	-0.492	6.588	4.215	0.0401	107	1	2
RP11-509E16.1	0.501	2.511	4.203	0.0404	108	1	4
RP4-765A10.1	-0.355	6.265	4.199	0.0405	109	1	3
H3F3BP1	-0.380	3.390	4.188	0.0407	110	1	3
RPL28	-0.472	10.921	4.188	0.0407	111	1	2
RPS7P1	-0.386	8.579	4.176	0.0410	112	1	2
ANKRD39	-0.378	3.983	4.131	0.0421	113	1	1
RPL14	-0.412	10.017	4.115	0.0425	114	1	2
RDH14	-0.494	1.765	4.102	0.0428	115	1	4
RPS7P11	-0.382	7.101	4.070	0.0437	116	1	2
CHCHD2P6	-0.445	2.735	4.068	0.0437	117	1	1
GNG11	-0.451	6.475	4.064	0.0438	118	1	1
RP11-565J7.3	-0.387	5.770	4.048	0.0442	119	1	2
CHD1	0.476	3.923	4.042	0.0444	120	1	4
C8orf59	-0.398	4.548	4.038	0.0445	121	1	1
RPS16	-0.447	10.642	4.033	0.0446	122	1	2
LIG4	0.515	1.901	4.008	0.0453	123	1	4
RPS24	-0.395	10.311	4.007	0.0453	124	1	2
TMEM18	-0.390	5.765	3.993	0.0457	125	1	2
PIGH	-0.356	4.956	3.993	0.0457	126	1	3
TMEM50A	-0.303	5.354	3.979	0.0461	127	1	3
MIF4GD	-0.361	3.726	3.977	0.0461	128	1	1
ATP5L	-0.371	7.685	3.967	0.0464	129	1	1
HOXD3	-0.499	2.558	3.949	0.0469	130	1	1
AC007969.5	-0.438	7.113	3.949	0.0469	131	1	2
RPL13	-0.429	10.998	3.941	0.0471	132	1	2
TBCA	-0.332	7.497	3.939	0.0472	133	1	3
RP11-16F15.2	-0.406	5.427	3.928	0.0475	134	1	2
RANBP1	-0.309	8.165	3.926	0.0475	135	1	1
PRAF2	-0.455	2.938	3.925	0.0476	136	1	1
RP1-292B18.1	-0.493	1.277	3.910	0.0480	137	1	2
H3F3AP6	-0.302	5.276	3.882	0.0488	138	1	3
H3F3AP4	-0.255	8.503	3.870	0.0492	139	1	3
RP11-215A21.2	-0.413	3.020	3.868	0.0492	140	1	3
CLN5	-0.343	3.364	3.868	0.0492	141	1	4
RPL32	-0.425	10.467	3.857	0.0495	142	1	2

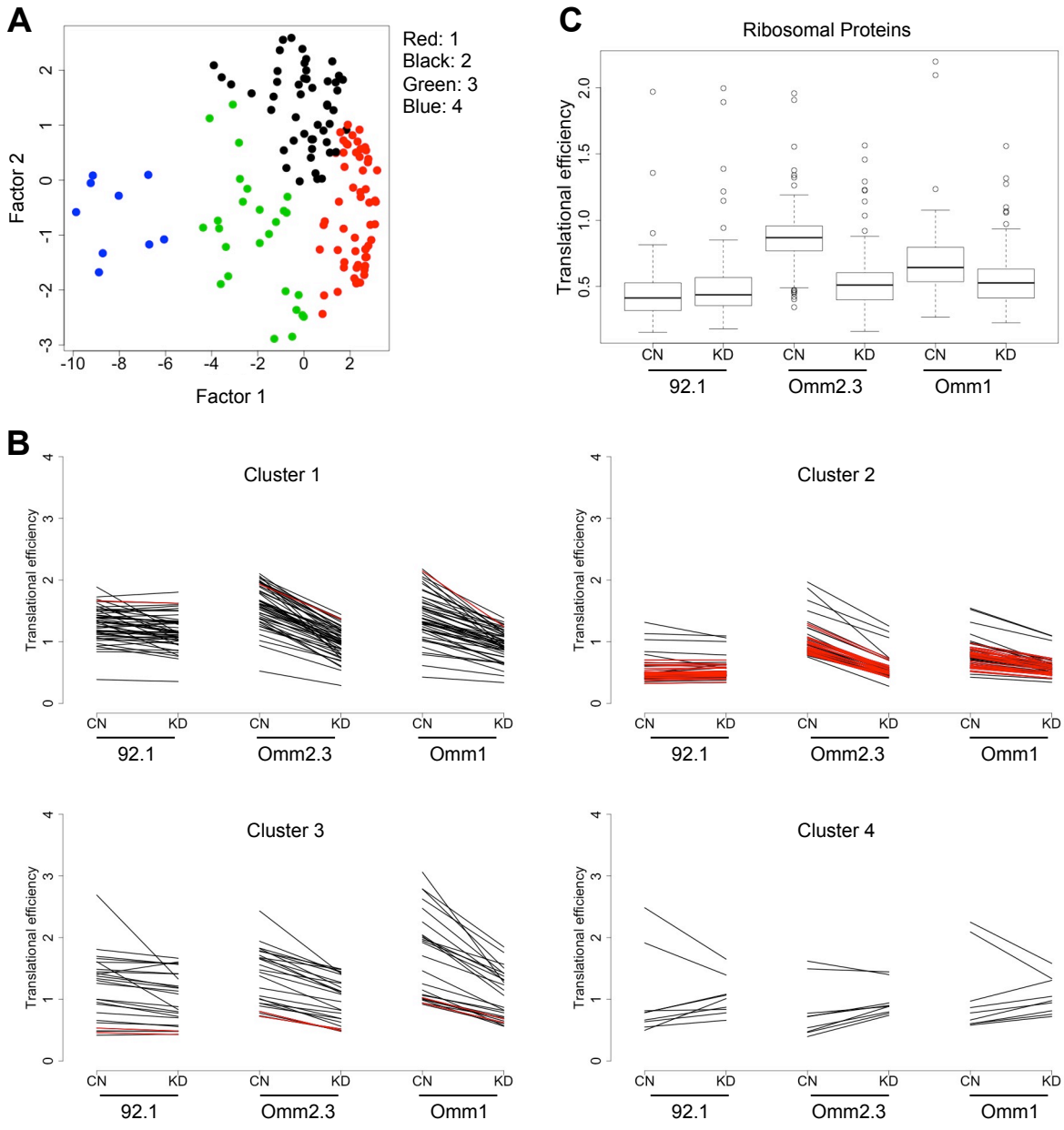

Figure 2.9. Genes with significant changes in translational efficiency (TE) following EIF1AX knockdown cluster into 4 groups. (A) Principle component analysis depicts 4 color-coded clusters of 141 genes. **(B)** The trend in TE is depicted for each cluster in cells expressing control shRNAs (CN) or EIF1AX shRNAs (KD). TE was calculated as polysome CPM / total CPM. **(C)** Boxplots demonstrate the distribution of the TEs of 78 ribosomal proteins in cells as in (B).

Discussion

In this study, we sequenced the exomes of 61 UM primary tumor/normal pairs. To our knowledge, this represents one of the largest UM cohorts to undergo comprehensive genomic characterization to date. Consistent with prior studies, recurrent mutations were observed in *GNAQ*, *GNA11*, *BAP1*, *EIF1AX*, and *SF3B1* (39, 40, 49, 59, 60); no additional genes met the threshold for significance. This study confirms the relative mutually exclusive nature of *BAP1*, *SF3B1*, and *EIF1AX* gene mutations. Our data further demonstrate that in contrast to cutaneous melanoma, which has the highest somatic gene mutation frequency of any cancer type (104), UM lacks a UV-radiation mutation signature and has a low mean somatic mutation rate. Recent data suggest that clinical benefit to immune checkpoint blockade therapy (e.g., anti-CTLA4) in cutaneous melanoma is associated with higher mutational burden (127). A higher mutation frequency is thought to generate a diversity of neoantigens that can be recognized by the immune system. Thus, the low somatic gene mutation frequency we detected in this large cohort of WES UM tumors may explain the lower response rates thus far reported for UM tumors using the recently FDA-approved immune checkpoint blockade inhibitors in cutaneous melanoma (98, 128).

In two cases, we sequenced multiple tumors from the same patient. This allowed us to track enrichment or depletion of specific somatic alterations over the course of disease progression. To date, monosomy 3 and mutated *BAP1* have been associated with UM metastasis (35, 49), but comprehensive sequencing of metastatic tumors has not been reported. In UM45 in this cohort, a *SMARCA4* mutation was detected in the metastatic sample. *SMARCA4* mutations were recently reported in metastatic UM tumors, although matched primary tumor DNA was not sequenced for comparison (129). Conceivably, then, SMARCA4 may contribute to the establishment or maintenance of metastatic disease, although functional studies are needed to confirm this hypothesis. Some *SMARCA4*-mutant cancer cells may be

sensitive to inhibition of the second SWI/SNF catalytic subunit (130-132). If SWI/SNF mutations are recurrently linked to metastatic disease in UM, the relevance of this synthetic lethal relationship to residual SWI/SNF complex function may merit additional exploration.

We identified *EIF1AX*-NTT mutations in approximately 20% of primary UM tumors, consistent with prior studies (60). Putative driver mutations in this translation factor are of interest given that increased protein synthesis is frequently observed in rapidly proliferating cancer cells. Both upstream signaling pathways and aberrant translation factor expression contribute to this phenomenon (133). Indeed, several translation initiation factors that are overexpressed in human cancer, including EIF4E, EIF4G, EIF3A, EIF3C, and EIF3H may also contribute to tumorigenesis (134). Consistent with these general observations, our RNAi knockdown experiments suggest an essential role for EIF1AX in both wildtype and mutant settings. EIF1AX is the first translation initiation factor reported as recurrently mutated in cancer, and is significantly mutated in both uveal melanoma and papillary thyroid carcinoma (62).

Recent ribosome footprinting experiments demonstrate that translation of the protein synthesis machinery is suppressed by pharmacologic inhibition of mTOR, a well-known regulator of translation (135, 136). We performed RNA sequencing of polysome-associated mRNAs and observed similar suppression of the translational efficiency of ribosomal proteins following EIF1AX knockdown in wild type *EIF1AX* cells. In contrast, mutant *EIF1AX* cells did not display this phenotype. There are at least two possible explanations for these observations. First, the level of knockdown achieved may not be sufficient to impair mutant EIF1AX function (thus, ribosomal proteins continue to be translated sufficiently by this mechanism). This model could be operant if mutated EIF1AX has enhanced function over wild type. However, the observed 80s accumulation following shRNA expression is consistent with the notion that the magnitude of EIF1AX knockdown achieved here is functionally consequential. Second, translation in the setting of mutant EIF1AX may be less efficient overall, such that knockdown does not further impair ribosomal functions. This model may also imply that mutant EIF1AX

harbors previously unrecognized yet essential functions that may or may not be related to translation. For example, one could posit a neomorphic role for EIF1AX, resulting in regulation of a unique set of mRNAs or a translation-independent activity contributing to tumorigenesis. However, no evidence for such a neomorphic effect currently exists. Additional studies will be necessary to tease apart the biological consequences of N-terminal mutations in *EIF1AX* in UM as well as other cancer types.

In summary, this study utilized systematic genomic approaches to probe the somatic genetics of primary and metastatic UM, as well as the function of mutated EIF1AX. This is the first study of deregulated translation by a mutated initiation factor in cancer and may represent a novel therapeutic avenue. Future work should focus on further developing approaches to target the described genetic lesions, in particular in patients with metastatic potential.

Materials and Methods

Tumor Specimens

This study was approved by the institutional review board of the Massachusetts Eye and Ear Infirmary, MD Anderson Cancer Center, Dana-Farber Cancer Institute, and the Broad Institute. All patients provided written informed consent. Biopsy samples were obtained from 62 patients with uveal melanoma. Primary tumor samples were from enucleated eye specimens, while metastatic samples were from core biopsies obtained by interventional radiology. Fresh tissue was immediately flash frozen at -80°C. Germline DNA was obtained from adjacent normal tissue or peripheral blood mononuclear cells.

DNA Extraction and Whole Exome Sequencing

The blood samples were extracted using Gentra Puregene Blood kit (Qiagen) and the fresh frozen tissue samples were extracted using QIAamp DNA Mini kit (Qiagen) according to

manufacturer's protocol. For all samples except Trio 2, DNA libraries and whole exome sequencing data were generated as previously described (137). Tumor and normal DNA went through shearing, end repair, adenylation, and adapter ligation using barcoded adapters. Hybrid capture was performed on size-selected DNA using the SureSelect v2 Exome Target Enrichment System (Agilent). Resulting libraries were quantified by qPCR using the KAPA Biosystems Library Quantification Kit, then pooled and sequenced across multiple HiSeq flow cell lanes (Illumina). 101x mean target coverage was achieved. For trio 2, DNA libraries and sequencing data were generated as previously described (138), with the following modification: hybrid capture was performed using the SureSelect v2 Exome baits (Agilent).

Sequence Data Processing and Quality Control

Standard methods developed at the Broad were used for data processing and analysis, as previously described (139-141). Sequence data were aligned to hg19 and BAM files were generated using Picard (http://picard.sourceforge.net/), and then input into Firehose for analysis (http://www.broadinstitute.org/cancer/cga/Firehose). All BAM files will be deposited in dbGaP (http://www.ncbi.nlm.nih.gov/gap). Tumor and normal pairs were confirmed using genotyping. Sample cross-contamination was estimated using ContEst (142) and ranged from 0.1 to 8.2%. Copy number profiles were reviewed and nonaberrant tumor samples or aberrant normal samples were removed from the analysis set (N=8). One hypermutated sample was excluded.

Somatic Mutation Calling and Significance Analysis

Somatic base pair substitutions and small insertions or deletions were identified using MuTect (143) and Indelocator (http://www.broadinstitute.org/cancer/cga/indelocator), respectively, and annotated using Oncotator (http://www.broadinstitute.org/cancer/cga/oncotator). DNA oxidation related artifacts were identified and filtered using a published method (144). The significance of mutated genes was

determined using MutSigCV (104). Mutations were manually reviewed by visual inspection using IGV (145, 146). For copy number analysis, segment files were generated using sequencing coverage data compared to a panel of normal samples. The circular binary segmentation algorithm was applied (147). The presence of disomy 3 or monosomy 3 was determined by manual review of CapSeg plots. Samples with noisy copy number data were labeled indeterminate.

Trio Analysis

The percentage of tumor cells (CCF) harboring each genetic alteration was determined using the previously described algorithm ABSOLUTE (106, 107). Clonal events were those with a cancer cell fraction (CCF) of close to 1, while all other events were subclonal. Phylogenetic trees were assembled after comparing the clonal and subclonal events in each sample from a given individual.

Mutation Validation

Targeted resequencing of select mutations was performed using microfluidic PCR (Fluidigm). 22 assays were designed to cover 37 targets with amplicons ranging from 149-164bp in size. The entire analysis set (51 pairs and 1 trio) was assayed using all primer sets across three 48.48 Access Array IFC chips (Fluidigm). Resulting amplicons were pooled and sequenced on MiSeq (Illumina) with 150 base paired-end reads. Resulting BAM files were manually reviewed at sites of interest using IGV. GNAQ (R183 and Q209), GNA11 (Q209), SF3B1 (R625), and EIF1AX (exon 2) hotspot mutations were assessed across all samples.

Cell Lines

92.1, Mel202, Mel270, Omm2.3, Omm2.5, Omm1, and Mel285 were kindly provided by Martine Jager in 2011 (Leiden University, The Netherlands). The origins and GNAQ and

GNA11 mutational status of these cell lines have been previously described (148). Cells were maintained in RPMI-1640 with 10% heat-inactivated FBS and identity was confirmed by fingerprinting using the GenePrint 10 kit (Promega) in January 2014. STR profiles were consistent with published data (148). An EIF1AX mutation in exon 1 or 2 was observed in only the 92.1 cell line of the 7 lines tested.

DNA Extraction and Sanger Sequencing

Cell line genomic DNA was extracted using DNeasy Blood & Tissue Kit (Qiagen) according to manufacturer's instructions. Exons 1 and 2 of EIF1AX were PCR amplified using AccuPrime *Pfx* SuperMix (Life Technologies). PCR products were purified using QIAquick PCR Purification Kit (Qiagen) and then Sanger sequenced. Traces were visualized using SeqMan Lasergene 8 software (DNASTAR). Primers (purchased from Integrated DNA Technologies) include:

Exon 1 forward (5'-GAAAAGCGACGCAAAGAGTC-3')

Exon 1 reverse (5'-CTGGGTGACCTGCAATCTAC-3')

Exon 2 forward (5'-GAAGGGTAGGGAGGTGATAATG-3')

Exon 2 reverse (5'-AGGCTGAAGTGGAAGGACTG-3')

Lentiviral Infections of shRNAs

shRNA expression constructs were obtained from The RNAi Consortium of the Broad Institute in the lentiviral expression plasmid pLKO.1 and include:

shLuc (TRCN0000072243, CTTCGAAATGTCCGTTCGGTT)

sh1AX 18 (TRCN0000062618, CCGAGACTACCAGGATAACAA)

sh1AX 21 (TRCN0000062621, CCTGGAGATGATGATGAAATT)

Lentivirus was produced by transfecting 2.4e6 293T cells with 3μg pLKO.1, 2.7μg Δ8.9 (*gag, pol*), and 0.3μg VSV-G plasmids in the presence of 18μL Xtreme Gene 9 (Roche). Virus was

harvested 72h after transfection and filtered using a 0.45μm syringe. For shRNA expression, cells were seeded at 2 to 4 x 10^5 cells/well in 6-well plates for immunoblot assays and polysome profiling and 1 to 2 x 10^3 cells/well in 96-well plates for cell viability assays. Cells were infected 24h later (1:40 to 1:50) in the presence of polybrene (Millipore; 5μg/mL) and then centrifuged at 2,250 RPM for 30 minutes at 37°C followed by a media change. To confirm infection efficiency, puromycin (1μg/mL) was added 24h after infection to half the 96-well plate. For polysome profiling, cells were passaged into 10cm dishes 24h prior to harvesting.

Viability Assays

Cells were infected in 96-well format (as described). Fresh media was added 72h after shRNA infection and proliferation was assessed in triplicate after another 72h (6 days total) using CellTiter96 Aqueous assay (Promega). Viability was calculated as a percentage of the control (shLuc) after background subtraction.

Project Achilles Analysis

The shRNA level scores for EIF1AX and RPS6 from Project Achilles v2.4.3 (216 cell lines) (http://www.broadinstitute.org/achilles/) (120) were visualized using histograms in Gene-E (www.broadinstitute.org/cancer/software/GENE-E/).

Immunoblot Analysis

Cells were washed twice with cold PBS and lysed in RIPA buffer containing Halt protease and phosphatase inhibitor single-use cocktail (Pierce). Lysates were quantified using Bradford assay (Bio-Rad) and resolved by SDS gel electrophoresis (Invitrogen), and then transferred to nitrocellulose (Invitrogen) or PVDF (Millipore) membranes. Membranes were blocked with 5% milk and then probed with primary antibodies for EIF1AX (Pierce 1:1,000) and

Vinculin (Calbiochem 1:5,000). HRP-linked secondary antibodies (anti-rabbit, anti-mouse IgG; 1:2,000 dilution, Santa Cruz) followed by chemiluminescence (Pierce) were used for detection.

Polysome Fractionation and RNA Isolation

Sub-confluent cells were treated with 100µg/mL cycloheximide for 3 minutes at 37°C and then washed twice with cold PBS containing 100µg/mL cycloheximide. Cells were lysed in buffer (5mM Tris (pH7.4), 2.5mM $MgCl_2$, 1.5mM KCl, 2mM DTT, 0.5% Triton-X, 0.5% NaDOC, 0.1units/µL RNasin, 100µg/mL cycloheximide, and 1x Halt protease and phosphatase inhibitor single-use cocktail), and then incubated on ice (20 min) and centrifuged at 13,000 RPM (10 min; 4°C). Lysates were quantified using Abs260 and equal amounts (based on OD units) were loaded onto 12mL 10%-50% sucrose gradients (15mM Tris (pH7.4), 15mM $MgCl_2$, 150mM NaCl, 100µg/mL cycloheximide). Gradients were centrifuged at 35,000 RPM for 2 hours at 4°C (SW40Ti rotor) and then 1mL fractionated with Auto Densi-Flow connected to RediFrac with monitoring of absorbance at 254nm.

RNA was extracted from input lysate and polysome fractions by Trizol LS (Invitrogen). Briefly, 500µL per polysome fraction or 100µL of input lysate was extracted at a ratio of 3:1 reagent to sample. After adding 200µL of chloroform (per 1mL), samples were vigorously mixed and centrifuged at 14,000 RPM for 10 minutes at 4°C. The aqueous phase was extracted and equal amounts of phenol:chloroform:isoamyl alcohol (25:24:1) were added to remove residual trizol. Samples were vortexed and spun again for 10 minutes. The aqueous phase was removed and precipitated with isopropanol and glycogen at -80°C. Samples were centrifuged at 14,000 RPM for 25 minutes at 4°C, pellets washed with 70% ethanol, and then resuspended in 100µL water (pellets from polysome fractions were pooled at this step). After addition of 250µL 100% ethanol and 10µL 3M Sodium acetate, RNA was precipitated at -80°C overnight.

Samples were centrifuged at 14,000 RPM for 25 minutes at 4°C, washed with 70% ethanol, and RNA resuspended in water.

RNA Sequencing and Analysis

The Quant-iT RiboGreen RNA Assay Kit (Invitrogen) was used to quantify total RNA. cDNA library construction was performed using the TruSeq RNA Sample Preparation protocol (Illumina, Revision A, 2010). Briefly, mRNA was selected from total RNA by oligo dT beads, followed by heat/ion fragmentation and double-stranded cDNA synthesis. End repair, adenylation, adapter ligation, and PCR enrichment were performed. Resulting libraries were quantified by qPCR using the KAPA Biosystems Library Quantification Kit for Illumina Sequencing Platforms and then pooled and sequenced using Illumina HiSeq to a depth of 45-50 million reads per sample.

The standard Broad Picard Pipeline was used to generate BAM files. Sequence data were aligned to hg19 using TopHat 1.4.1 (149). Read counts and RPKM (reads per kilobase of transcript per million mapped reads) were determined using RNA-SeQC (150). The resulting RPKM list was filtered for protein-coding HUGO symbol genes (http://www.genenames.org/), and then for genes expressed in total RNA samples (RPKM≥1 in all 6 total mRNA samples for each cell line). Polysome RPKM was then divided by total RPKM for each gene to determine the sample-specific translational efficiency. Biological replicates (sh1AX: 2 per shRNA, 4 total; shLuc: 2) were then averaged and fold change values were calculated by taking the $\log_2$ of sh1AX divided by shLuc.

Translational efficiency (TE) = polysome RPKM/total RPKM

$\text{Log}_2(\Delta \text{ TE}) = \text{Log}_2((\text{average sh1AX TE})/(\text{average shLuc TE}))$

Z-scores were calculated for each gene. Genes with $z<-2$ were functionally annotated using UniProt (www.uniprot.org) and PubMed (www.ncbi.nlm.nih.gov/gene). To determine whether

ribosomal proteins (RPS/RPL) were significantly enriched in the *z*<-2 group, a two-tailed Fisher exact test was applied using GraphPad.

For the interaction model, the counts for each gene were used to normalize the data using the TMM method (126). Genes whose translation efficiency was affected by the knockdown of EIF1AX were then identified using the edgeR package (125). To this end, we fitted the following generalized linear model, based on a negative binomial distribution, after estimating the expression level-detrended and gene-wise overdispersion.

$count_i \sim \alpha_i$*cell_line + β_i*replicate + γ_i*knockdown + δ_i*fraction + ζ_i*knockdown*fraction + ε_i

where:

$count_i$ is the normalized gene counts for gene i

cell line is the vector representing the cell line effect (levels=92.1 Omm2.3, Omm1)

replicate is the vector representing the replicate experiments (two independent replicate experiments performed)

fraction is the vector representing the profiling of total or polysomal RNA

The interaction effect ζ_i*knockdown*fraction models genes with transcripts that display a shift in the ratio between the polysomal and total RNA fraction (=translational efficiency) upon EIF1AX suppression. The genes of interest have a coefficient ζ_i significantly different from zero. Genes were nominated based on an interaction p-value threshold of 0.05 and an expression threshold of at least 50% of the samples containing a counts per million (CPM) greater than 2. Genes were then grouped by a k-means clustering of the translational efficiencies using correlation-based similarity measures. 1 gene was removed due to division by 0 CPM (XKR6). 4 clusters were identified and the trend in the translational efficiencies across control and knockdown samples for each cell line was depicted. Here, translational efficiencies (TE) were defined as polysome CPM / total CPM. The average TE for control and knockdown was computed and graphed using line plots.

CHAPTER 3.

SYSTEMATIC IDENTIFICATION OF TARGETS FOR CO-INHIBITION WITH MEK AND PROTEIN KINASE C INHIBITORS IN UVEAL MELANOMA

Attributions

This chapter is reprinted from a manuscript in preparation with the following authorship:

Chelsea S. Place[1,2], Daniel J. Treacy[1], Glenn S. Cowley[2], Mudra Hegde[2], David E. Root[2], and Levi A. Garraway[1,2]

1) Dana-Farber Cancer Institute, Harvard Medical School, Boston, MA 02115
2) The Broad Institute of Harvard and MIT, Cambridge, MA 02142

All of the experiments and analysis were performed by Chelsea Place except as follows:

Glenn Cowley assisted with screen design and analysis. Mudra Hegde performed the shRNA seed ranking analysis. Dan Treacy performed ERK inhibitor immunoblots (**Figure 3.11C**) and ERK resistance allele experiments (**Figure 3.12**) and assisted with MEKDD experiments (**Fig. 3.10**).

Abstract

The majority of uveal melanoma (UM) tumors contain activating mutations in the heterotrimeric G-protein α subunits, GNAQ and GNA11. These mutations result in downstream activation of protein kinase C (PKC) and mitogen-activated protein kinase (MAPK) signaling. Both PKC and MEK inhibitors are currently in metastatic UM clinical trials, however, additional therapeutic innovation will likely be necessary to achieve durable responses in advanced UM, which is uniformly fatal. Here, we employed large-scale RNA interference screening to identify putative protein targets that may further sensitize UM cells to PKC or MEK inhibition. Several candidate proteins were identified through this approach, including the mitochondrial folate pathway enzyme, MTHFD2. However, the most generalizable target identified overall was BRAF, whose co-inhibition enhanced sensitivity to MEK inhibition in multiple UM contexts. Indeed, synergy was consistently observed following combined small molecule inhibition of two nodes of the MAPK pathway using pan-RAF, MEK, or ERK inhibitors. These results suggest that more potent inhibition of MAPK signaling in UM cells may improve clinical responses. Thus, combined pan-RAF/MEK or MEK/ERK inhibition warrants further investigation in UM clinical trials.

Introduction

Uveal melanoma (UM) is a deadly malignancy that comprises 5% of all melanoma cases (1). Primary tumors originating in the iris, ciliary body, or choroid of the eye metastasize to the liver in 50% of patients (102). Once metastatic, UM patients have poor outcomes, with a median survival of only 6 months (17).

Oncogenic mutations in *GNAQ* and *GNA11,* which encode α subunits of heterotrimeric G proteins, are observed in the vast majority of UM tumors in a mutually exclusive fashion (39, 40). These mutations primarily involve residues Q209 and R183, and produce constitutively active G protein isoforms (39, 40). GNAQ/11 signals predominately through phospholipase C-β (PLCβ) to release second messengers such as inositol trisphosphate (IP_3) and DAG (151). In turn, these effectors may engage multiple downstream signaling pathways. In UM, oncogenic GNAQ/11 has been shown to activate protein kinase C (PKC), which itself may up-regulate the RAF, MEK, and ERK (MAP kinase) cascade in UM cells (45, 46, 79). Mutated GNAQ/11 may augment additional downstream pathways as well, including AKT (46) and YAP oncoproteins (47, 48).

Based on the altered signaling dynamics produced by oncogenic GNAQ/11, several protein constituents of the aforementioned pathways have been nominated for therapeutic intervention. For example, MEK and PKC can be targeted by small molecules in clinical use or development, and indeed such agents have demonstrated efficacy against UM cells *in vitro* as either single agents or in combination (39, 45, 79-81). Accordingly, MEK and PCK inhibitors are currently being evaluated in UM clinical trials. In one study, MEK inhibition was associated with a modest improvement in progression free survival (76), but this observation awaits further confirmation in follow up studies – some of which will leverage more potent MEK inhibitors. New therapeutic strategies that combine MEK inhibition with additional agents will undoubtedly be needed to achieve more robust and durable clinical responses in metastatic UM.

In the past, RNA interference screens have been used to nominate co-targets of anticancer drugs. These studies have identified putative enhancers of both chemotherapy (152, 153) and targeted therapy (154-157) across a range of drugs and cancer types. Given the possible benefits of combination therapy for treatment of UM, the RNAi enhancer screening approach might be well suited to identify putative co-targets of drugs that are currently in UM clinical trials. In this study, we applied a systematic genome-scale loss of function screening

approach to identify genes whose silencing further sensitizes a panel of UM cell lines to MEK and PKC inhibitors.

Results

Genome-scale drug enhancer screens in GNAQ/11-mutant cells

To identify proteins whose suppression might augment MEK or PKC inhibition in *GNAQ/11*-mutant UM cells, we employed an unbiased RNA interference drug enhancer screening approach (**Figure 3.1A**). A *GNAQ*-mutant UM cell line derived from a liver metastasis (Omm2.3) was screened using drug doses empirically determined to inhibit downstream signaling (**Figure 3.1B**). Phospho-MARCKS was used as a read out for PKC inhibition, as previously described (79), while phospho-ERK was used to assess MEK inhibition and confirm PKC inhibition. As expected, MEK inhibitor treatment caused phospho-MEK levels to increase; this phenomenon likely results from release of ERK-dependent negative feedback mechanisms (158).

Omm2.3 cells were infected with a pooled library of ~98,000 shRNAs targeting ~17,000 genes and cultured in the presence of vehicle control (DMSO), MEK inhibitor (1μM AZD6244), or PKC inhibitor (1μM AEB071) (**Fig. 3.1C**). After culturing the cells for 21 days, genomic DNA was extracted and the relative shRNA abundance was quantified using massively parallel sequencing. In principle, cells expressing shRNAs that enhance drug activity should be selected against during prolonged cell culture. Quantities of individual shRNAs in the presence of drug were compared to DMSO controls to identify shRNAs that became significantly depleted during drug exposure. The corresponding genes were ranked using the RNAi gene enrichment (RIGER) 2nd best shRNA analysis method (159). Here, we considered top candidate enhancer genes to be those with low normalized enrichment scores for which at least two shRNAs

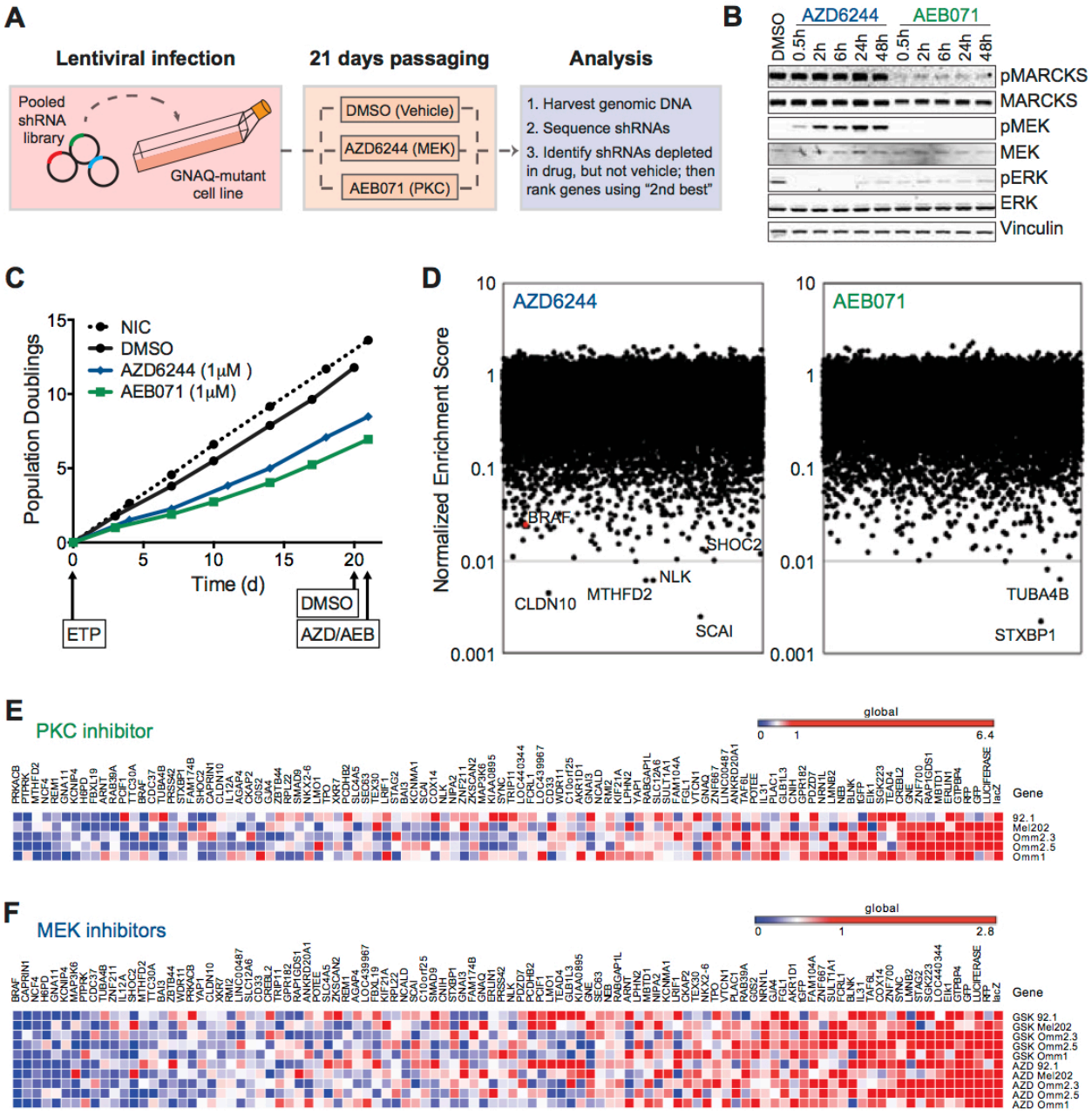

Figure 3.1. RNA interference drug enhancer screens identify novel MEK and PKC inhibitor sensitizers in UM cells. **(A)** Overview of screening approach using pooled shRNA library. **(B)** Immunoblot analysis of pathway inhibition following MEK (1μM AZD6244) or PKC (1μM AEB071) inhibitor treatment in Omm2.3 cells. **(C)** Growth of non-infected Omm2.3 cells (NIC), or those infected with genome-scale shRNA library and cultured in the presence of indicated drugs for up to 3 weeks. Arrows indicate when cells were harvested for DNA and ETP represents early time point. Data from 3 replicates per treatment arm are included. **(D)** Genes ranked by RIGER 2nd best shRNA method for AZD6244 (left) or AEB071 (right) in comparison to DMSO controls. Top hits are labeled. **(E)** Genes from PKC inhibitor validation screens ranked by average normalized enrichment score (NES) from 2nd best shRNA across 5 cell lines (AEB071). Low NES indicates more sensitivity to PKC inhibitor. **(F)** As in (E), but for MEK validation screens using two inhibitors (AZD6244 and GSK212).

showed selective depletion in the presence of drug (**Figure 3.1D**; see **Table 3.1 and 3.2** for the top 100 genes and corresponding shRNAs).

The strongest MEK and PKC inhibitor sensitizers were SCAI and STXBP1, respectively, neither of which has been previously implicated in UM (**Figure 3.1D**). Several genes had low normalized enrichment scores in both screens, although the top-ranking gene for each remained drug-specific (**Figure 3.2A**). In addition, YAP1 ranked within the top 50 genes in our MEK inhibitor screen (**Table 3.1**), and within the top 10% in our PKC screen. This finding validates the recently described role of YAP1 as a downstream dependency of GNAQ/11 in mutated UM cells (47, 48).

One major challenge with RNAi screens is mitigating the signal driven by off-target RNAi effects. In particular, transcripts containing sequences in their 3'-untranslated region that complement short 7-nucleotide seed sequences within an shRNA can be down regulated by shRNAs through a mechanism similar to miRNA regulation (160-162). All shRNAs have both an on-target effect and an off-target effect driven by its seed sequence. The relative contribution of the phenotype driven by both on-target and off-target effects are context dependent. Conceivably, then, shRNAs could emerge as candidate effectors from a phenotypic screen because of the effects of their seed sequences on transcripts other than the intended target genes.

Putative candidate genes that might have resulted from off-target miRNA seed effects were identified and removed. Each shRNA in the library was categorized by two 7-nucleotide seed sequences from positions 11-17 or 12-18. The shRNA depletion values from the previously described RIGER analysis were then used to score seeds with 2 or more shRNAs in the most depleted 2%. Seeds with multiple shRNAs demonstrating drug enhancement were then elucidated. This analysis generated a ranked list of seed sequences with drug enhancer phenotypes. Those shRNAs containing highly ranked seeds (top 10 or 7 for MEK and PKC, respectively) were removed from the total shRNA list and gene-level analysis was repeated

Table 3.1. The top 100 genes from the MEK inhibitor screen ranked by 2nd best shRNA.

Gene	# Hairpins	NES	Gene rank	p-value	p-value rank	# Hairpins 500	# Hairpins 1000	# Hairpins 5000	# Hairpins 10000
SCAI	5	0.002461	1	0.0002	2	2	2	2	2
CLDN10	4	0.004431	2	0.0002	4	2	2	2	2
NLK	10	0.006134	3	0.0001	1	2	2	3	3
MTHFD2	5	0.006188	4	0.0002	3	2	2	3	3
MAP3K6	10	0.009844	5	0.0003	5	2	2	2	3
SMAD9	5	0.01019	6	0.0005	6	1	2	3	3
POTEE	9	0.01045	7	0.0009	13	2	2	3	3
ERLIN1	5	0.01078	8	0.0006	7	1	2	2	2
ANKRD20A1	5	0.01106	9	0.0007	12	1	2	2	2
ZNF700	9	0.01174	10	0.001	15	2	2	2	2
SHOC2	10	0.01263	11	0.0007	9	2	2	4	6
LRIF1	5	0.01291	12	0.0007	11	1	2	2	3
SEC63	10	0.01313	13	0.0007	10	2	2	2	2
GTPBP4	5	0.01331	14	0.0007	8	0	2	2	2
KIF21A	5	0.01529	15	0.001	14	1	2	2	2
GPR182	9	0.01534	16	0.0018	27	1	2	2	4
PCIF1	5	0.01621	17	0.001	16	1	2	2	3
GLB1L3	10	0.01631	18	0.0016	23	1	2	2	2
BAI3	5	0.01673	19	0.0011	17	1	2	2	2
RAP1GDS1	5	0.01739	20	0.0013	18	1	1	2	2
MBTD1	5	0.01796	21	0.0014	21	1	1	2	2
SLC12A6	5	0.01799	22	0.0014	20	0	1	2	2
CD33	5	0.0182	23	0.0014	19	0	1	2	3
GNE	15	0.0186	24	0.0023	49	2	2	2	2
WDR11	5	0.01927	25	0.0017	24	0	1	2	2
LMO1	5	0.01959	26	0.0018	26	1	1	2	2
PRSS42	9	0.01963	27	0.0024	53	1	2	3	3
KIAA0895	5	0.01985	28	0.0018	25	0	0	2	2
NCALD	10	0.01996	29	0.0024	52	1	2	3	3
LINC00487	10	0.02044	30	0.0024	55	1	2	2	2
FBXL19	5	0.02146	31	0.0019	29	1	1	2	3
IL31	5	0.02172	32	0.0019	28	1	1	2	2
CNIH	5	0.02191	33	0.002	33	0	1	2	2
LOC439967	5	0.02196	34	0.002	32	1	1	2	2
CAPRIN1	5	0.02201	35	0.002	31	0	1	2	4
TTC30A	5	0.02205	36	0.002	30	1	1	2	3
RMI2	5	0.02283	37	0.0021	37	0	1	2	2
CREBL2	5	0.02286	38	0.0021	42	1	1	2	2
NCF4	5	0.02291	39	0.0021	41	0	1	2	3
SLC4A5	5	0.02298	40	0.0021	34	1	1	2	3
YAP1	5	0.02328	41	0.0021	36	1	1	3	3
BLNK	5	0.02343	42	0.0021	40	1	1	2	2
C10orf25	5	0.02364	43	0.0021	39	0	1	2	3
CKAP2	7	0.02377	44	0.0016	22	0	1	2	2
ZBTB44	5	0.02389	45	0.0021	38	0	1	2	2
AGAP4	10	0.02412	46	0.003	61	1	2	3	5
PCDHB2	5	0.0242	47	0.0021	35	1	1	2	2
ARNT	8	0.02456	48	0.0022	46	1	1	4	5
TEAD4	5	0.02458	49	0.0022	47	0	1	3	3
BRAF	9	0.02465	50	0.0034	64	1	2	4	7
IFIT3	5	0.0247	51	0.0022	48	1	1	2	2
THRAP3	5	0.02494	52	0.0022	45	1	1	2	3
SLC30A8	5	0.02508	53	0.0022	43	0	1	2	2
AWAT2	5	0.02513	54	0.0022	44	1	1	2	2
RPGRIP1L	5	0.0255	55	0.0023	51	1	1	2	2
WDR69	5	0.02584	56	0.0023	50	0	1	3	3
BCL6	5	0.02636	57	0.0024	54	0	0	2	3
EMB	9	0.02694	58	0.0039	80	1	2	2	2
INPP4B	5	0.02725	59	0.0025	58	0	0	2	2
TAF7	5	0.02728	60	0.0025	57	0	1	3	3
ATP8B4	5	0.02739	61	0.0025	56	0	0	2	2

Table 3.1 (Continued).

LRRC7	5	0.02832	62	0.0028	59	1	1	3	4
GTF2H5	5	0.02922	63	0.0031	62	1	1	2	2
LINC00326	4	0.03005	64	0.0029	60	0	0	2	2
LIN52	5	0.03016	65	0.0034	63	0	1	2	3
SALL1	5	0.03028	66	0.0034	65	0	0	2	2
PIK3C2G	9	0.0309	67	0.0048	103	0	0	2	2
JTB	5	0.03092	68	0.0035	66	1	1	2	2
TUBA4B	5	0.03096	69	0.0035	67	1	1	2	2
APOL3	8	0.03131	70	0.0039	81	0	0	2	3
PLAC1	10	0.03145	71	0.0049	104	0	0	2	4
ORC4	5	0.0316	72	0.0036	70	0	0	2	2
PBX2	5	0.03169	73	0.0036	77	1	1	2	2
BARD1	5	0.03174	74	0.0036	72	0	1	2	2
DAZ1	5	0.03215	75	0.0036	69	0	1	2	2
IL23R	5	0.03221	76	0.0036	68	1	1	2	2
PDCD4	5	0.03233	77	0.0036	75	0	1	2	2
FAM176A	5	0.03236	78	0.0036	73	0	1	2	2
SKA3	5	0.0326	79	0.0036	76	0	1	3	3
GABRA3	5	0.03266	80	0.0036	74	0	0	3	3
BHLHE22	5	0.03295	81	0.0036	71	0	0	2	2
PRKAB1	8	0.03297	82	0.0047	101	0	0	2	2
SSX2IP	5	0.03337	83	0.0038	78	1	1	3	3
TMBIM6	7	0.034	84	0.0044	90	1	1	2	2
WIPI1	5	0.03408	85	0.004	83	0	0	2	3
PARP10	5	0.03444	86	0.004	84	0	1	2	2
NCAM2	10	0.03459	87	0.0058	119	1	1	2	2
ZNF300	5	0.03475	88	0.004	82	0	0	2	2
GP5	10	0.03489	89	0.0058	118	0	1	2	4
CCDC59	5	0.03491	90	0.0041	86	0	0	2	2
RRAGC	5	0.03503	91	0.0041	85	1	1	2	3
OTOGL	4	0.03541	92	0.0038	79	0	0	2	2
SELV	5	0.03564	93	0.0042	87	0	0	2	2
HGF	5	0.03614	94	0.0043	88	1	1	2	2
YWHAG	5	0.03689	95	0.0044	95	0	0	2	2
MYLK3	10	0.03713	96	0.0063	134	0	1	3	4
TMEM236	5	0.03718	97	0.0044	91	0	0	3	3
LOC442075	19	0.03725	98	0.0087	172	0	2	3	3
AOC2	5	0.03767	99	0.0044	96	0	0	2	2
GSG2	9	0.0377	100	0.0069	140	0	1	2	3

Table 3.2. The top 100 genes from the PKC inhibitor screen ranked by 2nd best shRNA.

Gene	# Hairpins	NES	Gene rank	p-value	p-value rank	# Hairpins 500	# Hairpins 1000	# Hairpins 5000	# Hairpins 10000
STXBP1	5	0.002236	1	0.0002	2	2	2	2	2
TUBA4B	5	0.006327	2	0.0002	4	2	2	2	2
TEX30	5	0.007991	3	0.0002	3	2	2	2	2
RAB39A	5	0.009828	4	0.0005	5	1	2	2	2
H6PD	5	0.01017	5	0.0005	7	1	2	2	2
XKR7	5	0.01106	6	0.0007	11	1	2	2	2
IL12A	7	0.01165	7	0.0006	8	1	2	2	3
FAM104A	14	0.0125	8	0.001	18	2	2	3	3
CLDN10	4	0.01253	9	0.0005	6	1	2	2	2
REM1	5	0.0126	10	0.0007	12	1	2	2	3
TAF6L	3	0.01282	11	0.0001	1	0	1	2	2
PDZD7	10	0.0134	12	0.0007	9	2	2	2	2
NKX2-6	5	0.01352	13	0.0007	10	1	2	2	2
PRKACB	10	0.01406	14	0.0009	15	2	2	2	3
NRN1L	5	0.01449	15	0.0009	13	0	2	2	2
GJA4	5	0.01633	16	0.001	17	0	2	2	2
ARNT	8	0.01646	17	0.001	16	1	2	4	4
KCNMA1	5	0.01652	18	0.0011	19	0	2	2	2
TPO	5	0.01659	19	0.0011	20	0	2	2	3
KCNIP4	5	0.01693	20	0.0012	21	1	2	2	2
LOC440344	5	0.01829	21	0.0014	22	1	1	2	2
VTCN1	4	0.01846	22	0.0009	14	1	1	2	3
ZKSCAN2	5	0.01855	23	0.0015	23	0	1	2	3
SGK223	10	0.01861	24	0.002	34	1	2	3	3
COX14	10	0.0187	25	0.0022	41	1	3	3	3
TRIP11	5	0.01917	26	0.0016	24	1	1	2	2
FCRL1	5	0.01934	27	0.0018	30	0	1	2	2
RABGAP1L	5	0.01936	28	0.0018	26	1	1	2	2
ZNF211	5	0.0196	29	0.0018	27	0	1	2	2
LMNB2	5	0.01971	30	0.0018	29	0	0	2	2
AKR1D1	5	0.02019	31	0.0018	28	0	1	2	2
PTPRK	5	0.02057	32	0.0018	25	0	0	2	2
FAM174B	5	0.02153	33	0.0019	33	1	1	2	2
NLK	10	0.02154	34	0.0026	50	1	2	3	4
SULT1A1	5	0.02161	35	0.0019	31	1	1	2	2
PCDHB2	5	0.02165	36	0.0019	32	0	1	2	3
SYNC	5	0.02207	37	0.002	35	0	1	2	3
FBXL19	5	0.02239	38	0.0021	37	1	1	2	2
FGL1	9	0.02348	39	0.0032	60	0	2	2	3
STAG2	10	0.02358	40	0.0029	57	1	2	2	2
NIPA2	10	0.02361	41	0.0029	55	1	2	2	5
PLAC1	10	0.02379	42	0.003	58	0	3	4	4
CDC37	5	0.02409	43	0.0021	36	0	0	3	4
LRIF1	5	0.02411	44	0.0021	39	0	0	2	3
NEB	5	0.02416	45	0.0021	38	0	0	2	2
GNAI3	5	0.02458	46	0.0022	44	0	0	2	2
LPHN2	8	0.02473	47	0.0022	42	0	1	2	2
RPL22	5	0.02498	48	0.0022	40	0	0	2	2
G0S2	5	0.02519	49	0.0022	43	0	0	3	4
ZNF667	5	0.02538	50	0.0023	45	1	1	2	2
SDHB	9	0.02558	51	0.0034	66	1	2	2	2
LOC439967	5	0.02584	52	0.0023	48	0	1	2	2
PLA2G12A	5	0.02588	53	0.0023	47	0	0	2	2
SIPA1L1	5	0.02593	54	0.0023	49	0	0	2	2
SLC45A2	5	0.02603	55	0.0023	46	0	1	2	2
MAP3K6	10	0.02618	56	0.0035	72	1	2	4	4
STK17B	14	0.02679	57	0.0043	86	0	2	2	4
POTEE	9	0.02702	58	0.0039	78	1	2	2	3
TMEM176B	9	0.02765	59	0.0039	79	0	1	2	2
CTSL3	5	0.02775	60	0.0026	52	0	0	2	2
TM9SF3	5	0.02779	61	0.0026	51	0	0	2	2
SLC17A9	6	0.02847	62	0.0033	64	0	1	2	3

Table 3.2 (Continued).

ACAP3	5	0.0287	63	0.0028	53	1	1	4	4
SLC30A1	5	0.02874	64	0.0028	54	0	1	2	2
HOXA5	5	0.02914	65	0.0031	59	0	0	2	2
FAM188B	5	0.02959	66	0.0032	62	1	1	2	2
ST18	5	0.02966	67	0.0032	61	0	1	2	3
NUDT1	4	0.0298	68	0.0029	56	0	0	2	2
IL20RA	5	0.03009	69	0.0034	65	0	0	2	2
APLNR	8	0.03011	70	0.0033	63	0	1	2	2
ACTL9	5	0.03051	71	0.0035	69	0	1	2	2
C10orf81	5	0.03056	72	0.0035	70	0	0	2	2
HSD11B1L	5	0.03073	73	0.0035	71	0	1	2	2
METTL3	5	0.0311	74	0.0035	68	0	1	2	2
CHPT1	5	0.03111	75	0.0035	67	0	1	4	4
SLC22A24	5	0.03188	76	0.0036	73	0	0	2	3
ST14	5	0.03257	77	0.0036	75	0	0	2	2
ARHGAP39	5	0.03264	78	0.0036	74	0	0	2	2
PPM1F	5	0.03314	79	0.0037	76	0	0	2	2
LOC400499	5	0.03338	80	0.0038	77	1	1	2	3
GABRA3	5	0.03378	81	0.0039	80	0	0	2	2
ZNF512B	9	0.03388	82	0.0054	109	0	0	2	3
SPANXN5	10	0.03399	83	0.0058	113	1	1	3	3
KAT7	5	0.03399	84	0.004	83	0	0	2	2
COG5	5	0.03404	85	0.004	82	0	0	2	2
ZNF746	5	0.03481	86	0.004	81	0	0	2	2
ZCCHC3	5	0.03524	87	0.0041	84	0	0	2	2
QRSL1	5	0.03623	88	0.0043	85	0	0	2	2
INSL3	5	0.03675	89	0.0044	91	0	1	2	2
RPS6KB2	9	0.03715	90	0.0064	121	0	1	2	3
CDH4	5	0.03767	91	0.0044	88	0	0	2	3
PCDHGB2	5	0.0378	92	0.0044	93	0	0	2	2
FAM24B	5	0.03782	93	0.0044	90	1	1	2	2
SLC25A12	5	0.03825	94	0.0044	89	1	1	2	2
ANKHD1	10	0.03836	95	0.0064	120	0	0	2	2
PHF5A	5	0.03838	96	0.0044	92	1	1	3	4
SPATA7	5	0.03862	97	0.0044	87	0	0	2	2
CNTD2	5	0.03872	98	0.0045	94	0	1	2	2
ACTA2	5	0.03874	99	0.0046	96	0	0	2	4
MTHFD2	5	0.03888	100	0.0046	95	1	1	2	3

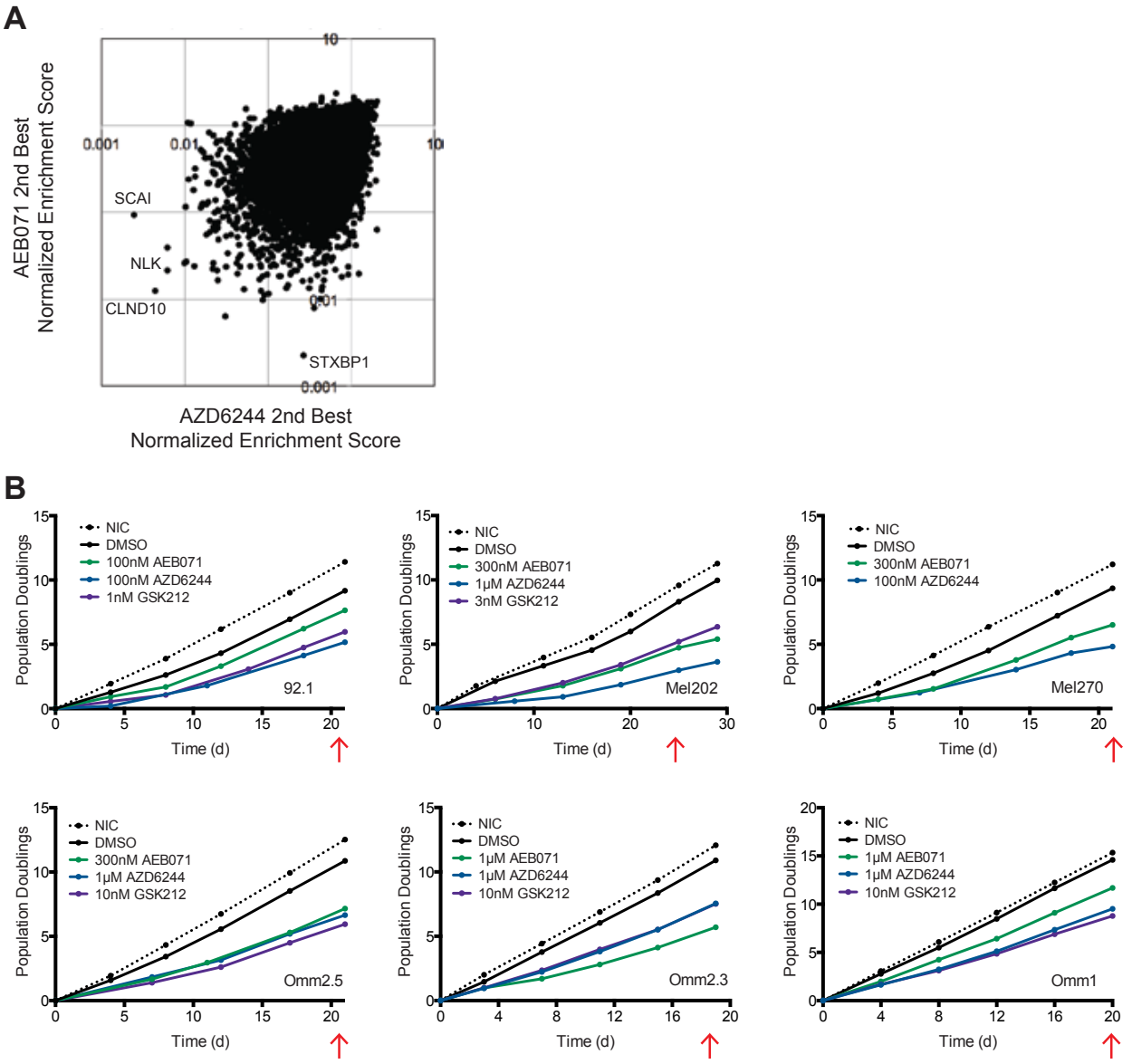

Figure 3.2. Primary screen comparison and validation growth curves. (A) Comparison of gene ranking scores for PKC inhibitor (AEB071) screen and MEK inhibitor (AZD6244) screen. Genes located on the diagonal have similar scores. Top hits are labeled. **(B)** Growth of non-infected cells (NIC), or those infected with custom shRNA library and cultured in the presence of indicated drug doses for 3-4 weeks. The red arrow indicates the time point that was sequenced and analyzed, in addition to an early time point at day 0. Data represent the average of 3 replicates per screen arm.

using RIGER 2nd best shRNA. This filtering step resulted in several genes dropping from the top 50 ranked enhancers, including the strongest PKC inhibitor enhancers (STXBP1 and TUBA4B), and several putative MEK inhibitor enhancers (NLK, MAP3K6, and POTEE; **Table 3.3**).

Candidate genes from drug enhancer validation screens

To confirm the primary screen findings, a custom lentiviral pool of ~600 shRNAs targeting the top 50 candidate MEK and PKC inhibitor enhancer genes was screened across six *GNAQ/11*-mutant UM cell lines (see **Table 3.4** for full list of genes and corresponding shRNAs). Genes with putative shRNA off-target effects were included based on the assumption that even seed effects could be used to validate the primary screen findings (**Figure 3.3**). A second MEK inhibitor, GSK1120212 (GSK212), was included in the validation studies alongside AZD6244 (MEK inhibitor) and AEB071 (PKC inhibitor). Drug concentrations that produced robust target inhibition were again determined empirically for each cell line and inhibitor. Library-expressing cells were cultured for 19-25 days, at which point the shRNAs were quantified by sequencing as described above (**Figure 3.2B**). One cell line, Mel270, and one replicate of the Omm2.5 GSK212 arm were removed from subsequent analysis due to poor replicate clustering. Candidate genes were again ranked using the RIGER 2nd best shRNA for each drug screen in each cell line. The average normalized enrichment score (NES) across the panel of cell lines was used to prioritize validated enhancer genes (**Figure 3.1E and F**). Here, the gene with the lowest average NES was considered to represent the most generalizable drug enhancer across the cell line panel. Genes for which the corresponding shRNAs showed no evidence of depletion during drug exposure included several negative control shRNAs targeting non-human transcripts such as GFP, LacZ, and Luciferase (**Figure 3.1E and F**).

Table 3.3. Genes that no longer score by 2nd best shRNA following removal of seed-nominated shRNAs.

MEK inhibitor screen		PKC inhibitor screen	
Genes gone from top 50	**Genes gone from 50-100**	**Genes gone from top 50**	**Genes gone from 50-100**
NLK	THRAP3	STXBP1	POTEE
MAP3K6	TUBA4B	TUBA4B	
POTEE	HGF	TAF6L	
ANKRD20A1		PRKACB	
GLB1L3		NLK*	
BAI3		FBXL19	
SLC12A6		STAG2	
LINC00487			
TTC30A			
NCF4			
ZBTB44			

* NLK was shifted to the 69th ranked gene.

Table 3.4. Genes and corresponding shRNA sequences included in the custom shRNA pool used for validation screens. Control genes are bolded.

Gene	# Hairpins	Hairpin Sequences
AGAP4	3	CACAAAGAGATGCAGATAGAT, CAGGAAGGTTATGTCATCTAT, CCCTCTCCTCATGCTAATAAA
AKR1D1	5	CAGCTAGATTATGTGGATCTT, CCCTAGAGATGAGAATGGCAA, CCGCTTTGTAGAATTGCTCAT, CCTTTGTTAAAGGATGCACTT, GCGATCATCCTGAATACCCAT
ANKRD20A1	5	CACAGGTCAAAGAAGGAAATA, GCACTGGACAAGGACAATAAT, GCAGAAGCTAAAGTGAATAAT, GCCTCATTTCTAGGAAATAAA, GCTGGCAGATTAACCCAACAA
ARNT	5	ACTAGGTCCCACAGCTAATTT, CATTGTCCAGAGGGCTATTAA, GAGAAGTCAGATGGTTTATTT, GCCTACACTCTCCAACACAAT, GGCTCAAGGAGATCGTTTATT
BAI3	4	ATAGCGGTTTGACGCTCAAAT, CCCGCATTACACCACAATCAA, TCGAGTATTTCCAACTAATTT, TTGGACAGATTTCGGGATATA
BLNK	5	CCATGATTCCAAACAACCATA, CCCATACCTCTGCCAAGATTT, CCCGTGGAAGATAATGATGAA, GCGATTTATTGAAGCAACAAA, TTCGCCAGAGGCGAGTATATA
BRAF	8	AGAACACTTGTGTGGTTAAAG, CAGCTTTCAGTCAGATGTATA, CCCAAATTCTCGCCTCTATTG, CCGCTGTCAAACATGTGGTTA, GAACATATAGAGGCCCTATTG, GCATAATCCACCATCAATATA, GTCATCAGAATGCAAGATAAA, TTACCTGGCTCACTAACTAAC
C10orf25	5	CCAACCTAGAAACTGCATACT, CCGTAAGAGATAGGAATTGTT, CCTGAAGTAATACAGTGGTTT, GAACCAAGGCTCAGAGAAGAA, GCCAGAGGTATGTCAACTAAA
CAPRIN1	5	CCTCAGCAGAACACTGGATTT, CGCCCTTCATTCTCTAACACT, GCCACGTTAGTGTCACAAATT, GCCAGTTATAACCAGAGCTTT, GCCGTTTCTAAGTACCAGGAA
CD33	5	GCAATGGGTTTATAGACATTA, GCCACAAACAAGCTAGATCAA, GCCCTGGCTATGGATCCAAAT, GCTATATTAACATCATCTTAG, TCACTCCTCGGTGCTCATAAT
CDC37	4	CCAGACAATCGTCATGCAATT, CGGCAGTTCTTCACTAAGATT, GACAGCCAATTACCTGGTCAT, GCCCATTCAAGTCTCTGCTTT
CKAP2	5	ATATGACTGCCACTACTAAAT, CCGCATTTGTTACTAACTGAA, CGACCTCCTATTAGAAGTCAT, GCAAGAGTTGTCCTCTACATT, TATGAGGCTGATACAACATAA
CLDN10	4	CCTGGGCTTCTTTGGTTCCAT, CGCTCTTTGGAATGAAGTGTA, CGGACAAAGTATCATGGTGGA, GCAGCAAGTTATCTGGTAGAA
CNIH	5	ACCTATATGGCATGATCTATG, CAGGACTCTATGACCCTACAA, CATCTGTCATGTCGATGATTA, CCCTCTTGGCATATCATATTT, TTCGCCATTTGGCACATTATA
COX14	5	CAACAGGACTAGAGCGTTGAT, CATGATGCTTCTCACTGTGTA, CCGAGTCTACCACTATTTCCA, GAAGAACAGAAGACCTCAGGA, GACCTTCTCTACCTCCATGAT
CREBL2	5	CAAAGTAAAGAAGCCCGGTAA, GAGTTGGTATCCAGTCGAGAA, GCAGAACAAATCTCAGCAGAA, GCTGGCTAATTGACAGTATTT, GCTGGGAAGACAGATGCTAAT
Elk1	3	CCTCTATTCTACCTTCACAAT, CCATCCATCTATGCTCCTGAA, CGGTACTACTATGATAAGAAT
ERLIN1	5	CCGAATAGAAGTGGTTAATAT, CGCATTTCTGAAATCGAAGAT, GCAGATTATGACAAGACCTTA, GCCCACATAGTGTGGAACAAA, GCGAAAGCAGATGCTGAATAT
FAM104A	5	CCTGTGTAACAGGAGAACAAT, CTACTTCCACATCAACCAGAC, GAAGTAGCAGAAACCCTGTCT, GAATGGCAACGAAGAAGACAA, GCAGTTGTTTACTTGTGGTTT
FAM174B	4	AGATGAGGACTCCACAGTATT, CACAGTATTCGACATCAAATA, CGTGGCTAGTTCACAAAGAAT, GAGGTTAAAGAAGACACGCAA
FBXL19	5	AGCCTCATGGAGTGTACAATC, CAGGGAACAAAGACCAGTTAC, CGCTGGATCGAGGATGTTAAA, GCGGGAGCTGTGTATCTGCAT, GCTGCTTCTCAAGGACAGCTA
FCRL1	5	CCAAGAGTTCACCTACCTCAA, CCATTCTCCATGGCACTATTC, CTGACGTGTAAGATGCCCTTT, GTTTATTCACTGGCGTACTAT, TTACATGGATCATCGAGTTTC
FGL1	5	CTGAACATATCCATGCGCAAT, GAAGTCCAGTTCCTTGATAAA, GACGATCTGATGGCAGTGAAA, GAGAATGAAGTCCAGTTCCTT, GTGGGCTAGTCACCAAAGAAT
G0S2	3	CACTGCATTGTCATGACATTT, CATTTCCAACACTGTGTGAAT, GCTGACATCTAGAACTGACCT
GFP	27	ACAACAGCCACAACGTCTATA, ACGTCTATATCATGGCCGACA, AGTACAACTACAACAGCCACA, AGTTCGTGACCGCCGCCGGGA, CAACAGCCACAACGTCTATAT, CCACATGAAGCAGCACGACTT, CCCGACCACATGAAGCAGCAC, CCTACGGCGTGCAGTGCTTCA, CGACCACATGAAGCAGCACGA, CGACGTAAACGGCCACAAGTT, CGGCATGGACGAGCTGTACAA, CGGGATCACTCTCGGCATGGA, CTACGGCAAGCTGACCCTGAA, CTATATCATGGCCGACAAGCA, CTCTCGGCATGGACGAGCTGT, GAACGGCATCAAGGTGAACTT, GACCACATGAAGCAGCACGAC, GACCACCCTGACCTACGGCGT, GCACGACTTCTTCAAGTCCGC, GCCACAACATCGAGGACGGCA, GCGACGTAAACGGCCACAAGT, GCGCGATCACATGGTCCTGCT, GTCGAGCTGGACGGCGACGTA, TACAACAGCCACAACGTCTAT, TCTCGGCATGGACGAGCTGTA, TGACCCTGAAGTTCATCTGCA, TGCCCGACAACCACTACCTGA
GJA4	5	CCACCTACAATGGGCTCTCAT, CTCTGCTTCTAAGAAGCAGTA, GCAGTCAGATTTCGAGTGTAA, GCCAAGATCTCGGTGGCAGAA, GCTCTGCAAGAGTGTGCTAGA
GLB1L3	5	CAAACACAGTGTTGCCTACAA, CGTGTTCATCAATGGACGTAA, CTTCTACTGTGGGACCTTGAA, GACAACCAACAAGAGCTTCAT, GACGTAACCTTGGGCGATATT
GNA11	5	CGACAGCGACAAGATCATCTA, CGACCTGGAGAACATCATCTT, GAACGTGACATCCATCATGTT, GCTCAACCTCAAGGAGTACAA, GCTCAAGATCCTCTACAAGTA
GNAI3	5	CTTAAAGGAATGTGGACTTTA, CTTCAATCATTCTCTTCCTTA, GCAGGAGTGATTAAACGGTTA, GCCCTCAGTGATTATGACCTT, GCTCAATGATTCTGCTTCATA
GNAQ	5	CCTCGGTTATTCTGTTCTTAA, CCTGGAATCCAGGAATGCTAT, CTATGATAGACGACGAGAATA, GACACCGAGAATATCCGCTTT, GCACAATTAGTTCGAGAAGTT
GNE	5	ACCTATGAAGAGAGGATTAAT, GATGACCGTTTCTTAACAATC, GCCAGTCACTATATCCACATT, GTACCCTTGTTCAAAGATATA, TGCCAAAGCAGCTACAATAAT
GPR182	5	AGGGCTGATGAACCTCTACAT, CCTCTCATCACAGTCTTCAAT, CCTGAATGCTGTAGTCCATTA, GAGCTTTCAGGCACACCATTT, TCAAAGCACTCGTGGTCAATT
GTPBP4	5	GCGTAGTCTTGGTGTTGACAT, GCGTCAGCATTTATCCCGTTT, GCTCATCGAGTGGAAACCAAA, GCTGGAGAGTATGACAGTGTA, TGTCGGAATCCCGTGCTTAAA
H6PD	5	ACCGGGTGGACCATTACTTAG, ACCTGGCTAAGAAGTACTTAT, ATGGCCGTCTGTTGGACTTTG, CTCCGTCCTCTTATCCCATAT, CTCTGGATCAGGCAGATATAA

Table 3.4 (Continued).

IL12A	5	CCTGTGCCTTAGTAGTATTTA, CCTGTTTACCATTGGAATTAA, CTTTAATAGAAGGGCAAATAT, GAGACCTCTTTCATAACTAAT, TGATACCTCTGATCAAGTATT
IL31	5	CCAAGTGATGATGTACAGAAA, CCATGAATGTAAACGCTTCAT, CCTGACTATTTCTCAACAGTT, GCATATCTCAAGACAATCAGA, GCTGAGATGTGAATTTGTGAA
KCNIP4	5	CCAGACAACACGTTGAAACAT, CCCAGTGGTGTTGTTAATGAA, CGTCGTCTCCTGCTATTCAAA, GATCCTTTACAGAGGATTTAA, GTTACCATAGATGAGTTCATT
KCNMA1	5	CCCAATAGAATCCTGCCAGAA, CCGAGCTGGAATTGGAAAGAA, GCGTAGTATTCAAACCAGTAT, GTCAAGATAGAGTCAGCAGAT, TGGCAGAAATACTACTTGGAA
KIAA0895	5	CCAGCAAATCTCCTAACACTT, CCAGGTATACTTGGATGGAAT, CCTCAGTTTGAGTATGCCAAT, GCAGTTCTAGTTCCTGACTTT, GTTACAGGGAATGGCATAGTA
KIF21A	5	CCCAATTCTTAGAGCTCTATA, CCCGTAATGAACTGAATGTTT, GCCAACATAATGCAGATGGAA, GCGTGTAAGAATTAAAGCCAT, GCTGTGATAATACTCTGTATT
lacZ	20	ACTCTGGCTAACGGTACGCGT, CCAACGTGACCTATCCCATTA, CCCGTCAGTATCGGCGGAATT, CCGTCATAGCGATAACGAGTT, CGACCACGCAAATCAGCGATT, CGATCGTAATCACCCGAGTGT, CGCGATCGTAATCACCCGAGT, CGCGCCTTTCGGCGGTGAAAT, CGCTAAATACTGGCAGGCGTT, CGGATTCTCTGGCCGTCGTAT, CGTCGTATTACAACGTCGTGA, CTCTGGCTAACGGTACGCGTA, GCCGTCGTATTACAACGTCGT, GCGATCGTAATCACCCGAGTG, GCGCTAATCACGACGCGCTGT, GCGTTGGCAATTTAACCGCCA, GTCGGCTTACGGCGGTGATTT, GTTCCGTCATAGCGATAACGA, TCGTATTACAACGTCGTGACT, TGTTCGCATTATCCGAACCAT
LINC00487	5	CCTCTGGAATAATGATTGAAT, GAACAATTTGAGAGTGAGAAA, GAAGTTCAAGATCAAGGTGTT, GCTGAAATTCAAAGCTGATAA, GTTGGAAGGAAGCTCTGAGAA
LMNB2	5	AGTTTGGCGAGGAGGATCTTT, CAAGAGGCTGCTACGTGATGT, GAGCTCTGACCAGAACGACAA, TAGCGTCAGCATCGAGGAGAT, TCGGCAATAGCTCACCGTTTA
LMO1	5	ATGAGGAAGGGCAGCTCAATG, CAACATGATCTTGTGTCAGAT, CACCTTTGAATCCCAAGTTCA, CGCTCTCCTGCCACATTAGAA, GCTGAAGGCATTGGACAAGTA
LOC439967	5	CCAACCAGTATCGACAATAAT, CCCTACCATGTGGTTATTCAT, CGAGGTTCCAAAGCCCAAATA, CTCACGTCAAAGGTCTGTCTT, GTCAGCTTGAACAAAGGCAAA
LOC440344	5	CGGTTCAAGGAGCCGTTTGAT, CTTTCTGTGATAGGCGTGTTT, GAAGGAGAAATTCCAAAGAAA, GCAGAGAGAAACCTGCCCAAA, TGAGGCTTCAACCTGTGTTAA
LPHN2	5	CCACAGGGAAATTGCATATAA, GCCAATGAACTGGCTAAACAT, GCGATTGCATGCCCAATATTT, GGCAATAGTGATGGTTATATA, GGCATATCTCTTCACTATATT
LRIF1	5	CCAAGATAATCTACAGCCTTT, CCCAACTCCTAAGCAGTATTT, CCTCTGGAGAAGGTTTCGATT, GCAGCTTATGAACAAAGTCAT, GCCAGCCAGTTCTTCAAACTA
LUCIFERASE	25	ACACTCGGATATTTGATATGT, ACGCTGAGTACTTCGAAATGT, ACTTACGCTGAGTACTTCGAA, AGAATCGTCGTATGCAGTGAA, AGTACTTCGAAATGTCCGTTC, AGTCAAGTAACAACCGCGAAA, ATCACAGAATCGTCGTATGCA, ATGTTTACTACACTCGGATAT, CAAATCACAGAATCGTCGTAT, CACTCGGATATTTGATATGTG, CACTTACGCTGAGTACTTCGA, CAGAATCGTCGTATGCAGTGA, CGCTGAGTACTTCGAAATGTC, CTTCGAAATGTCCGTTCGGTT, GAATCGTCGTATGCAGTGAAA, GAATGTTTACTACACTCGGAT, GAGTACTTCGAAATGTCCGTT, GCGCCATTCTATCCGCTGGAA, GCGGTTGCCAAGAGGTTCCAT, GCTGAGTACTTCGAAATGTCC, GTTGTGTTTGTGGACGAAGTA, TCACAGAATCGTCGTATGCAG, TCTACTGGTCTGCCTAAAGGT, TGAGTACTTCGAAATGTCCGT, TGTCCGGTTATGTAAACAATC
MAP3K6	5	CGTGGAGAAGATGCAGTATTA, GAGCTGAATGAGGGCATCATA, GATGAATGGAGAGGACAAAGG, GCTTCAGCATGACCAACAATG, GTTGGAGTTTGATTATGAGTA
MBTD1	5	CTCCTAGAACTATTCAGCATA, GCCACAGTAACTCGAATTATT, GCCCATTAATACATCATATTG, TCTCATGGAGCCACGTTTAAT, TGGATTTATGTGCATTGTTAA
MTHFD2	5	CACTCCTATGTCCTCAACAAA, CGAATGTGTTTGGATCAGTAT, CGAGAAGTGCTGAAGTCTAAA, GCAGTTGAAGAAACATACAAT, GCTGGGTATATCACTCCAGTT
NCALD	5	CCACAGAAAGAGAGACATCAT, CCTGGACGGAAATGGCTATAT, GAGATGGGACAATAGACTTTA, GCCCAAATTCTCAAGGTTGTT, GTGATCGTGCAGGCAATCTAT
NCF4	5	AGAGAGGACATAGCTCTGAAT, CGAGAGTGACTTTGAACAGCT, CGTGAAGATCCTCAAAGACTT, CGTGGGTGTGAAACAGGAGAT, GCTGAATTTCAAAGCTGGAGA
NEB	5	CCGGGAATACAAGAAGGGATA, GCCAGGTTAAATACCGAGAAA, GCCTAGAGTCTTTCTCCATTA, GCCTATAATCTGAGTGATAAT, GCGGACATCTTCAGTGAGAAA
NIPA2	5	CATTGCTATCAAGGAGCTGTT, CGAGAAAGCAATGAATGGCAA, GACCTCAGCACATGACGATTT, GACGATGTCATTGGTACTTTG, GTCATTCATGCTCCAAAGGAA
NKX2-6	5	CAATCCGCTTTAAGGAGGATA, CGACGCTACAAATGCAAGAGA, CGCATTTATACGCGCACACAA, GAACCGTCAATACGAACCAAA, GCCCTTTAAGAGAACCGTCAA
NLK	5	CGGATAGACCTATTGGATATG, GAAGGCGCTAAGGCACATATA, GCAACTGTGTTCTAAAGATTT, GCTCAGATCATGTCAAAGTTT, GTGGGTAGAGAGAATGAGTTT
NRN1L	3	CAAACCGATGTGACACCATAT, CGTCCGAATAACTTGCACACT, GAATCACTACAGCAAGAAGCT
PCDHB2	5	ACTAACTATGTCGACACTTAT, CTACGGATTAGGGACGTAAAT, GACAGTCTCGATGGCATAATA, TCCAGACATACACAGTAAATA, TGGCTCCTTTGTGGCCAATTT
PCIF1	5	ACGACATTCCTATCAGGTTAT, CATCCAGACCAATGCTGTCAT, CGATGTGATTTCGGACCCTTT, CGTGGTCTGCATCCGGTATAA, GCAAGGTGGTAGACAAAGGAT
PDZD7	5	CCAATCCCAACTACTCTGGAA, GACGCTGATGAACCTCTTCTT, GCCTACAAGGAGATGGTTTCT, GTATCCTGCCTACAAGGAGAT, GTCTCCCAAAGTGCTAGGATT
PLAC1	5	CAGTGAAGAAGAGCATACCCA, CCTTGTGTCTTCAGTGAAGAA, CGGTTCAGGACAAAGTCCAAT, GATTGGTCTCTTCACACAGAT, GCCATCTCACTTTCTTGATAT
POTEE	5	CCAGTTACTTTCTGACTACAA, GAGTATGCTGTTTCTAGTCAT, GCAATGGTGATGATGGATTAA, GCCAAAGCACTGCTCTTATAT, GCTCTGATAAAGGCCGTACAA
PRKACB	5	ACTCAGAATAATGCCGGACTT, CCTCCATTCACTAGACCTCAT, GAGCATACTTTGAATGAGAAA, GCCAACTGACTTAACAACATT, GCTCAGATAGTGCTAACATTC
PRSS42	5	CATCTACTAAGGATGTAATAA, CCGCTTGGCCTGTGAATATAA, CCGTTTCCATTACAGTGTCAA, GAGATCGGAGTGTCTATAATG, GGGATGGTCTGTGGCTATAAA
PTPRK	5	CATACTTTCTACGTGGCATTT, CCAATGAATATCAGGTAATAT, CTTAAGATCTCGGCGTATTAA, GCCGGGTTAAATGCTATAAAT, TAGATCCAGATACCGAATATG

Table 3.4 (Continued).

RAB39A	5	AGCTTCACAACGTCAAGTTAC, ATCTTGACGAGAGACATATAT, CGCAACTCAGTTGGTGGATTT, GCCTCCAAAGTGCTGGAATTA, TCAGCAAAGGATGCTACAAAT
RABGAP1L	5	ACCGGACCTGCATAGCCATTT, CGAGATATTCATCGTACATTT, CGTAATGAAGTAGAGGCTTTA, GCCTAAGGATAGAGATAAATT, TCCAATCTATAAGGTGTTATT
RAP1GDS1	5	CCCTTATACGACACAGTAAAT, GCAGAACTTGAGTCAAGTAAA, GCCAGTACAAACATTGCTGAA, GCTAACATCATAGCAGAAGTA, GCTGAACAATTGGGAAAGAAT
REM1	4	CAGATGATTGGTCTTCTGAAT, CCCTCAGAAACCCTCACAATA, GAGGCCGAGAAACTGGATAAA, GCTGTGGTGTTCGACTGTAAA
RFP	19	ACTACACCATCGTGGAACAGT, CAACGAGGACTACACCATCGT, CAGTTCCAGTACGGCTCCAAG, CCACTACGACGCCGAGGTCAA, CCGTAATGCAGAAGAAGACCA, CGAGTTCGAGATCGAGGGCGA, CGCGTGATGAACTTCGAGGAC, CGTAATGCAGAAGAAGACCAT, CTACAAGACCGACATCAAGCT, CTACACCATCGTGGAACAGTA, CTCAGTTCCAGTACGGCTCCA, GAACGGCCACGAGTTCGAGAT, GCTCCGTGAACGGCCACGAGT, GCTTCAAGTGGGAGCGCGTGA, GTAATGCAGAAGAAGACCATG, GTACGGCTCCAAGGCCTACGT, GTGGGAGCGCGTGATGAACTT, TCAGTTCCAGTACGGCTCCAA, TGCAGAAGAAGACCATGGGCT
RMI2	5	CGGACACCACTCAAACATTTA, GAACTGGAGGTAGAAGATTTA, GATGACAGACCTTTCTGATAA, GCAGGAAGACAGACTGTGTAA, GTAGAAGATTTACACAGGAAT
RPL22	5	CCCTGTAGAAGATGGAATCAT, CGAATTACGTTACTTCCAGAT, CGTGACTGGTTGCGCGTAGTT, GCACACAATTATGTCTGCTAA, GTTCTGAAGTTCACTCTTGAT
SCAI	5	CACAAGTATCTGCTCTACAAA, CCCAGATGAATAAACCAGGAA, CGGATGTTACAAGCTCTGGAA, GCGGATCCTGTAATGGTATTA, GTTAAGAGATTTGCCACAATA
SEC63	5	CCATTGAAGTTGGAAGTTCAT, CCCTTGAAGAAGATCAGCAAT, GCAAATGGAGTCGTTGGGAAT, GCCCTACTTCAAGAAATGGTT, GTGGTATCGTTTACGGTTATT
SGK223	5	CGGAGGATGACAGTGATCAAA, GAGTCGTCAGTGCCGGATAGA, GCACAACTGGATCGACATGAA, GTACCGCAAGTTCGATGAGTT, TCGTCTCCTCTCTGCACTAAG
SHOC2	5	CGTTTCTCTTGAGGTTCTTAT, GAGAACCTAGAAGAACTGTAT, GATGCTTGATTTACGGCATAA, GCAGTGCACTTGAAGAATTAA, GCTTAGCATTCGAGAGAACAA
SLC12A6	5	CCCATGAAGCAAAGCTGGTTT, CCGAAACTCAATGCTACGATT, CCGGTTTGCTTTGCTTCGATT, CGGACATAAGAAAGCTCGAAA, GCTAAATAACATGCGTGTCTA
SLC4A5	5	ACCGCTCCTTAGCTGACATTG, ATCGCAGGAATTGATGAATTT, CCCTATCAATATGGACTTCAA, CCCTCTTTACAGAGATGGATA, GCCAGCTTTATCATCAAATAT
SMAD9	5	CACGGCTTTGAAGTCGTGTAT, CCCTATCAACACTCAGACTTT, CGACCCTTCAAATAACAGGAA, CGTGTATGAACTGACCAAGAT, GCAGAAAGAAGTGTGCATTAA
STAG2	5	CCACTGATGTCTTACCGAAAT, CCTCTGCTGGATTTCTGTTTA, GAGAGGAAGCACTAACAGATA, GCAAGCAGTCTTCAGGTTAAA, GCAGTTCTTACAGCTTTGTTT
STXBP1	5	CCTCAGTTTCAGATACTTCAT, GACACTATTGAGGACAAACTT, GACTGTATGAAGCATTACCAA, GCAGAAACTAAAGCAGCAAAT, GCTCAGATGAAGAATCCTATA
SULT1A1	5	ACCAAGCGGCTCAAGAATAAA, GACATGAAGGAGAACCCGAAA, GAGAAGTTCATGGTCGGAGAA, GCTGAGGTGGGAGGATCATTT, TGCCCTTCCTTGAGTTCAAAG
SYNC	5	CAGAAGAACAAAGAGATGGAA, CAGCTGGAGGAAATGGAAGAA, CCAGAAACTTGGCAAGCAATT, GAAATGAAGGAGGCTCTGAGA, GCCAAATCTGTAACCCGGAAA
TAF6L	5	ATGACCTTCTCAAGTACTATC, CACGCAGAATAGCTCTCAGTT, CAGGCTGTGCTGGATGATTAT, GCACGGAGCCTATTTCGTAAT, TATCTAATGCCCAGGTCAAAG
TEAD4	5	CCTTTCTCTCAGCAAACCTAT, CGAGATCCAGGCCAAGCTAAA, GAAGAGACGTGTGTGCAGGAA, GAGACAGAGTATGCTCGCTAT, GCTGTGCATTGCCTATGTCTT
TEX30	5	CCACTGGATTGAGAAGGCAAA, GCACTGTTACAGTTGTATAAA, GCATCCCATCTTGCATCTCAT, GCTTCTGTAATGTGTCACATT, TGAAGACCTCTTTCGTTTAAA
tGFP	3	ACCGACAAGATCATCCGCAGC, ACCTGCTGAGCCACGTGATGG, GGACAGCCACATGCACTTCAA
TPO	5	CCCTACGAGTTAGGAGACGAT, CGACAAGATCCTGGACTTGTA, CGAGAGGGAAAGAACTCCTTT, GCTGAGCATCATTGCAAACAT, GTCACAGATGATGACCGCTAT
TRIP11	5	CCACAGATTGTCTGATTCGAT, CGGCAGCTGTACCTCTTATTA, GCAAAGGAACAAGAACTCAAT, GCAATCTACAAGTTACCGAAA, GCACAAGTTCAGCACAGCATT
TTC30A	5	CCACTTCTCAATCAGCAAATA, CGATTCTGTATAAGCCACATA, CTCTACAAGGAGGGACAGTAT, GCCAAAGGAAACTATGAGTTT, GCTCCTGAAGAGGCTTTCATT
TUBA4B	5	CATTCCTGATGGAGTGGCTTT, CCAACCTCAATCGCCTCATTA, CCACAGGCTTTAAGGTTGATA, GCATGGCACATACCGCCAGAT, GCCTTCATGGTGGACAACAAA
VTCN1	5	CATGAGTTCAAAGAAGGCAAA, CCTGACATCAAACTTTCTGAT, GAAGTGAATGTGGACTATAAT, GCTCTACAATGTTACGATCAA, GGAATGCTAACCTTGAGTATA
WDR11	5	ACGTGTTCGAAGATCTTATAA, CGCTTGGAAAGGTGATACATT, GAACGTGAATGCTTAAGATTT, GCAGTCGTATTCAGAGATAAA, GCAGTTTAAGAAGTGGCAGAA
XKR7	5	CCAGAGCATAGCGAACAAGAA, CGAACAAGAATGAACTCCTTA, GAAATGTTTGAAGGAGCCATT, GATTGACTTGCCTCGCAAGAA, GCAGAATCAACACACCTACTT
YAP1	4	CAGGTGATACTATCAACCAAA, CCCAGTTAAATGTTCACCAAT, GACCAATAGCTCAGATCCTTT, GCCACCAAGCTAGATAAAGAA
ZBTB44	5	CGAAGAAGATGTCCGGTCAAA, CGGTAGAAGAATGGCTGATTA, GAAACCAACCAGTTGACTCTT, GAATGGCTGATTATGTGACTT, GTCTAGATGCTGGACAAGAAA
ZKSCAN2	5	CCCAGTAAACACTGAAGGAAA, CCGCAAATGCTTCAGGCAATT, CGAAGCAACTACGTCAAGGAA, GATTTCGAGAACATCGGAGAA, GCGTTCTACAAGGAGATGGAT
ZNF211	5	CCACACAGTGTGTATCATTTA, GCCATAGCTCCAACCTTAAGA, GCCTGGTCTTGAGAGATATTT, GCTGTAAATCTAACCTCATTA, GCTTCAGTTCACATCGGAAAG
ZNF667	5	CAACCCTTATTCTGCATCTAA, CAACGAATGAGGCTATCAAAC, CGAATATCTCTCACACGACAT, CGCCAATCATTTCTTATTGAA, GTCGAAGCTTCTCTCTTAAAC
ZNF700	5	CTGGAGTGAAACCCTATGAAT, GAGTGACCAGAACATTGAATA, GAGTGTATTCTAGTTCCGTTT, GATGTTGCAATTCCCTTCGAT, GCCAAGTCATTTCAAACACAT

These validation experiments confirmed the drug enhancer effects of shRNAs corresponding to several candidate genes identified through our initial screens. In particular, these shRNAs were significantly depleted in the presence of drug across several independent UM cell lines (**Figure 3.1E and F**). The most generalizable MEK and PKC inhibitor enhancer genes encoded multiple distinct protein types, including kinases, phosphatases, and metabolic enzymes. Enzymes are particularly amenable to small molecule inhibition, suggesting that these hits may represent novel or pre-existing drug targets. The top-ranking shRNAs from the primary screens (e.g., those directed against SCA1 and STXBP1) validated in the originally screened cells (Omm2.3), but were not strong enhancers across the cell line panel (**Figure 3.1E and F**).

To prioritize targets for further study, several filtering steps were applied (**Figure 3.3**). Candidate genes were first required to reach an average NES of less than 0.33. This threshold was selected based on the score distribution across the gene set; 0.33 represented one standard deviation below the mean of the MEK inhibitor data. Next, we excluded genes that were not expressed in UM based on RNA sequencing of UM cell lines (data not shown). Finally, genes for which the corresponding shRNAs did not pass the miRNA seed effect analysis were excluded from further analysis. Overall, five PKC and five MEK inhibitor enhancer genes both fit our prioritization criteria and showed enhancer phenotypes in at least 3 UM cell lines—these were considered validated drug enhancer genes. Interestingly, GNA11 shRNAs emerged as enhancers to growth suppression by both PKC and MEK inhibitors. GNA11 was not a candidate gene from either primary screen; rather, it was included in our validation experiments as a positive control for essentiality. The fact that *GNA11* knockdown conferred an enhancer phenotype despite its known essentiality in *GNA11*-mutant UM cells (45) suggests that its knockdown (and perhaps that of other enhancer genes) may have been partial. In this case, co-suppression of PKC and MEK—known downstream effectors of oncogenic GNA11 signaling—would be expected to produce an enhancer phenotype. GNA11 also scored as an enhancer in

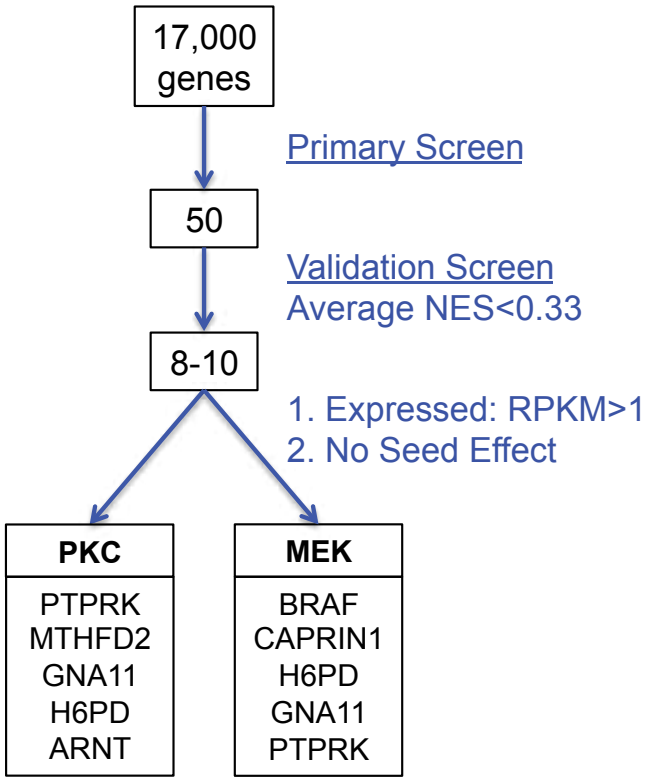

Figure 3.3. Schematic of enhancer gene selection steps. The top 50 genes from the primary screen were tested in validation screens across a panel of cell lines. Generalizable enhancers were nominated based on an average normalized enrichment score (NES) threshold of less than 0.33. These genes were then filtered based on whether they were expressed in UM cell lines according to RNA sequencing and finally whether they passed the analysis of off-target seed effects.

some *GNAQ*-mutant cell lines treated with PKC and MEK inhibitors (**Figure 3.1E and F**). These data suggest that GNA11 may also confer a dependency in *GNAQ*-mutant settings.

The overarching goal of these drug enhancer screens is to identify possible UM targets that might be co-inhibited together with MEK or PKC inhibition. Protein targets for which therapeutics are already in clinical use or development were considered high priorities in this regard. Toward this end, the top PKC inhibitor enhancer genes to emerge from our validation studies included PTPRK and MTHFD2. *PTPRK* encodes a tyrosine phosphatase that has been proposed to directly dephosphorylate CD133 (163) and STAT3 (164), and to regulate β-catenin activity (165, 166). Although the specific function of PTPRK is not well understood, it has been implicated as a putative tumor suppressor in several cancer contexts (reviewed in 167). Our data raise the possibility that PTPRK inhibition may augment the effects of PKC inhibition. However, small molecule inhibitors of PTPRK do not currently exist.

MTHFD2 encodes the enzyme methylenetetrahydrofolate dehydrogenase (NADP+ dependent) 2, methenyltetrahydrofolate cyclohydrolase, a member of the mitochondrial folate pathway. The folate pathway is involved in one-carbon metabolism and has both cytoplasmic and mitochondrial functions that contribute to nucleotide biosynthesis, the generation of methyl donors, and glycine production (168). The cytoplasmic folate pathway has been a long-standing target for cancer therapy (169). The FDA-approved drug methotrexate targets dihydrofolate reductase (DHFR), a component of the cytoplasmic folate pathway. Although compartmentalized, the cytoplasmic and mitochondrial folate pathways are interconnected; the cytoplasmic pathway provides 1C units predominately in the form of serine or glycine to fuel the mitochondrial reactions, while the mitochondrial pathway generates formate to be used by the cytoplasmic enzymes (170). The mitochondrial pathway, which consists of the enzymes SHMT2, MTHFD2, MTHFD1L, AMT, and ALDH1L2, has only recently been implicated in cancer: increased expression of MTHFD2 is associated with breast cancer metastasis (171, 172), many cancer cell lines require MTHFD2 for growth (172), and SHMT2 knockdown results

in glycine auxotrophy in several cancer cell lines (173). Given the translational relevance of the folate pathway, MTHFD2 was chosen for further study.

To expand upon our screening findings, we first determined the extent of drug sensitization when MTHFD2 knockdown and PKC inhibition were combined. Mock-infected cells or those expressing control or MTHFD2 shRNAs were plated at low density and treated with DMSO or PKC inhibitors for 2 weeks. Analysis of cell proliferation indicated a partial dependency on MTHFD2 in cells treated with DMSO and drug enhancement in PKC inhibitor treated cells (**Figure 3.4A and C**). The magnitude of growth impairment was consistent with the extent of MTHFD2 knockdown (**Figure 3.4A-D**). These data confirm that MTHFD2 is a PKC inhibitor enhancer and suggest that it also represents a partial dependency in UM cells.

Given the metabolic link between the cytoplasmic and mitochondrial folate pathways (170), we next hypothesized that inhibition of the cytoplasmic pathway using methotrexate might synergize with PKC inhibition in UM cells. Co-treatment with methotrexate did not further sensitize UM cells to PKC inhibition (**Figure 3.4E**). These data suggest that the cytoplasmic and mitochondrial folate pathways are not entirely inter-dependent in UM cells.

BRAF suppression sensitizes UM cells to MEK inhibition

The top MEK inhibitor sensitizer was BRAF (**Figure 3.1F**). BRAF encodes one of three isoforms of RAF kinase, which is situated directly upstream of MEK in the MAPK pathway. A second member of the MAPK pathway, the C-RAF-scaffold protein SHOC2, also sensitized cells to MEK inhibition (**Figure 3.1F**). These data may underscore the importance of MAPK signaling for UM cell proliferation. Moreover, they raise the possibility that inhibition of MEK alone may be insufficient to fully extinguish MAPK pathway activity in UM cells.

Since multiple therapeutics that target the MAP kinase pathway are clinically available (or in clinical trials), we sought to explore whether combinatorial inhibition of RAF together with MEK inhibition might prove synergistic in UM cells. To test this, we first determined the extent

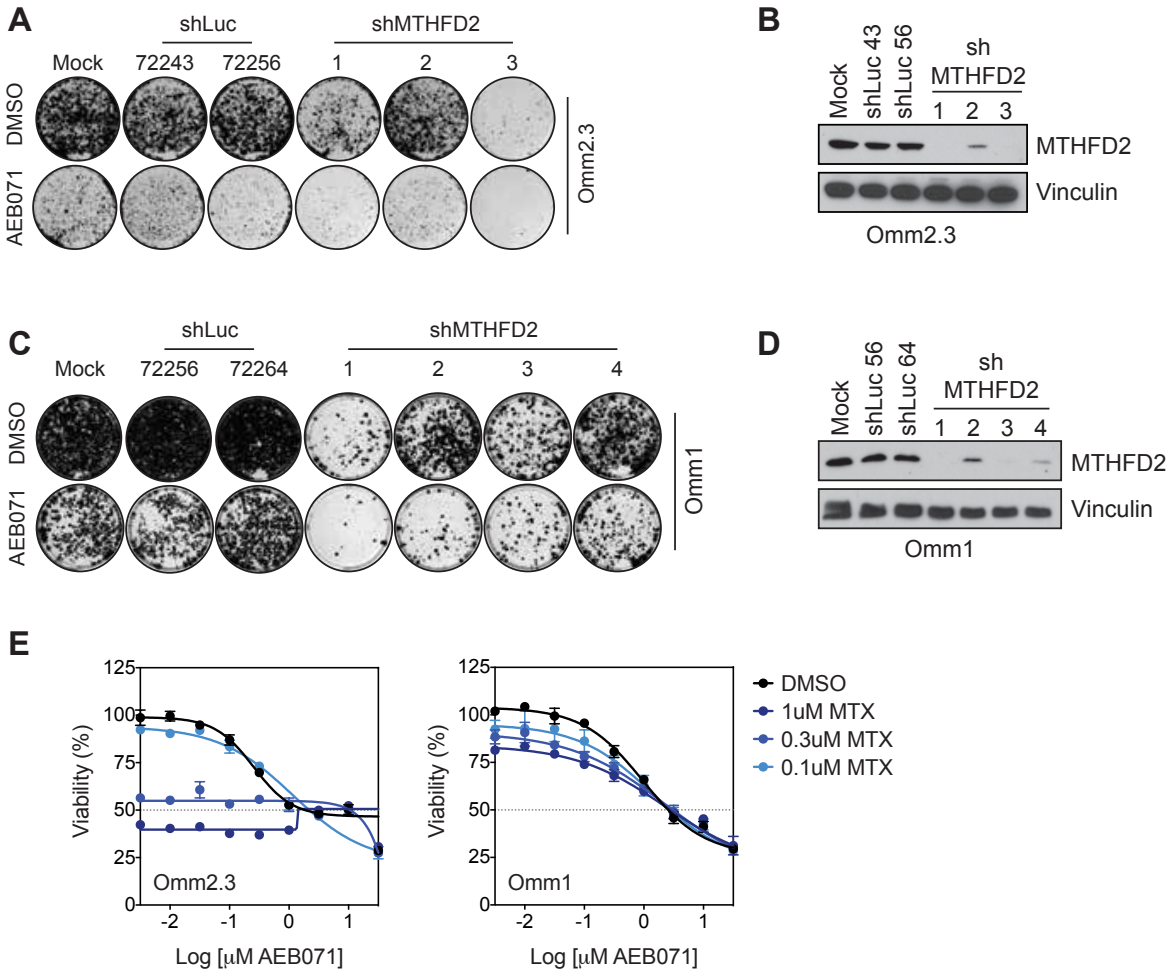

Figure 3.4. MTHFD2 is a novel dependency in UM cells. (A) Mock infected or indicated shRNA-expressing Omm2.3 cells were treated with DMSO or PKC inhibitor (0.3μM AEB071) for 2 weeks, and then stained with crystal violet and imaged. **(B)** Immunoblot analysis confirming MTHFD2 knockdown in cells as in (A). **(C)** As in (A), but for Omm1 cells treated with 1μM AEB071. **(D)** As in (B), but for Omm1 cells. **(E)** Indicated cells were treated with 9 doses of PKC inhibitor AEB071 in combination with indicated doses of methotrexate (MTX) for 4 days and cell viability was determined using MTS. Error bars represent SD.

to which concomitant BRAF knockdown might affect sensitivity to MEK inhibition in pharmacologic growth inhibition experiments. UM cells were infected with control or BRAF-targeting shRNAs and then treated with MEK inhibitors for 5 days. The relative sensitivity of shRNA-expressing cells was then determined by cell viability curves. Omm1 cells expressing BRAF shRNAs demonstrated a 10-fold reduction in the AZD6244 MEK inhibitor dose at which 50% growth inhibition was achieved (GI50) (**Figure 3.5A**). Sensitization to the MEK inhibitor GSK212 was more modest (**Figure 3.6A**). Two additional cell lines also showed a similar pattern of reduced AZD6244 GI50 values following BRAF knockdown, although the 92.1 cell line showed only a modest trend towards increased drug sensitivity (**Figure 3.5D; Figure 3.6E**). Drug enhancement with the GSK212 MEK inhibitor was less profound than AZD6244 in these cell lines as well (**Figure 3.6C and E**). MEK inhibitor sensitivity was also tested using colony-formation assays over a 10-16 day treatment regimen, a context that more closely mirrors our screening approach. Cells expressing BRAF shRNAs exhibited less growth in the presence of MEK inhibitors than control cells (**Figure 3.5B and E; Figure 3.6B and D**). These data confirmed the results from our enhancer screens, and endorsed the notion that concomitant BRAF knockdown sensitizes *GNAQ/11*-mutant UM cells to MEK inhibition.

To determine the effect of combined MEK inhibition and BRAF knockdown on MAPK pathway activity, we assessed the levels of phospho-ERK following treatment of shRNA-expressing cells. Combined BRAF knockdown and MEK inhibition resulted in additional reductions in ERK phosphorylation (**Figure 3.5C and F; Figure 3.6F**). These data suggest that reduced proliferation with this combination may be due to enhanced blockade of MAPK signaling.

We next sought to assess the effect of combined BRAF and MEK inhibition using an orthogonal genetic ablation method. To accomplish this, we generated UM cell lines that stably express both Cas9 and short guide RNAs (sgRNAs) targeting GFP (control) or BRAF. BRAF sgRNA-expressing Omm1 cells were more sensitive to MEK inhibition than control cells in

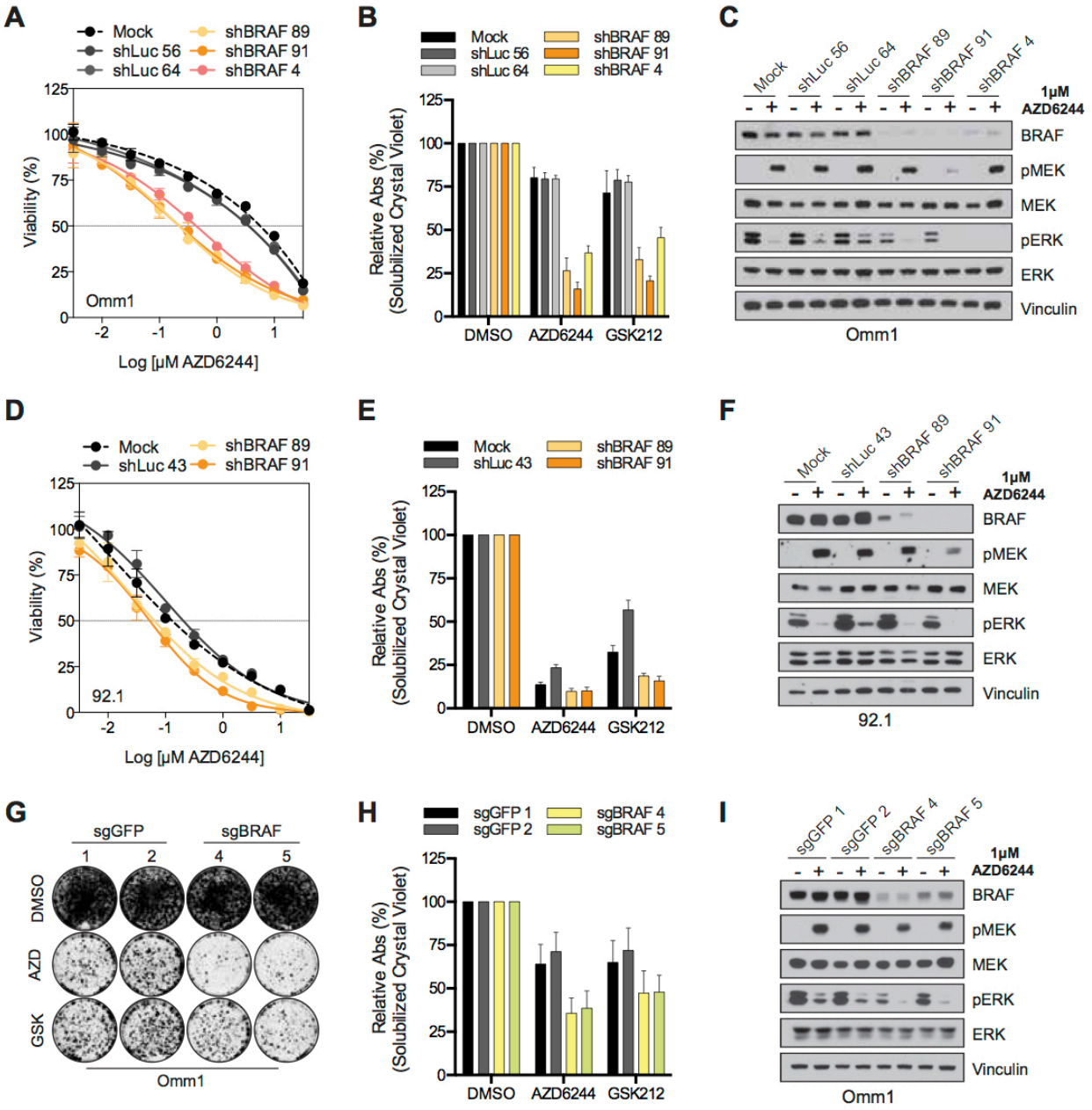

Figure 3.5. Suppression of BRAF expression sensitizes UM cells to MEK inhibition. (A) Mock-infected or indicated shRNA-expressing Omm1 cells were treated with 9-doses of MEK inhibitor AZD6244 for 5 days and cell viability was determined using MTS. Error bars represent SD. **(B)** Cells as in (A) were treated with DMSO or MEK inhibitors (1μM AZD6244, 10nM GSK212) for ~2 weeks, after which cells were stained with crystal violet, imaged, and then solubilized and quantified by Abs595. Data represent mean ± SEM of 4 independent experiments. Controls for Omm1 DMSO-treated cells only are the same as those depicted in Figure 3.4C. **(C)** Immunoblot analysis of shRNA-expressing cells following overnight treatment with DMSO or MEK inhibitor. **(D-F)** As in (A-C), but for 92.1 cell line. **(G)** Omm1 cells expressing Cas9 and GFP or BRAF targeting sgRNAs were treated with DMSO or MEK inhibitors (1μM AZD6244, 10nM GSK212) for ~2 weeks, and then stained with crystal violet and imaged. **(H-I)** As in (B-C), but for Omm1 sgRNA-expressing cells as in (G).

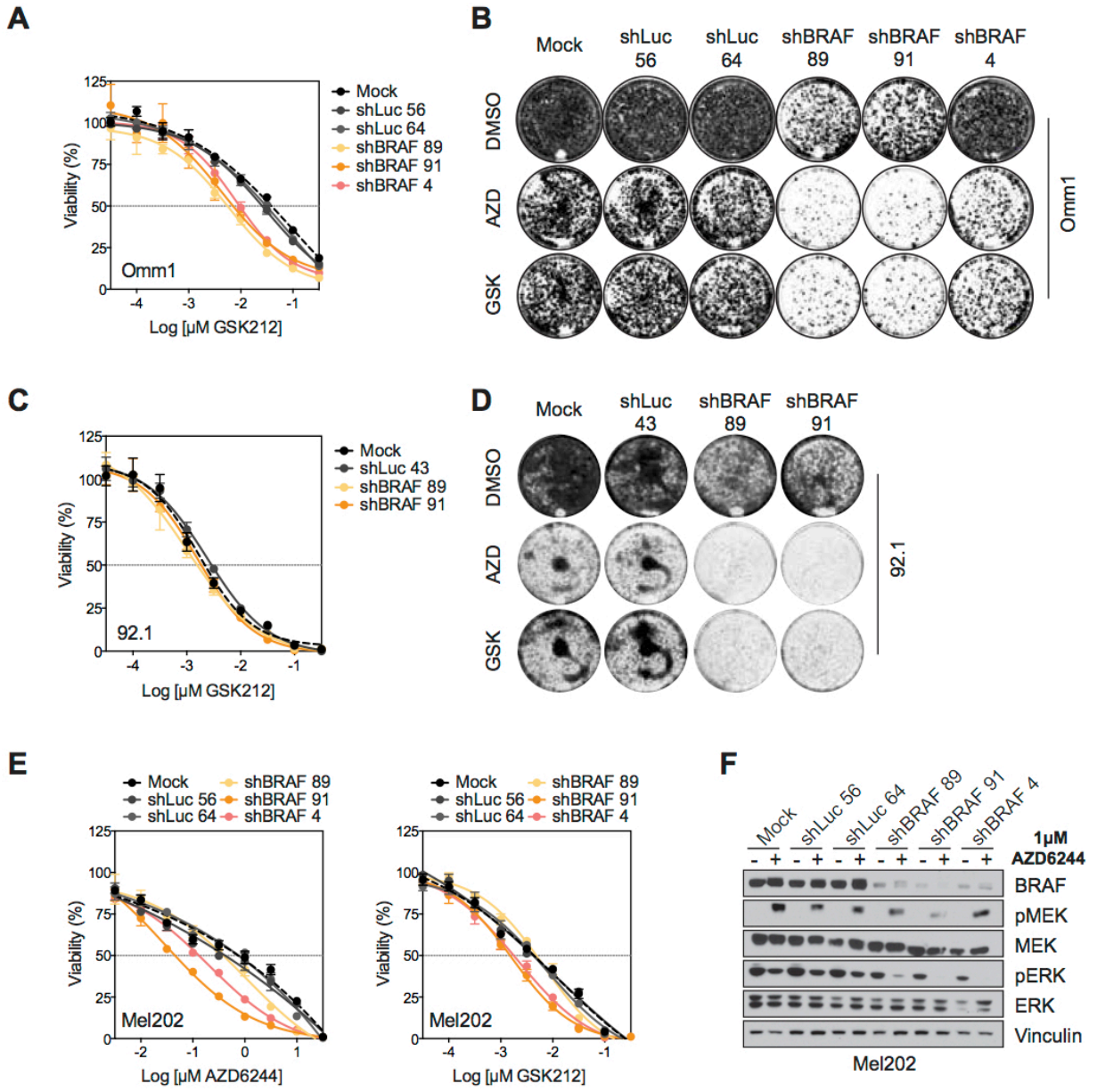

Figure 3.6. BRAF shRNAs further sensitize UM cells to MEK inhibition. (A) Mock infected or indicated shRNA-expressing Omm1 cells were treated with 9-doses of MEK inhibitor GSK212 for 5 days and cell viability was determined using MTS. Error bars represent SD. **(B)** Representative crystal violet images from the quantification presented in Figure 3.5B. Omm1 cells were treated with DMSO or MEK inhibitors (1μM AZD6244, 10nM GSK212) for 12 days, and then stained with crystal violet and imaged. **(C)** As in (A), but for 92.1 cells. **(D)** Representative images from Figure 3.5E. 92.1 cells were treated with DMSO or MEK inhibitors (0.1μM AZD6244, 1nM GSK212) for 11 days, and then stained with crystal violet and imaged. **(E)** As in (A), but for Mel202 cell line treated with AZD6244 (left) or GSK212 (right). **(F)** Immunoblot analysis of cells as in (E) following overnight treatment with DMSO or MEK inhibitor.

colony-formation assays (**Figure 3.5G and H**). Combined BRAF knockout and MEK inhibition resulted in lower phosphorylation of ERK when compared to controls (**Figure 3.5I**). These data indicate that the drug enhancer phenotype identified by RNAi was also detectable using CRISPR-based genome editing in Omm1 cells. However, in a second cell line (Omm2.3), we observed no incremental effect with combined BRAF knockout and MEK inhibition (**Figure 3.7A and B**). This result was somewhat surprising given that Omm2.3 cells were used in the primary drug enhancer screens described above. This apparent discrepancy could relate to either incomplete BRAF knockout by CRISPR in Omm2.3 cells (**Figure 3.7C**) or signaling rewiring that may conceivably occur during the genome editing process. Alternatively, single-agent MEK inhibition may have been sufficient to suppress both ERK signaling and proliferation to near maximal levels in Omm2.3 cells under these experimental conditions (**Figure 3.7**).

Combined RAF/MEK or MEK/ERK inhibition is synergistic in UM cells

The RNAi and CRISPR data suggest that further suppression of the MAPK pathway beyond single-agent MEK inhibition may augment growth inhibition in UM cells. We hypothesized that improved pathway suppression might be achieved by inhibiting the pathway at multiple nodes, and in particular that combined pharmacologic inhibition of the MAPK pathway might prove synergistic in UM cells. To test this hypothesis, we first performed combinatorial cell growth inhibition studies *in vitro* using pan-RAF and MEK inhibitors.

For these experiments, we chose to test pan-RAF inhibitor tool compounds instead of the RAF inhibitors currently in clinical use, because the latter have been shown to induce paradoxical activation of the MAPK pathway in BRAF wild type cells containing active Ras (174-176). Similar paradoxical activation of MEK/ERK signaling has been observed in UM cells (78). Immunoblot analyses demonstrated increased phospho-ERK levels upon RAF inhibitor treatment in *GNA11*-mutant cells, confirming the previously described paradoxical activation (**Figure 3.8A**). In contrast, $BRAF^{V600E}$-mutant UM cells demonstrated a dose-dependent

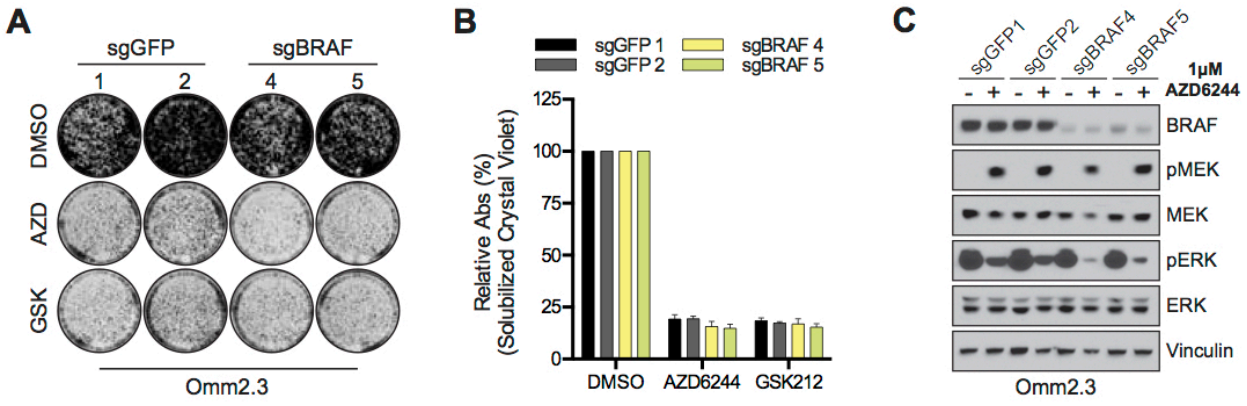

Figure 3.7. Sensitivity of Omm2.3 cells to MEK inhibition following BRAF knockout. (A) Omm2.3 cells expressing Cas9 and GFP or BRAF targeting sgRNAs were treated with DMSO or MEK inhibitors (1μM AZD6244, 10nM GSK212) for ~2 weeks, and then stained with crystal violet and imaged. **(B)** Crystal violet stains from (A) were solubilized and quantified by Abs595. Data represent the mean ± SEM of 3-5 independent experiments. **(C)** Immunoblot analysis of cells as in (A) following overnight treatment with DMSO or MEK inhibitor.

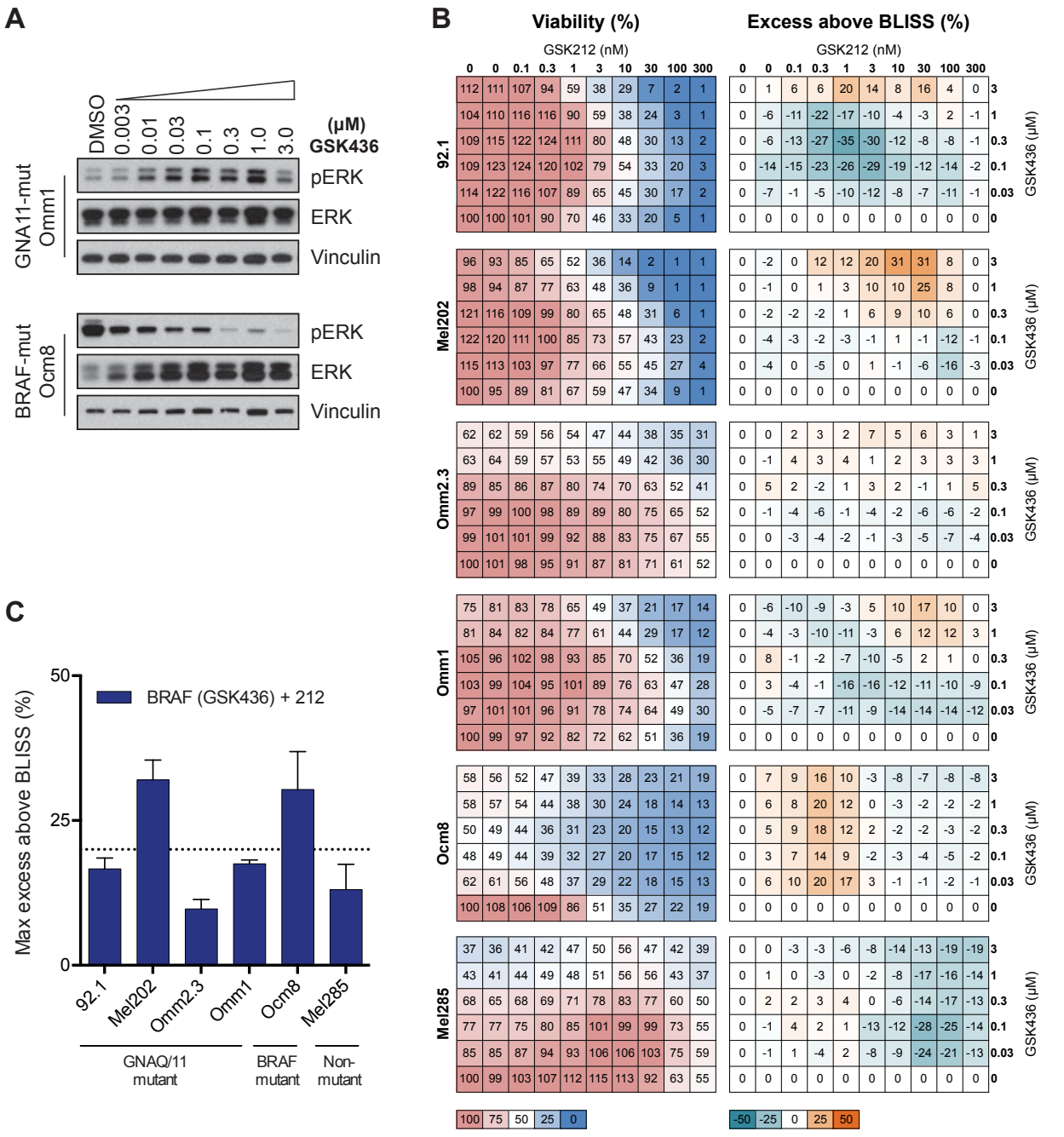

Figure 3.8. BRAF inhibition results in paradoxical pathway activation in *GNAQ/11*-mutant cells. (A) Immunoblot analysis of indicated cells treated overnight with vehicle or increasing doses of RAF inhibitor GSK436. **(B)** Cells were treated with indicated doses of MEK inhibitor GSK212 and RAF inhibitor GSK436 for 4 days and cell viability was determined using MTS (left). Percent excess above BLISS was calculated for each drug combination (right). **(C)** Maximal percent excess above BLISS from (B) is shown. Data represent the mean ± SEM of 3-4 independent experiments.

decrease in MAPK activity, as expected (**Figure 3.8A**). We then tested cell viability following combined treatment with the MEK inhibitor GSK212 and the RAF inhibitor GSK436 across a panel of UM cell lines (*GNAQ/11*-mutant, *BRAF*-mutant, and non-mutant) (**Figure 3.8B and C**). Synergy was determined using the percent excess above BLISS calculation, which determines whether the effect of the combination is greater than what would be expected if it were additive (177). In *GNAQ/11*-mutant cells, synergy was observed only at the highest RAF inhibitor doses (GSK436 ≥ 1μM), while antagonism was observed at doses under 1μM (**Figure 3.8B**). Antagonism is represented by negative values, indicating that the combination does not achieve the percent growth inhibition expected for additivity (177). Our subsequent combination studies therefore focused on pan-RAF inhibitors in order to mitigate the paradoxical activation observed in *GNAQ/11*-mutant settings.

Next, a panel of UM cells, including *GNAQ/11*-mutant, *BRAF*-mutant, and non-mutant lines, were co-treated with pan-RAF inhibitors and MEK inhibitors. Synergy was observed in all UM cell lines treated with the pan-RAF inhibitors AZ628 or MLN2480 in combination with the MEK inhibitor GSK212 (**Figure 3.9A and B**). The *BRAF*-mutant cell line, Ocm8, demonstrated synergy at lower drug doses than *GNAQ/11*-mutant (Mel202 and Omm1) and non-mutant (Mel285) cells, consistent with the stronger sensitivity of these cells to MAPK pathway inhibitors (**Figure 3.9A**). Interestingly, the highest percent excess above BLISS was observed in the wild type cell line, Mel285, suggesting that UM cells depend on MAPK signaling regardless of mutational presence.

We next sought to determine the effect of combined inhibition of RAF and MEK for a longer time course. Cells co-treated with pan-RAF/MEK inhibitors for up to 2 weeks demonstrated minimal outgrowth when compared to single agent treatments (**Figure 3.9C**). These data confirm our short-term experiments and suggest that combination therapy could delay the emergence of resistant populations, although additional experiments are necessary to confirm this observation.

Figure 3.9. Combined pan-RAF and MEK inhibition is synergistic in UM cells. (A) Cells were treated with indicated doses of MEK inhibitor GSK212 and pan-RAF inhibitor AZ628 for 4 days and cell viability was determined using MTS (left). Percent excess above BLISS was calculated for each drug combination (right). **(B)** Maximal percent excess above BLISS from (A) is presented and expanded to indicated cell lines and drugs in combination with MEK inhibitor GSK212. Data represent mean ± SEM of 3-5 independent experiments. **(C)** Cells were treated with MEK inhibitor (1 or 10nM GSK212), pan-RAF inhibitor (0.3μM AZ628), or the combination for 2 weeks and then stained with crystal violet and imaged. **(D)** Immunoblot analysis of cells treated overnight with vehicle, pan-RAF inhibitors (1μM MLN2480 or AZ628), MEK inhibitor (30nM GSK212), or indicated combinations. **(E)** Immunoblot analysis of 92.1 cells treated overnight with indicated doses of pan-RAF inhibitor AZ628, MEK inhibitor GSK212, or combinations.

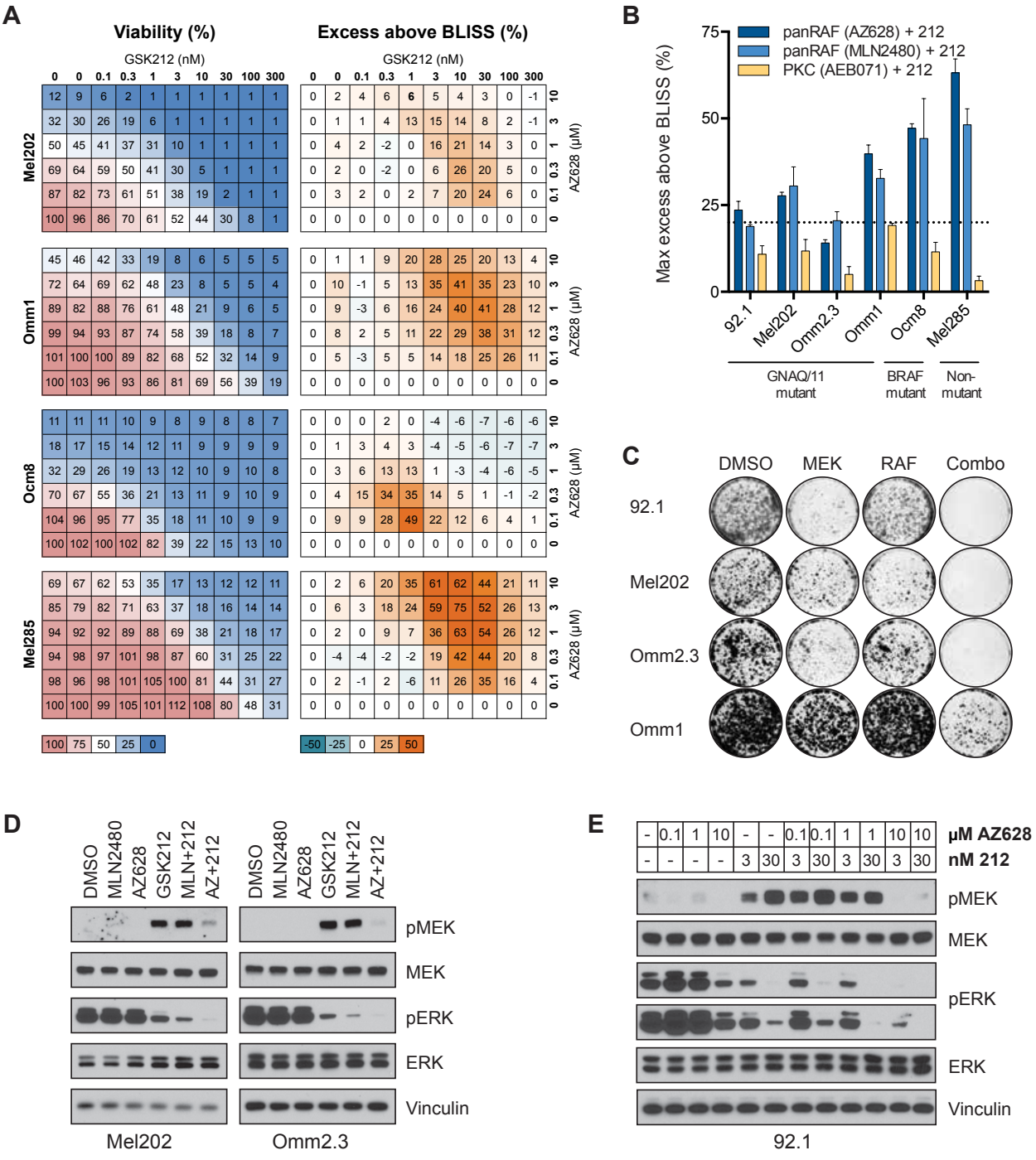

Figure 3.9 (Continued).

To determine the effect of co-treatment with pan-RAF and MEK inhibitors on MAPK signaling, immunoblot analysis of drug treated cells was performed. Treatment with both MLN2480 or AZ628 and GSK212 together resulted in reduced phospho-ERK levels when compared to single agent treatments (**Figure 3.9D and E**). Here, single agent AZ628 did not reduce phospho-ERK levels until doses upwards of 10μM were applied; however, 1μM AZ628 effectively suppressed phospho-MEK induced by GSK212 and further decreased phospho-ERK when combined with GSK212 (**Figure 3.9D and E**). These data suggest that the impaired viability with combination treatments may be due to stronger blockade of MAPK signaling.

We also sought to determine whether the anti-proliferative effects of our pan-RAF inhibitors resulted from RAF inhibition as opposed to possible off-target effects of the tool compounds. Here, we tested a constitutively active version of MEK (MEKDD) that remains sensitive to MEK inhibition, but is resistant to RAF inhibition in $BRAF^{V600E}$-mutant contexts (178). MEKDD was expressed under an inducible promoter such that drug treatment coincided with induction of plasmid DNA expression. Doxycycline treatment induced over expression of MEKDD and enhanced MAPK signaling through phospho-ERK (**Figure 3.10A**). MEKDD expression conferred resistance to the pan-RAF inhibitor AZ628 in three UM cell lines, confirming the on-target inhibition of RAF (**Figure 3.10B-D**). Cell lines with higher levels of MEKDD and phospho-ERK showed greater resistance (**Figure 3.10**). These results indicated that a substantial proportion of the pan-RAF inhibitor effect resulted from inhibition of MAPK signaling.

Given that combined inhibition of RAF and MEK was synergistic in UM cells, we next sought to determine whether co-targeting of ERK together with MEK would also be synergistic. BLISS analysis revealed synergy with combined inhibition of MEK and ERK in UM cells (**Figure 3.11A and B**). To assess whether MEK/ERK co-treatment further reduced pathway activity, the levels of phospho-ERK were assayed following drug treatment. Co-treatments using

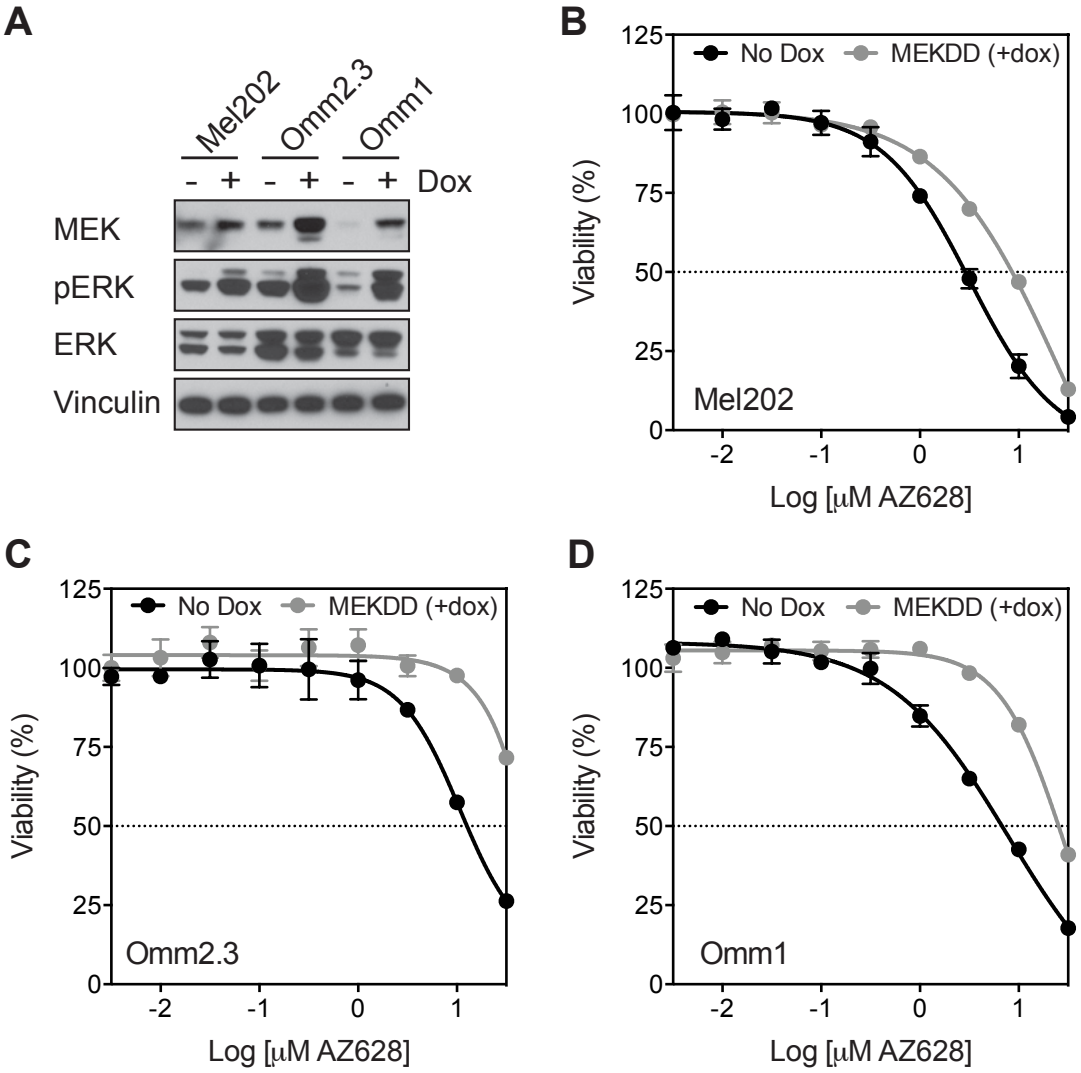

Figure 3.10. MEKDD confers resistance to pan-RAF inhibition in UM cells. (A) Immunoblot analysis shows induction of MEKDD expression and phospho-ERK levels following 24h dox treatment. **(B)** Mel202, **(C)** Omm2.3, **(D)** Omm1 cells were co-treated with 9 doses of pan-RAF inhibitor AZ628 and dox for 4 days and cell viability was determined using MTS.

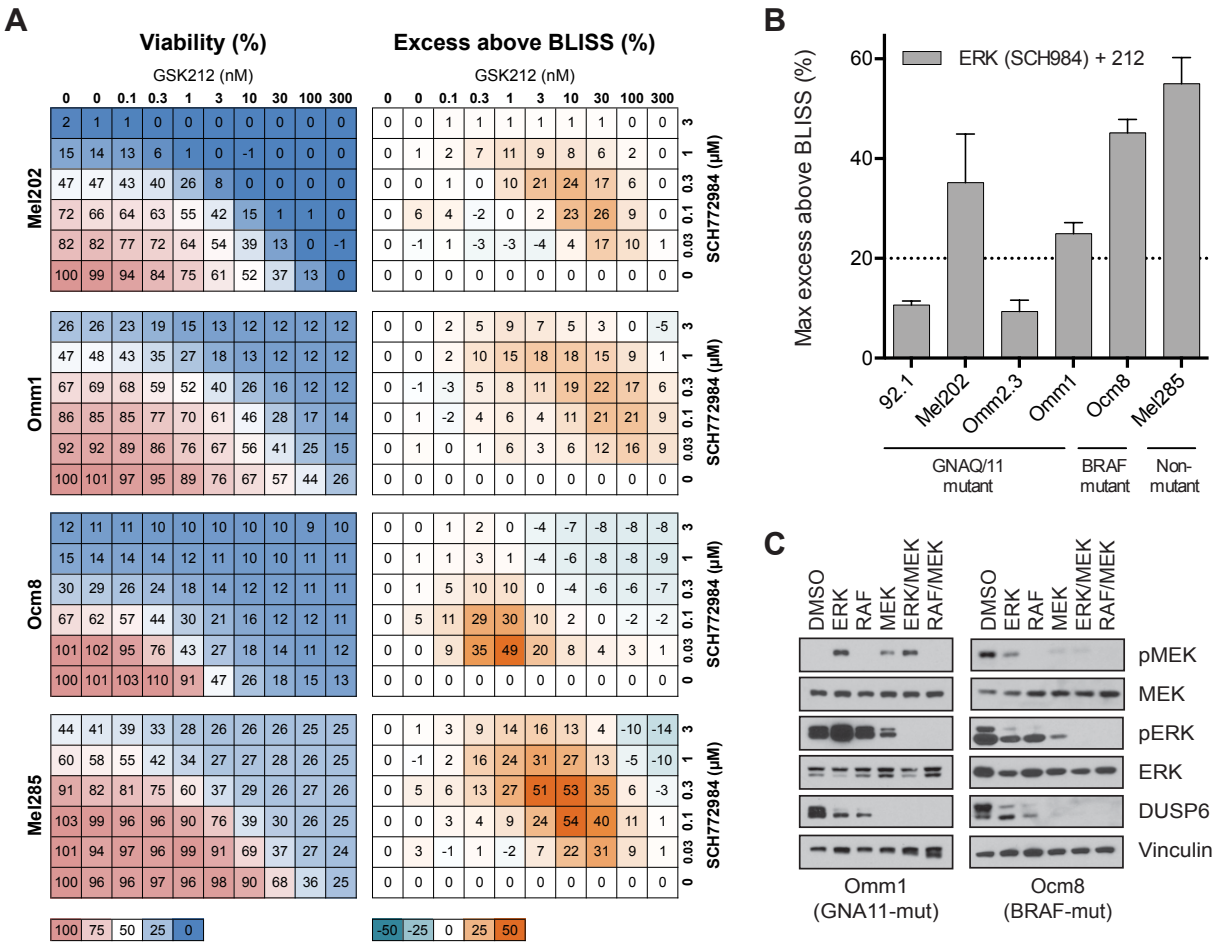

Figure 3.11. Co-targeting of MEK and ERK is synergistic in UM cells. (A) Cells were treated with 9 doses of MEK inhibitor GSK212 and 5 doses of ERK inhibitor SCH984 for 4 days and cell viability was determined using MTS (left). Percent excess above BLISS was calculated for each drug combination (right). **(B)** Maximal percent excess above BLISS from (A) is graphed and extended to additional cell lines. The mean ± SEM of 3 independent experiments is shown. **(C)** Immunoblot analysis of cells treated overnight with vehicle, ERK inhibitor (0.3μM SCH984), pan-RAF inhibitor (1μM AZ628), MEK inhibitor (30nM GSK212), or indicated combinations.

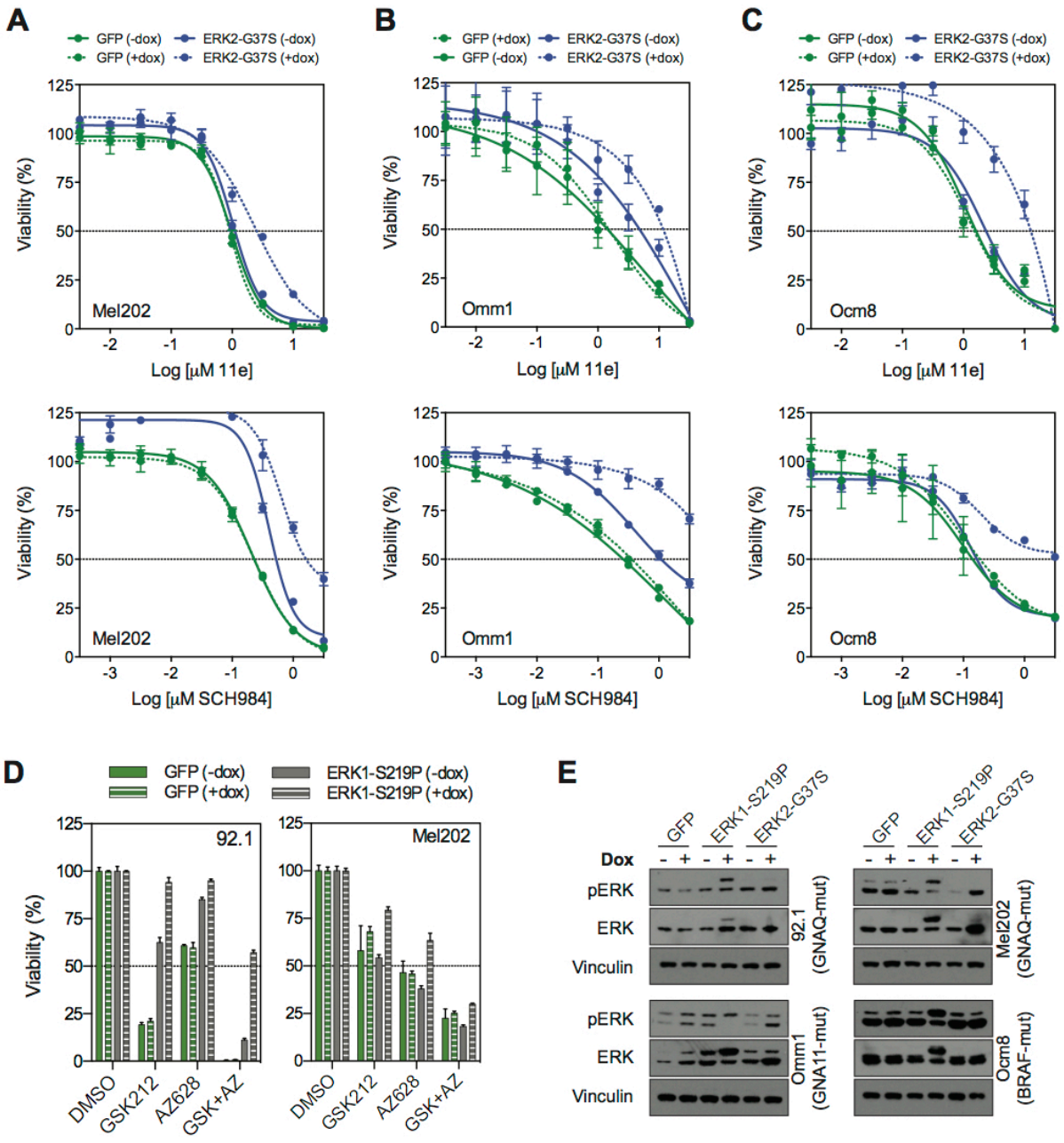

Figure 3.12. ERK resistance alleles confer resistance to MAPK inhibitors in UM cells. (A) Mel202 (*GNAQ*-mutant), **(B)** Omm1 (*GNA11*-mutant) **(C)** Ocm8 (*BRAF*-mutant) UM cells were co-treated with 9 doses of ERK inhibitor 11e (top) or SCH984 (bottom) and dox for 4 days and cell viability was determined using MTS. **(D)** Cells were co-treated with indicated drugs (GSK212/AZ628: 92.1 10nM/0.3μM; Mel202 1nM/1μM) and dox for 4 days and cell viability was determined using MTS. **(E)** Immunoblot analysis confirms ERK allele expression in dox-treated cells (24h).

pan-RAF/MEK or MEK/ERK combinations resulted in stronger reduction in phospho-ERK levels than single agent treatments (**Figure 3.11C**). These data indicate that combined inhibition of MEK and ERK achieves stronger pathway suppression.

We also sought to confirm the on-target inhibition of ERK in these cells. Known ERK inhibitor resistant ERK alleles (179) were expressed in UM cells and ERK inhibitor sensitivity was determined. ERK allele expression conferred resistance to ERK inhibitors in several UM cell lines (**Figure 3.12A-C**). In addition, ERK alleles known to confer resistance to RAF/MEK inhibition (179) also conferred resistance to pan-RAF/MEK inhibition in UM cells (**Figure 3.12D**). Induction of ERK allele expression was confirmed using immunoblots (**Figure 3.12E**). These data confirm the on-target effect of ERK inhibition, as well as further validate the on-target effect of RAF/MEK combinations in UM cells.

Discussion

Metastatic UM represents a major unmet medical need. In rare cancers like UM, extensive preclinical evidence is necessary to understand which therapeutic combinations should be tested in the clinic. In the absence of large numbers of patients, combinations cannot be effectively tested empirically. Instead, one needs to leverage large-scale screening approaches to identify rational co-targets of existing drugs. We performed genome-scale shRNA enhancer screens and identified several biologically interesting and near-term clinically applicable co-targets with MEK and PKC inhibitors.

There are both advantages and limitations of RNAi based enhancer screens. One obvious advantage is that the genome-scale library captures the full range of possible targets and pathways operant within a cell. In addition, multiple drugs can readily be tested, demonstrating the versatility of this approach. However, by limiting our genome-scale screen to only one cell line, we could be insensitive to additional enhancer genes that may also operate in

GNAQ/11-mutant UM contexts. Conversely, cell line specific false positives may remain problematic, effectively reducing the efficiency of validation screening. In the future, a larger effort could be initiated to test multiple cell lines at genome-scale in order to capture the maximum set of co-targeting opportunities.

The MEK and PKC inhibitor enhancer screens performed here identified a variety of potential co-targets. In principle, the corresponding enhancer genes may comprise two categories. One category may consist of shRNAs that partially, but not entirely, suppress growth on their own, and thus enhance drug sensitivity in combination contexts. A second category may represents "true" synthetic lethal effectors that have little effect on cell viability in the absence of drug. Targets from either category may produce an enhancer phenotype in the screening approach described herein. Several enhancer genes identified here emerged in the setting of both PKC and MEK inhibition. This finding reinforces the link between PKC and MAPK signaling in *GNAQ/11*-mutant cells.

Several new cellular targets were discovered by the enhancer screens, including PTPRK. Although PTPRK is a poorly understood gene, the phosphatase activity of this protein could be important for UM tumorigenesis. H6PD, CAPRIN1, and ARNT were also nominated by these studies, none of which have been previously implicated in UM.

The mitochondrial folate pathway was also identified as a novel pathway that may be important for UM proliferation. The mitochondrial folate pathway enzyme MTHFD2 validated as a PKC inhibitor enhancer. However, targeting the cytoplasmic portion of the folate pathway using methotrexate did not enhance PKC inhibitor sensitivity. This may occur if the cytoplasmic and mitochondrial folate pathways are not entirely dependent on one another. Although methotrexate did not represent a surrogate for MTHFD2 suppression in these studies, direct inhibitors of MTHFD2 could be relevant for combination therapy in the future. Overall, our screens identified new targets for combination therapy and uncovered novel biology of the

networks operant in UM. Expanding our understanding of these networks represents an extensive opportunity for future studies.

The PI3K/AKT/mTOR signaling node was previously nominated for co-inhibition with MEK or PKC in UM (45, 46, 77, 88). Synergy was observed using these drug combinations *in vitro* (45, 46, 77, 88), and several clinical trials were subsequently initiated. Our approach did not identify any members of the AKT pathway as enhancers. These genes may represent false-negatives due to the described limitation of screening only one cell line, or if the library lacked effective shRNAs targeting these transcripts. Alternatively, the enhancers nominated by our screens may represent stronger drug sensitizers than AKT pathway members.

Our enhancer screening approach identified MAPK signaling as crucial for UM cell proliferation. This result is consistent with a recent report nominating RAS activation as a mechanism of resistance to MEK inhibition in UM (180). Furthermore, we demonstrate that targeting more than one MAPK pathway member is necessary to ablate phospho-ERK signaling and block proliferation. Co-treating with inhibitors of two pathway members may be more effective than dialing up dosage of a single agent. It is possible that inhibition of 1 pathway member may be unable to reach 0% pathway activity; however, combined inhibition of two pathway members may achieve stronger downstream suppression.

Two recent reports demonstrate enhanced sensitivity to MEK inhibition following CRAF suppression in *KRAS*-mutant cells (181, 182). These studies paired with our findings suggest that activation of the MAPK pathway by oncogenic GNAQ/11 or oncogenic RAS may occur using similar mechanisms. This hypothesis would suggest that observations made in *RAS*-mutated cells might in some cases be relevant in the *GNAQ/11*-mutant context.

Treating UM patients with combined pan-RAF/MEK or MEK/ERK inhibitors in the clinic is imminently tractable. All three kinases currently have multiple small molecules in clinical studies, and the MEK inhibitor trametinib is FDA approved. One could even imagine future studies combining two MAPK pathway inhibitors with PKC inhibitors as well. Various dosing and

scheduling regimens could be applied to achieve robust and sustained pathway inhibition in UM patients.

In summary, large-scale enhancer screens can identify a range of co-dependencies. This study provides a framework to rapidly identify novel pathways for co-inhibition with existing small molecule inhibitors. We demonstrate efficacy with combinatorial blockade of multiple nodes of the MAPK pathway. Such an approach warrants further study in a clinical setting.

Materials and Methods

Cell lines and inhibitors

UM cell lines provided by Martine Jager in 2011 (Leiden University, The Netherlands) were maintained in RPMI-1640 + 10% heat-inactivated FBS. The previously published establishment and *GNAQ/11* mutations (148) were confirmed using exon PCR and STR profiling (GenePrint10 kit; Promega). Cells containing inducible constructs were maintained in RPMI-1640 containing 10% TET approved FBS (Clontech). Compounds include: AZD6244, AEB071, AZ628, and GSK2118436 (Selleck), GSK1120212 and VX-11e (ChemieTek), MLN2480 (ChemScene), SCH772984 (synthesized by J & W PharmLab as described in (179) and Selleck), and methotrexate (Sigma).

Pooled screens

The primary screen was performed as previously described (183). Omm2.3 cells were infected in 12-well plates (1.5e6 cells/well) with a pooled library of ~98,000 shRNAs at an infection efficiency of 30-50%. Cells were centrifuged at 2,000 RPM for 2 hours at 30°C, after which media was changed. Cells were pooled the next day and replated in puromycin (1µg/mL) for 3 days. Following selection, at least 3e7 cells were plated for each replicate in large stacker and T225 flasks, treated with DMSO, 1µM AZD6244, or 1µM AEB071, and passaged for up to 3

weeks. A non-infected control was also passaged in parallel using T75 flasks. At least 3e7 cells were harvested in PBS and frozen at -20°C for genomic DNA extraction. shRNAs were PCR-amplified (~200µg per replicate) and then sequenced (Illumina). Sample-specific shRNA representation was determined by calculating: Log_2[(shRNA reads/total reads)*1e6]. The 3 drug replicates were then compared to 3 DMSO control replicates to identify shRNAs depleted in the drug arm, but not the control arm. Candidate genes were nominated using the RIGER 2nd best shRNA ranking method in Gene-E (www.broadinstitute.org/cancer/software/GENE-E/) (159). For the validation screens, the same protocol and analysis method was used as the primary screen. A custom pooled shRNA library of 629 shRNAs was generated. At least 1e6 cells were maintained at each cell passaging in T75 flasks and at least 1e6 cells were harvested for genomic DNA extraction and shRNA sequencing. The normalized enrichment score from 2nd best shRNA was averaged across cell lines to prioritize candidate genes.

Seed analysis

To identify shRNA seed sequences that function as drug enhancers, the STARS algorithm, which is the subject of a manuscript currently in preparation, was applied to the primary screening ranked shRNA results (Hegde, M et al., In preparation). Seeds were defined as the 7 bases following position 11 or 12 in the shRNA sequence. shRNAs were ranked based on their depletion in drug-treated cells, but not DMSO. Seeds with 2 or more shRNAs in the top 2% were ranked. Those shRNAs containing seeds with an average score > 9 were removed and RIGER 2nd best shRNA analysis was repeated. 10 seeds corresponding to 324 shRNAs were removed from the MEK inhibitor analysis, while 7 seeds corresponding to 211 shRNAs were removed from the PKC inhibitor analysis. Genes that no longer scored following seed filtering were then identified.

Expression constructs

All shRNAs were expressed from the pLKO.1 or pLKO_TRC005 lentiviral vectors. CRISPR reagents included the previously described lentiviral vectors: pXPR_101-Cas9 and pXPR_003-sgRNA (184). All shRNA and CRISPR reagents were obtained from the RNAi Consortium and the Broad Institute Genetic Perturbation Platform. MEKDD, GFP, ERK1-S219P, and ERK2-G37S were expressed from V5-tagged tet-inducible construct, pLIX_403, as previously described (32, 179). The shRNA and sgRNA constructs included:

shLuc 43 (TRCN0000072243, CTTCGAAATGTCCGTTCGGTT)

shLuc 56 (TRCN0000072256, ACGCTGAGTACTTCGAAATGT)

shLuc 64 (TRCN0000072264, GCTGAGTACTTCGAAATGTCC)

shBRAF 89 (TRCN0000006289, GCAGATGAAGATCATCGAAAT)

shBRAF 91 (TRCN0000006291, GCTGGTTTCCAAACAGAGGAT)

shBRAF 4 (TRCN0000231130, TTACCTGGCTCACTAACTAAC)

shMTHFD2 1 (TRCN0000036551, CGAGAAGTGCTGAAGTCTAAA)

shMTHFD2 2 (TRCN0000290805, CACTCCTATGTCCTCAACAAA

shMTHFD2 3 (TRCN0000290880, GCAGTTGAAGAAACATACAAT)

shMTHFD2 4 (TRCN0000290881, CGAATGTGTTTGGATCAGTAT)

sgGFP 1 (GGCATCGACTTCAAGGAGGA)

sgGFP 2 (GAAGGGCATCGACTTCAAGG)

sgBRAF 4 (GGCTCTGTTCAACGGGGACA)

sgBRAF 5 (CGGTGGTGGCGGCGCGGAGC)

Lentiviral infections

To generate lentivirus, 293T cells were transfected with 3μg expression plasmid, 2.7μg Δ8.9, and 0.3μg VSV-G in 10cm plates with Xtreme Gene 9 (18μL; Roche). Virus was

harvested 3 days later and filtered (0.45μm). Uveal melanoma cells were plated in 6-well dishes (1.5e5-4e5 cells/well) and then infected 1-2 days later in the presence of polybrene (Millipore; 5μg/mL). For shRNA expression, cells were infected at 1:40-1:50 viral dilution, centrifuged at 2,000 RPM for 30 minutes at 37°C, and then replated in puromycin (1μg/mL) the following day and selected for 4-6 days. For CRISPR experiments, cells were infected with Cas9 at 1:4, centrifuged, and then replated in blasticydin (5μg/mL) 2 days later. After 3-4 days selection, cells were infected with sgRNAs at 1:10, centrifuged, and then replated in puromycin (1μg/mL) the following day. Cells were selected for at least 10 days to allow for genome editing. For inducible ORF expression, cells were infected at 1:3 in media lacking TET, centrifuged, and then selected using puromycin (1μg/mL) for 3-4 days. For all assays, selected UM cells were plated for drug sensitivity and immunoblot analysis in parallel.

Drug sensitivity assays

For single agent kill curves, cells were seeded in 96-well plates (1.5e3-4e3 cells/well), and then treated with a 9-point drug dilution in triplicate the following day. For resistance studies, expression vectors were induced by co-treatment with 1μg/mL doxycycline (Clontech). For drug combination assays, cells were treated in duplicate or triplicate with 2D drug matrices including 9-doses of drug 1 and 5-doses of drug 2. Cell viability was determined 4-5 days later using CellTiter96 Aqueous assay (Promega). Viability was calculated as a percentage of the vehicle-treated cells, following background subtraction. For combination studies, synergy was determined using the excess above BLISS calculation: X – [A+B – A*B], where X is the effect of combination treatment, while A and B are the effects of single agent treatment at specific dose (177). For longer-term drug exposure experiments, cells were seeded in 12-well plates (5e3-1.5e4 cells/well), and then treated with drug in triplicate the following day. Drug media was changed every 3-5 days for approximately 2 weeks, after which cells were fixed using methanol, stained with crystal violet (0.1%), washed with water, and then imaged. Dye was solubilized

using 10% acetic acid and quantified by absorbance at OD595. Relative absorbance was calculated as a percentage of vehicle-treated cells.

Immunoblots

In advance of protein harvesting, cells were exposed to inhibitors overnight or dox (1μg/mL) for 24h. Cells were washed twice with cold PBS and then lysed using RIPA buffer containing protease and phosphatase inhibitors (Roche). Equal amounts of protein were resolved by SDS-page (Invitrogen) and then transferred to nitrocellulose membranes (Invitrogen). Antibodies used to detect proteins included: BRAF (Santa Cruz Biotechnology), phospho-ERK1/2 (T202/Y204) (Santa Cruz Biotechnology and Cell Signaling Technology), phospho-MEK1/2 (Ser217/S221), MEK1/2, ERK1/2, phospho-MARCKS (Ser152/156), MARCKS (Cell Signaling Technology), Vinculin (Calbiochem and Cell Signaling Technology), MTHFD2 and DUSP6 (Abcam).

CHAPTER 4.

CONCLUSION AND FUTURE DIRECTIONS

Summary

The work described in this thesis used genomic approaches to further our understanding of UM biology and therapeutic development. First, we performed whole exome sequencing to comprehensively understand the somatic genetic events that drive UM tumorigenesis. These studies confirmed the prevalence of *GNAQ*, *GNA11*, *BAP1*, *SF3B1*, and *EIF1AX* mutations and nominated two novel putative driver genes (*SMARCA4* and *IQGAP1*) that were mutated exclusively in metastatic samples. In addition, we used loss of function tools to demonstrate that the translation initiation factor EIF1AX is required for the viability of both wild type and N-terminal tail mutated cancer cells. We then applied RNA sequencing of polysome-associate mRNAs to identify transcripts regulated by EIF1AX at the level of translation. These studies provide the first insights into the functional effect of a mutated translation initiation factor in cancer.

Paired with these genome characterization efforts, we also applied a functional genomic approach to nominate targets for combination therapy with MEK or PKC inhibitors, which are currently in clinical trials for UM. A near genome-scale shRNA library was used to screen a single UM cell line for genes that when suppressed, sensitize cells to MEK or PKC inhibitors. Several of the candidate drug enhancer genes nominated by this screen validated across a panel of cell lines. Both the mitochondrial folate pathway enzyme MTHFD2 and the MAPK pathway kinase BRAF were selected for follow-up studies based on their generalizability and imminent potential to target. MTHFD2 was important for the growth of UM cells and sensitized these cells to PKC inhibition when suppressed. In addition, BRAF inhibition using multiple genetic and pharmacologic methods enhanced the effect of MEK inhibition across our UM cell lines. Combined inhibition of two MAPK pathway members, including RAF/MEK and MEK/ERK, was synergistic in UM cells. These data suggest that stronger inhibition of the MAPK pathway through combination therapy may be an effective strategy to improve clinical outcomes using

MEK inhibitors in metastatic UM patients. These studies provide compelling results that expand our current understanding of UM tumorigenesis and identify novel targets for drug development. However, several of the limitations of this work should be addressed.

Limitations of this study

One major limitation of this work involves the heavy reliance on existing tumor cell lines as a model for UM biology and therapeutic sensitivity. Historically, UM cell lines have been difficult to generate from patient tumor samples, thereby limiting the number of cell lines established. In addition, UM is a relatively rare disease, making tumor samples difficult to acquire and accumulate. At the time when this work was initiated, there were very few established UM cell lines on which *in vitro* studies could be performed (148). In addition, these cell lines do not accurately recapitulate the genetic heterogeneity observed in patient populations. Although many of the cell lines harbor *GNAQ/11* activating mutations, none are *BAP1*-mutant. Generating cell lines from *BAP1*-mutant tumors is particularly important due to the association of BAP1 loss with more aggressive disease, yet establishing these lines has been a challenge in the field for several years (49, 93). Fortunately, two recent studies report the generation of new UM models using both *in vitro* approaches as well as patient-derived tumor xenografts (185, 186). Importantly, several of these models harbor BAP1 loss (185, 186). The addition of novel cell lines that incorporate the full genetic landscape observed in UM will aid in future mechanistic and drug discovery studies. In addition, patient-derived tumor xenografts will be hugely important for the discovery and validation of new therapies for UM patients.

Along similar lines, one additional limitation of this work was the reliance of the functional studies of mutant EIF1AX on a single mutated cell line (see chapter 2). Including a larger number of mutated cell lines in our panel might have strengthened our viability and polysome

profiling studies. Additional *EIF1AX*-mutant cell lines would have been included if they were available at the time these studies were performed.

Alternatively, we could have generated an isogenic genetic system using CRISPR-Cas genome engineering methods to tease apart the contribution of mutant EIF1AX to UM viability and translation. This could have involved knocking a wild type version of EIF1AX into a mutant background, or vice versa, and then performing mRNA sequencing of polysome-bound transcripts in each setting. This approach could provide a more compelling result for mutant EIF1AX specific mRNA regulation at the level of translation. In addition, it could be used to differentiate the impact of each individual mutation observed in EIF1AX in UM and other cancer types. In particular, the impact of N-terminal tail mutations in comparison to mutations in other regions of the protein could be elucidated. Overall, the work presented in chapter 2 of this thesis provides a framework for future studies of mutant EIF1AX in cancer, including those described above.

Another limitation of this work involves the selection of candidate genes from our drug enhancer screening efforts. As discussed in chapter 3, several genes nominated by our genome-scale shRNA screen scored well in our validation screens across a panel of *GNAQ/11*-mutant cell lines. In order to maximize the translational opportunity of drug enhancers, we then prioritized candidates with existing drugs for follow-up studies (MTHFD2 and BRAF). However, several other interesting candidates lacking drugs were also nominated (such as the receptor tyrosine phosphatase PTPRK). Future studies should therefore seek to understand the role of these other candidate genes in UM biology and drug sensitivity.

There are a few additional limitations of genome-scale shRNA screens in general. First, by screening only one cell line using the genome-scale library, we may have missed strong drug enhancers that perform well across other UM cell lines. Second, not all of the shRNAs included in the library down regulate their target gene. Many shRNAs could have off-target effects, as discussed in chapter 3. In addition, different shRNAs that target the same transcript can cause

near complete knockout to no knockdown at all; thus, identifying multiple shRNAs with the same phenotype can be difficult. By using 2nd best shRNA to nominate candidate genes, we may have missed genes for which only 1 shRNA scored. These genes may represent real on-target drug enhancers, but only 1 shRNA was functional of the 5 or more included in the pooled library. Despite these limitations, our screening approach identified several interesting targets for further study.

Future directions for UM studies

Genome characterization

The genome characterization study presented in chapter 2 represents a foundation for our understanding of the somatic genetic drivers of primary and metastatic UM. Future studies will be necessary to build upon these findings in order to better understand the underlying events important for UM tumorigenesis. Several possible studies are suggested here.

First, our understanding of the genetic drivers of metastatic UM needs to be expanded. We present highly interesting, novel, and potentially targetable findings from whole exome sequencing of only 3 metastatic tumor samples. These types of approaches should be applied to larger cohorts of metastatic UM samples, ideally paired with primary tumor and normal samples in order to define the recurrent genetic drivers of progression from primary to metastatic disease. Given that metastatic UM currently has no effective therapies, these studies are of the utmost importance in order to nominate new strategies to target metastatic disease based on the underlying genetic basis.

In addition to whole exome sequencing efforts, additional genome characterization approaches should be applied to both primary and metastatic tumor sample cohorts. Whole exome sequencing is effective at identifying somatic point mutations and small insertions and deletions, but other technologies, such as whole genome sequencing and transcriptome

sequencing, are better equipped to identify translocations, expression changes, and splice variants that may also drive tumorigenesis. One whole genome sequencing study in UM has been reported, however, only 12 samples were analyzed (10). Larger sample sizes are necessary to identify recurrent alterations. Fortunately, some of these points will be addressed by the ongoing Cancer Genome Atlas (TCGA) effort to analyze 80 UM samples using several methods including whole exome and transcriptome sequencing, as well as methylation studies (http://cancergenome.nih.gov/).

To complement and extend these genome characterization studies, additional efforts to further our understanding of the functional consequence of recurrent mutations are needed. This work presents the first functional studies of mutant EIF1AX in cancer. Future studies should seek to answer several open questions regarding EIF1AX biology in cancer, including whether mutant EIF1AX is sufficient to transform cells in the presence or absence of oncogenic GNAQ/11? Does each of the N-terminal tail mutations behave in the same way, or differently? Do mutations outside of the N-terminal tail behave in the same way, or differently? In addition, mutant EIF1AX mRNA is preferentially expressed over wild type mRNA in mutant cells (reported in (60) as well as chapter 2), suggesting that wild type EIF1AX could be tumor suppressive. Understanding if this indeed is true would be of interest. Finally, as EIF1AX is also recurrently mutated in papillary thyroid carcinoma (62), understanding the role for mutant EIF1AX in different tumor contexts would also be of interest.

Targeted therapy

The work described in chapter 3 provides the basis for several avenues for future study. First, combined pan-RAF and MEK inhibition is proposed as a possible new avenue for UM therapy. The described results relied on *in vitro* approaches and should next be expanded using *in vivo* models such as tumor xenograft growth in mice. We are currently working on such an *in vivo* study to assess the efficacy of combining RAF and MEK inhibition in a xenograft

model using the 92.1 cell line. Following efficacy in these *in vivo* studies, a future clinical trial could be initiated to test the effect of combined RAF and MEK inhibition in metastatic UM patients. The pan-RAF inhibitor MLN2480 is currently in clinical trials as a single agent therapy in the setting of metastatic melanoma (NCT01425008). In addition, a combined pan-RAF and MEK inhibition study using RAF265 and MEK162 was completed for RAS or $BRAF^{V600E}$ mutant tumors (NCT01352273). Our data suggest that applying such a combination in the context of UM could be beneficial over treating patients with a MEK inhibitor alone.

In addition to pan-RAF plus MEK combinations, our data also suggest that ERK inhibitors may be clinically beneficial for UM patients as single agents and in combination with MEK inhibitors. Multiple distinct ERK inhibitors are currently in clinical development (NCT01781429 and NCT01875705). Future studies should seek to further understand the convergence of GNAQ/11 signaling on ERK, and whether UM cell lines are sensitive to ERK inhibitors *in vivo*.

Future follow-up studies could also seek to further understand the biochemical mechanism underlying the synergy observed using pan-RAF/MEK inhibitors. The MAPK pathway is often visualized as a linear cascade (shown in **Figure 1.1**), however, these proteins actually form complexes within the cell that include scaffold proteins such as KSR, SHOC2, and 14-3-3 (187). Small molecule inhibitors are capable of changing complex formations. In *KRAS*-mutant cells, treatment with specific MEK inhibitors induces MEK to bind to RAF, resulting in a MEK protein that is more resistant to MEK inhibitors than unbound MEK (181). One could imagine that combined treatment with both a RAF and a MEK inhibitor could disrupt MEK-RAF binding, allowing for more successful inhibition of MEK. Indeed, Lito and colleagues show in a *KRAS*-mutant model that co-treatment with a RAF and MEK inhibitor results in greater lethality than single agent treatments (181). These types of studies should be performed in the *GNAQ/11*-mutant context in order to understand the effect of MEK inhibitors and MEK/RAF combinations at the biochemical level. These studies could be performed by using tagged

versions of RAF and MEK to pull them down and then subsequently identify their binding partners in the presence and absence of each drug or combination. This type of study would aid in understanding MAPK signaling downstream of oncogenic GNAQ/11, which may or may not mimic the effects seen in mutated RAS settings.

In addition to BRAF, our screening efforts also nominated MTHFD2 as an interesting new gene in UM. Our work only begins to reveal the role of one-carbon metabolism in UM. The folate pathway had not been previously implicated in UM and there are many future studies that one could envisage. First, one would want to expand our dependency studies to determine whether MTHFD2 or other enzymes in the mitochondrial folate pathway are required for the viability of a larger panel of UM cell lines with various genetic backgrounds. Second, one would want to determine whether suppression of these enzymes results in glycine auxotrophy in UM cells, as has been reported for SHMT2 knockdown in some cancer cells (173). In addition to these dependency experiments, one would also want to perform expression analyses. MTHFD2 is not typically expressed in adult tissue, however, it is over expressed in some cancers (171, 172). One would therefore want to determine the levels of MTHFD2 expression in primary and metastatic UM tumors. Together, these studies should help to determine whether MTHFD2 or the mitochondrial folate pathway in general represents a viable therapeutic target. If yes, one could then envisage designing drug screens to identify MTHFD2 or other pathway member inhibitors for the treatment of UM.

The studies described above and in chapter 3 relied on targeting oncogenic GNAQ/11 by inhibiting downstream signaling. However, renewed efforts to directly target mutated GNAQ/11 may be warranted. Genetic strategies to reduce GNAQ/11 function, such as RNAi or CRISPR-Cas genome editing may represent novel approaches to directly suppress the predominant genetic driver of UM. If one could successfully deliver these molecules to either the eye or the liver, one could change GNAQ/11 at the genomic or expression level. For genome engineering, one could target a guide RNA to the mutated allele specifically and then

either introduce deletions to prevent protein activity or correct the mutated copy back to the wild type sequence. Targeting the mutant allele may prevent on-target toxicities in normal cells that could potentially receive these molecules. For RNAi, one could potentially deliver short interfering RNAs that target the GNAQ or GNA11 transcript to down regulate expression levels. These approaches may represent novel opportunities to effectively shut down activity of the main driver in UM.

Given that UM metastasizes to the liver, this strengthens the likelihood of success using these gene therapy approaches. Multiple reports have shown that siRNAs conjugated to cholesterol molecules can be targeted to liver cells and achieve sustained decreases in target gene expression (188-190). Although these studies target normal hepatocytes, one could imagine using a similar approach to target UM cells located in the liver. In addition to siRNA therapy, CRISPR genome-editing molecules were recently delivered to adult mouse liver cells using multiple distinct methodologies (191-193). Metastatic UM in the liver is well poised to benefit from these gene therapy approaches in the future.

Mechanisms of resistance

Chapter 3 of this thesis described a functional genomic approach to identify drug sensitizers. In parallel, identifying mechanisms of resistance to targeted agents is also warranted. Several different approaches could be applied in UM to understand resistance to therapies in preclinical and clinical investigation, including: PKC, MEK, combined PKC/MEK, as well as the combination therapies suggested in chapter 3, pan-RAF/MEK and MEK/ERK. A few of the possible approaches are described here.

First, one could utilize functional genomic approaches to identify genes that when down regulated or over expressed confer resistance to targeted therapy. These studies could help to predict resistance mechanisms that may occur in patients. By understanding these mechanisms, one can develop ways to overcome resistance or prevent it from occurring. This

type of approach was successfully applied using both ORF over expression and CRISPR transcriptional activation screening approaches in *BRAF*-mutant melanoma treated with MAPK pathway inhibitors (194-196). Complementarily, loss of function approaches using shRNAs and CRISPR knockout methods also identified genes that when suppressed, confer resistance to targeted agents (183, 197). These functional genomic tools could be applied in the setting of UM to systematically identify mechanisms of resistance to targeted agents in genetic backgrounds of interest.

In addition to these functional genomic approaches, one could also probe resistance by culturing sensitive cell lines to resistance by gradual drug exposure. This method was applied in UM on one occasion using a MEK inhibitor (180). Sustained MEK inhibition resulted in increased RAS activity (180). These studies could be expanded to test additional cell lines and inhibitors to look for common or differential mechanisms of resistance in cell lines with different genetic backgrounds or those treated with multiple targeted agents.

Finally, mechanisms of resistance to targeted agents could also be uncovered by analyzing tumor samples from patients treated with these therapies. In cutaneous melanoma, next-generation sequencing of pre-treatment and post-relapse tumor samples revealed genetic events that were sufficient to confer resistance to MAPK pathway inhibitors (32, 198, 199). This approach could be executed alongside UM clinical trials to understand why some patients respond and then relapse, or never respond. By understanding the genetic events that contribute to resistance, one could design rational combination therapies to prevent, postpone, or overcome relapse.

Concluding Remarks

The work presented in this thesis expands our existing knowledge of the genetic basis and underlying dependencies of UM. Our genome characterization studies provide a

comprehensive view of somatic genetic drivers of primary tumors, and begin to lay the foundation for future studies focusing on metastatic disease. In addition, we report the first functional studies of a mutated translation initiation factor in cancer, thereby paving the way for future studies to expand upon these initial observations. We also utilize systematic genome-scale loss of function screens to identify genes that enhance the effects of targeted agents. Such an approach could be applied to any genetic context and targeted therapy in order to nominate putative combination therapies. Ultimately, translating biological findings into clinical treatments for metastatic UM patients is of the utmost importance. Future work in UM should seek to expand our understanding of the metastatic state as well as translate drug combinations proposed here into clinical investigation.

REFERENCES

1. Chang AE, Karnell LH, Menck HR. The National Cancer Data Base report on cutaneous and noncutaneous melanoma: a summary of 84,836 cases from the past decade. The American College of Surgeons Commission on Cancer and the American Cancer Society. Cancer. 1998;83:1664-78.

2. Singh AD, Turell ME, Topham AK. Uveal melanoma: trends in incidence, treatment, and survival. Ophthalmology. 2011;118:1881-5.

3. Stang A, Parkin DM, Ferlay J, Jockel KH. International uveal melanoma incidence trends in view of a decreasing proportion of morphological verification. Int J Cancer. 2005;114:114-23.

4. Keenan TD, Yeates D, Goldacre MJ. Uveal melanoma in England: trends over time and geographical variation. Br J Ophthalmol. 2012;96:1415-9.

5. Damato BE, Heimann H, Kalirai H, Coupland SE. Age, survival predictors, and metastatic death in patients with choroidal melanoma: tentative evidence of a therapeutic effect on survival. JAMA Ophthalmol. 2014;132:605-13.

6. Weis E, Shah CP, Lajous M, Shields JA, Shields CL. The association between host susceptibility factors and uveal melanoma: a meta-analysis. Arch Ophthalmol. 2006;124:54-60.

7. Guenel P, Laforest L, Cyr D, Fevotte J, Sabroe S, Dufour C, et al. Occupational risk factors, ultraviolet radiation, and ocular melanoma: a case-control study in France. Cancer Causes Control. 2001;12:451-9.

8. Shah CP, Weis E, Lajous M, Shields JA, Shields CL. Intermittent and chronic ultraviolet light exposure and uveal melanoma: a meta-analysis. Ophthalmology. 2005;112:1599-607.

9. Weis E, Shah CP, Lajous M, Shields JA, Shields CL. The association of cutaneous and iris nevi with uveal melanoma: a meta-analysis. Ophthalmology. 2009;116:536-43 e2.

10. Furney SJ, Pedersen M, Gentien D, Dumont AG, Rapinat A, Desjardins L, et al. SF3B1 mutations are associated with alternative splicing in uveal melanoma. Cancer Discov. 2013;3:1122-9.

11. Schwartz GG. Eye cancer incidence in U.S. states and access to fluoridated water. Cancer Epidemiol Biomarkers Prev. 2014;23:1707-11.

12. Eskelin S, Kivela T. Mode of presentation and time to treatment of uveal melanoma in Finland. Br J Ophthalmol. 2002;86:333-8.

13. Shields CL, Shields JA. Ocular melanoma: relatively rare but requiring respect. Clin Dermatol. 2009;27:122-33.

14. Gragoudas ES, Seddon JM, Egan K, Glynn R, Munzenrider J, Austin-Seymour M, et al. Long-term results of proton beam irradiated uveal melanomas. Ophthalmology. 1987;94:349-53.

15. Margo CE. The Collaborative Ocular Melanoma Study: an overview. Cancer Control. 2004;11:304-9.

16. Kujala E, Makitie T, Kivela T. Very long-term prognosis of patients with malignant uveal melanoma. Invest Ophthalmol Vis Sci. 2003;44:4651-9.

17. Gragoudas ES, Egan KM, Seddon JM, Glynn RJ, Walsh SM, Finn SM, et al. Survival of patients with metastases from uveal melanoma. Ophthalmology. 1991;98:383-9.

18. Diener-West M, Reynolds SM, Agugliaro DJ, Caldwell R, Cumming K, Earle JD, et al. Development of metastatic disease after enrollment in the COMS trials for treatment of choroidal melanoma: Collaborative Ocular Melanoma Study Group Report No. 26. Arch Ophthalmol. 2005;123:1639-43.

19. Bottaro DP, Rubin JS, Faletto DL, Chan AM, Kmiecik TE, Vande Woude GF, et al. Identification of the hepatocyte growth factor receptor as the c-met proto-oncogene product. Science. 1991;251:802-4.

20. Hendrix MJ, Seftor EA, Seftor RE, Kirschmann DA, Gardner LM, Boldt HC, et al. Regulation of uveal melanoma interconverted phenotype by hepatocyte growth factor/scatter factor (HGF/SF). Am J Pathol. 1998;152:855-63.

21. Ye M, Hu D, Tu L, Zhou X, Lu F, Wen B, et al. Involvement of PI3K/Akt signaling pathway in hepatocyte growth factor-induced migration of uveal melanoma cells. Invest Ophthalmol Vis Sci. 2008;49:497-504.

22. Woodward JK, Elshaw SR, Murray AK, Nichols CE, Cross N, Laws D, et al. Stimulation and inhibition of uveal melanoma invasion by HGF, GRO, IL-1alpha and TGF-beta. Invest Ophthalmol Vis Sci. 2002;43:3144-52.

23. Mallikarjuna K, Pushparaj V, Biswas J, Krishnakumar S. Expression of epidermal growth factor receptor, ezrin, hepatocyte growth factor, and c-Met in uveal melanoma: an immunohistochemical study. Curr Eye Res. 2007;32:281-90.

24. Economou MA, All-Ericsson C, Bykov V, Girnita L, Bartolazzi A, Larsson O, et al. Receptors for the liver synthesized growth factors IGF-1 and HGF/SF in uveal melanoma: intercorrelation and prognostic implications. Acta Ophthalmol. 2008;86 Thesis 4:20-5.

25. Onken MD, Worley LA, Ehlers JP, Harbour JW. Gene expression profiling in uveal melanoma reveals two molecular classes and predicts metastatic death. Cancer Res. 2004;64:7205-9.

26. Onken MD, Ehlers JP, Worley LA, Makita J, Yokota Y, Harbour JW. Functional gene expression analysis uncovers phenotypic switch in aggressive uveal melanomas. Cancer Res. 2006;66:4602-9.

27. Worley LA, Onken MD, Person E, Robirds D, Branson J, Char DH, et al. Transcriptomic versus chromosomal prognostic markers and clinical outcome in uveal melanoma. Clin Cancer Res. 2007;13:1466-71.

28. Onken MD, Worley LA, Tuscan MD, Harbour JW. An accurate, clinically feasible multi-gene expression assay for predicting metastasis in uveal melanoma. J Mol Diagn. 2010;12:461-8.

29. Onken MD, Worley LA, Char DH, Augsburger JJ, Correa ZM, Nudleman E, et al. Collaborative Ocular Oncology Group report number 1: prospective validation of a multi-gene prognostic assay in uveal melanoma. Ophthalmology. 2012;119:1596-603.

30. Flaherty KT, Puzanov I, Kim KB, Ribas A, McArthur GA, Sosman JA, et al. Inhibition of mutated, activated BRAF in metastatic melanoma. N Engl J Med. 2010;363:809-19.

31. Beroukhim R, Mermel CH, Porter D, Wei G, Raychaudhuri S, Donovan J, et al. The landscape of somatic copy-number alteration across human cancers. Nature. 2010;463:899-905.

32. Van Allen EM, Wagle N, Sucker A, Treacy DJ, Johannessen CM, Goetz EM, et al. The genetic landscape of clinical resistance to RAF inhibition in metastatic melanoma. Cancer Discov. 2014;4:94-109.

33. Prescher G, Bornfeld N, Becher R. Nonrandom chromosomal abnormalities in primary uveal melanoma. J Natl Cancer Inst. 1990;82:1765-9.

34. Horsman DE, White VA. Cytogenetic analysis of uveal melanoma. Consistent occurrence of monosomy 3 and trisomy 8q. Cancer. 1993;71:811-9.

35. Prescher G, Bornfeld N, Hirche H, Horsthemke B, Jockel KH, Becher R. Prognostic implications of monosomy 3 in uveal melanoma. Lancet. 1996;347:1222-5.

36. Kilic E, van Gils W, Lodder E, Beverloo HB, van Til ME, Mooy CM, et al. Clinical and cytogenetic analyses in uveal melanoma. Invest Ophthalmol Vis Sci. 2006;47:3703-7.

37. Aalto Y, Eriksson L, Seregard S, Larsson O, Knuutila S. Concomitant loss of chromosome 3 and whole arm losses and gains of chromosome 1, 6, or 8 in metastasizing primary uveal melanoma. Invest Ophthalmol Vis Sci. 2001;42:313-7.

38. Zuidervaart W, van Nieuwpoort F, Stark M, Dijkman R, Packer L, Borgstein AM, et al. Activation of the MAPK pathway is a common event in uveal melanomas although it rarely occurs through mutation of BRAF or RAS. Br J Cancer. 2005;92:2032-8.

39. Van Raamsdonk CD, Bezrookove V, Green G, Bauer J, Gaugler L, O'Brien JM, et al. Frequent somatic mutations of GNAQ in uveal melanoma and blue naevi. Nature. 2009;457:599-602.

40. Van Raamsdonk CD, Griewank KG, Crosby MB, Garrido MC, Vemula S, Wiesner T, et al. Mutations in GNA11 in uveal melanoma. N Engl J Med. 2010;363:2191-9.

41. Onken MD, Worley LA, Long MD, Duan S, Council ML, Bowcock AM, et al. Oncogenic mutations in GNAQ occur early in uveal melanoma. Invest Ophthalmol Vis Sci. 2008;49:5230-4.

42. Kalinec G, Nazarali AJ, Hermouet S, Xu N, Gutkind JS. Mutated alpha subunit of the Gq protein induces malignant transformation in NIH 3T3 cells. Mol Cell Biol. 1992;12:4687-93.

43. De Vivo M, Chen J, Codina J, Iyengar R. Enhanced phospholipase C stimulation and transformation in NIH-3T3 cells expressing Q209LGq-alpha-subunits. J Biol Chem. 1992;267:18263-6.

44. Van Raamsdonk CD, Fitch KR, Fuchs H, de Angelis MH, Barsh GS. Effects of G-protein mutations on skin color. Nat Genet. 2004;36:961-8.

45. Khalili JS, Yu X, Wang J, Hayes BC, Davies MA, Lizee G, et al. Combination small molecule MEK and PI3K inhibition enhances uveal melanoma cell death in a mutant GNAQ- and GNA11-dependent manner. Clin Cancer Res. 2012;18:4345-55.

46. Ambrosini G, Musi E, Ho AL, de Stanchina E, Schwartz GK. Inhibition of mutant GNAQ signaling in uveal melanoma induces AMPK-dependent autophagic cell death. Mol Cancer Ther. 2013;12:768-76.

47. Feng X, Degese MS, Iglesias-Bartolome R, Vaque JP, Molinolo AA, Rodrigues M, et al. Hippo-independent activation of YAP by the GNAQ uveal melanoma oncogene through a trio-regulated rho GTPase signaling circuitry. Cancer Cell. 2014;25:831-45.

48. Yu FX, Luo J, Mo JS, Liu G, Kim YC, Meng Z, et al. Mutant Gq/11 promote uveal melanoma tumorigenesis by activating YAP. Cancer Cell. 2014;25:822-30.

49. Harbour JW, Onken MD, Roberson ED, Duan S, Cao L, Worley LA, et al. Frequent mutation of BAP1 in metastasizing uveal melanomas. Science. 2010;330:1410-3.

50. Jensen DE, Proctor M, Marquis ST, Gardner HP, Ha SI, Chodosh LA, et al. BAP1: a novel ubiquitin hydrolase which binds to the BRCA1 RING finger and enhances BRCA1-mediated cell growth suppression. Oncogene. 1998;16:1097-112.

51. Ventii KH, Devi NS, Friedrich KL, Chernova TA, Tighiouart M, Van Meir EG, et al. BRCA1-associated protein-1 is a tumor suppressor that requires deubiquitinating activity and nuclear localization. Cancer Res. 2008;68:6953-62.

52. Scheuermann JC, de Ayala Alonso AG, Oktaba K, Ly-Hartig N, McGinty RK, Fraterman S, et al. Histone H2A deubiquitinase activity of the Polycomb repressive complex PR-DUB. Nature. 2010;465:243-7.

53. Machida YJ, Machida Y, Vashisht AA, Wohlschlegel JA, Dutta A. The deubiquitinating enzyme BAP1 regulates cell growth via interaction with HCF-1. J Biol Chem. 2009;284:34179-88.

54. Yu H, Mashtalir N, Daou S, Hammond-Martel I, Ross J, Sui G, et al. The ubiquitin carboxyl hydrolase BAP1 forms a ternary complex with YY1 and HCF-1 and is a critical regulator of gene expression. Mol Cell Biol. 2010;30:5071-85.

55. Matatall KA, Agapova OA, Onken MD, Worley LA, Bowcock AM, Harbour JW. BAP1 deficiency causes loss of melanocytic cell identity in uveal melanoma. BMC Cancer. 2013;13:371.

56. Testa JR, Cheung M, Pei J, Below JE, Tan Y, Sementino E, et al. Germline BAP1 mutations predispose to malignant mesothelioma. Nat Genet. 2011;43:1022-5.

57. Abdel-Rahman MH, Pilarski R, Cebulla CM, Massengill JB, Christopher BN, Boru G, et al. Germline BAP1 mutation predisposes to uveal melanoma, lung adenocarcinoma, meningioma, and other cancers. J Med Genet. 2011.

58. Wiesner T, Obenauf AC, Murali R, Fried I, Griewank KG, Ulz P, et al. Germline mutations in BAP1 predispose to melanocytic tumors. Nat Genet. 2011;43:1018-21.

59. Harbour JW, Roberson ED, Anbunathan H, Onken MD, Worley LA, Bowcock AM. Recurrent mutations at codon 625 of the splicing factor SF3B1 in uveal melanoma. Nat Genet. 2013;45:133-5.

60. Martin M, Masshofer L, Temming P, Rahmann S, Metz C, Bornfeld N, et al. Exome sequencing identifies recurrent somatic mutations in EIF1AX and SF3B1 in uveal melanoma with disomy 3. Nat Genet. 2013;45:933-6.

61. DeBoever C, Ghia EM, Shepard PJ, Rassenti L, Barrett CL, Jepsen K, et al. Transcriptome Sequencing Reveals Potential Mechanism of Cryptic 3' Splice Site Selection in SF3B1-mutated Cancers. PLoS Comput Biol. 2015;11:e1004105.

62. Cancer Genome Atlas Research N. Integrated genomic characterization of papillary thyroid carcinoma. Cell. 2014;159:676-90.

63. Kalirai H, Dodson A, Faqir S, Damato BE, Coupland SE. Lack of BAP1 protein expression in uveal melanoma is associated with increased metastatic risk and has utility in routine prognostic testing. Br J Cancer. 2014;111:1373-80.

64. Ewens KG, Kanetsky PA, Richards-Yutz J, Purrazzella J, Shields CL, Ganguly T, et al. Chromosome 3 status combined with BAP1 and EIF1AX mutation profiles are associated with metastasis in uveal melanoma. Invest Ophthalmol Vis Sci. 2014;55:5160-7.

65. Bedikian AY, Legha SS, Mavligit G, Carrasco CH, Khorana S, Plager C, et al. Treatment of uveal melanoma metastatic to the liver: a review of the M. D. Anderson Cancer Center experience and prognostic factors. Cancer. 1995;76:1665-70.

66. Schmittel A, Schmidt-Hieber M, Martus P, Bechrakis NE, Schuster R, Siehl JM, et al. A randomized phase II trial of gemcitabine plus treosulfan versus treosulfan alone in patients with metastatic uveal melanoma. Ann Oncol. 2006;17:1826-9.

67. Kivela T, Suciu S, Hansson J, Kruit WH, Vuoristo MS, Kloke O, et al. Bleomycin, vincristine, lomustine and dacarbazine (BOLD) in combination with recombinant interferon alpha-2b for metastatic uveal melanoma. Eur J Cancer. 2003;39:1115-20.

68. Lorusso PM, Adjei AA, Varterasian M, Gadgeel S, Reid J, Mitchell DY, et al. Phase I and pharmacodynamic study of the oral MEK inhibitor CI-1040 in patients with advanced malignancies. J Clin Oncol. 2005;23:5281-93.

69. Ohren JF, Chen H, Pavlovsky A, Whitehead C, Zhang E, Kuffa P, et al. Structures of human MAP kinase kinase 1 (MEK1) and MEK2 describe novel noncompetitive kinase inhibition. Nat Struct Mol Biol. 2004;11:1192-7.

70. Zhao Y, Adjei AA. The clinical development of MEK inhibitors. Nat Rev Clin Oncol. 2014;11:385-400.

71. Infante JR, Fecher LA, Falchook GS, Nallapareddy S, Gordon MS, Becerra C, et al. Safety, pharmacokinetic, pharmacodynamic, and efficacy data for the oral MEK inhibitor trametinib: a phase 1 dose-escalation trial. Lancet Oncol. 2012;13:773-81.

72. Falchook GS, Lewis KD, Infante JR, Gordon MS, Vogelzang NJ, DeMarini DJ, et al. Activity of the oral MEK inhibitor trametinib in patients with advanced melanoma: a phase 1 dose-escalation trial. Lancet Oncol. 2012;13:782-9.

73. Flaherty KT, Robert C, Hersey P, Nathan P, Garbe C, Milhem M, et al. Improved survival with MEK inhibition in BRAF-mutated melanoma. N Engl J Med. 2012;367:107-14.

74. Robert C, Karaszewska B, Schachter J, Rutkowski P, Mackiewicz A, Stroiakovski D, et al. Improved overall survival in melanoma with combined dabrafenib and trametinib. N Engl J Med. 2015;372:30-9.

75. Johnson DB, Flaherty KT, Weber JS, Infante JR, Kim KB, Kefford RF, et al. Combined BRAF (Dabrafenib) and MEK inhibition (Trametinib) in patients with BRAFV600-mutant melanoma experiencing progression with single-agent BRAF inhibitor. J Clin Oncol. 2014;32:3697-704.

76. Carvajal RD, Sosman JA, Quevedo JF, Milhem MM, Joshua AM, Kudchadkar RR, et al. Effect of selumetinib vs chemotherapy on progression-free survival in uveal melanoma: a randomized clinical trial. JAMA. 2014;311:2397-405.

77. Ho AL, Musi E, Ambrosini G, Nair JS, Deraje Vasudeva S, de Stanchina E, et al. Impact of combined mTOR and MEK inhibition in uveal melanoma is driven by tumor genotype. PLoS One. 2012;7:e40439.

78. Mitsiades N, Chew SA, He B, Riechardt AI, Karadedou T, Kotoula V, et al. Genotype-dependent sensitivity of uveal melanoma cell lines to inhibition of B-Raf, MEK, and Akt kinases: rationale for personalized therapy. Invest Ophthalmol Vis Sci. 2011;52:7248-55.

79. Chen X, Wu Q, Tan L, Porter D, Jager MJ, Emery C, et al. Combined PKC and MEK inhibition in uveal melanoma with GNAQ and GNA11 mutations. Oncogene. 2014;33:4724-34.

80. Wu X, Zhu M, Fletcher JA, Giobbie-Hurder A, Hodi FS. The protein kinase C inhibitor enzastaurin exhibits antitumor activity against uveal melanoma. PLoS One. 2012;7:e29622.

81. Wu X, Li J, Zhu M, Fletcher JA, Hodi FS. Protein kinase C inhibitor AEB071 targets ocular melanoma harboring GNAQ mutations via effects on the PKC/Erk1/2 and PKC/NF-kappaB pathways. Mol Cancer Ther. 2012;11:1905-14.

82. Mochly-Rosen D, Das K, Grimes KV. Protein kinase C, an elusive therapeutic target? Nat Rev Drug Discov. 2012;11:937-57.

83. Evenou JP, Wagner J, Zenke G, Brinkmann V, Wagner K, Kovarik J, et al. The potent protein kinase C-selective inhibitor AEB071 (sotrastaurin) represents a new class of

immunosuppressive agents affecting early T-cell activation. J Pharmacol Exp Ther. 2009;330:792-801.

84. Friman S, Arns W, Nashan B, Vincenti F, Banas B, Budde K, et al. Sotrastaurin, a novel small molecule inhibiting protein-kinase C: randomized phase II study in renal transplant recipients. Am J Transplant. 2011;11:1444-55.

85. Budde K, Sommerer C, Becker T, Asderakis A, Pietruck F, Grinyo JM, et al. Sotrastaurin, a novel small molecule inhibiting protein kinase C: first clinical results in renal-transplant recipients. Am J Transplant. 2010;10:571-81.

86. Tedesco-Silva H, Kho MM, Hartmann A, Vitko S, Russ G, Rostaing L, et al. Sotrastaurin in calcineurin inhibitor-free regimen using everolimus in de novo kidney transplant recipients. Am J Transplant. 2013;13:1757-68.

87. Naylor TL, Tang H, Ratsch BA, Enns A, Loo A, Chen L, et al. Protein kinase C inhibitor sotrastaurin selectively inhibits the growth of CD79 mutant diffuse large B-cell lymphomas. Cancer Res. 2011;71:2643-53.

88. Musi E, Ambrosini G, de Stanchina E, Schwartz GK. The phosphoinositide 3-kinase alpha selective inhibitor BYL719 enhances the effect of the protein kinase C inhibitor AEB071 in GNAQ/GNA11-mutant uveal melanoma cells. Mol Cancer Ther. 2014;13:1044-53.

89. Pan D. The hippo signaling pathway in development and cancer. Dev Cell. 2010;19:491-505.

90. Abdel-Rahman MH, Boru G, Massengill J, Salem MM, Davidorf FH. MET oncogene inhibition as a potential target of therapy for uveal melanomas. Invest Ophthalmol Vis Sci. 2010;51:3333-9.

91. Surriga O, Rajasekhar VK, Ambrosini G, Dogan Y, Huang R, Schwartz GK. Crizotinib, a c-Met inhibitor, prevents metastasis in a metastatic uveal melanoma model. Mol Cancer Ther. 2013;12:2817-26.

92. Gardner FP, Serie DJ, Salomao DR, Wu KJ, Markovic SN, Pulido JS, et al. c-MET expression in primary and liver metastases in uveal melanoma. Melanoma Res. 2014;24:617-20.

93. Landreville S, Agapova OA, Matatall KA, Kneass ZT, Onken MD, Lee RS, et al. Histone deacetylase inhibitors induce growth arrest and differentiation in uveal melanoma. Clin Cancer Res. 2011.

94. Faingold D, Marshall JC, Antecka E, Di Cesare S, Odashiro AN, Bakalian S, et al. Immune expression and inhibition of heat shock protein 90 in uveal melanoma. Clin Cancer Res. 2008;14:847-55.

95. de Lange J, Ly LV, Lodder K, Verlaan-de Vries M, Teunisse AF, Jager MJ, et al. Synergistic growth inhibition based on small-molecule p53 activation as treatment for intraocular melanoma. Oncogene. 2011.

96. Hodi FS, O'Day SJ, McDermott DF, Weber RW, Sosman JA, Haanen JB, et al. Improved survival with ipilimumab in patients with metastatic melanoma. N Engl J Med. 2010;363:711-23.

97. Maio M, Danielli R, Chiarion-Sileni V, Pigozzo J, Parmiani G, Ridolfi R, et al. Efficacy and safety of ipilimumab in patients with pre-treated, uveal melanoma. Ann Oncol. 2013;24:2911-5.

98. Luke JJ, Callahan MK, Postow MA, Romano E, Ramaiya N, Bluth M, et al. Clinical activity of ipilimumab for metastatic uveal melanoma: a retrospective review of the Dana-Farber Cancer Institute, Massachusetts General Hospital, Memorial Sloan-Kettering Cancer Center, and University Hospital of Lausanne experience. Cancer. 2013;119:3687-95.

99. Hodis E, Watson IR, Kryukov GV, Arold ST, Imielinski M, Theurillat JP, et al. A landscape of driver mutations in melanoma. Cell. 2012;150:251-63.

100. Krauthammer M, Kong Y, Ha BH, Evans P, Bacchiocchi A, McCusker JP, et al. Exome sequencing identifies recurrent somatic RAC1 mutations in melanoma. Nat Genet. 2012;44:1006-14.

101. Luscan A, Just PA, Briand A, Burin des Roziers C, Goussard P, Nitschke P, et al. Uveal melanoma hepatic metastases mutation spectrum analysis using targeted next-generation sequencing of 400 cancer genes. Br J Ophthalmol. 2014.

102. Singh AD, Bergman L, Seregard S. Uveal melanoma: epidemiologic aspects. Ophthalmol Clin North Am. 2005;18:75-84, viii.

103. Prescher G, Bornfeld N, Friedrichs W, Seeber S, Becher R. Cytogenetics of twelve cases of uveal melanoma and patterns of nonrandom anomalies and isochromosome formation. Cancer Genet Cytogenet. 1995;80:40-6.

104. Lawrence MS, Stojanov P, Polak P, Kryukov GV, Cibulskis K, Sivachenko A, et al. Mutational heterogeneity in cancer and the search for new cancer-associated genes. Nature. 2013;499:214-8.

105. Wan Y, Wu CJ. SF3B1 mutations in chronic lymphocytic leukemia. Blood. 2013;121:4627-34.

106. Carter SL, Cibulskis K, Helman E, McKenna A, Shen H, Zack T, et al. Absolute quantification of somatic DNA alterations in human cancer. Nat Biotechnol. 2012;30:413-21.

107. Landau DA, Carter SL, Stojanov P, McKenna A, Stevenson K, Lawrence MS, et al. Evolution and impact of subclonal mutations in chronic lymphocytic leukemia. Cell. 2013;152:714-26.

108. Kadoch C, Hargreaves DC, Hodges C, Elias L, Ho L, Ranish J, et al. Proteomic and bioinformatic analysis of mammalian SWI/SNF complexes identifies extensive roles in human malignancy. Nat Genet. 2013;45:592-601.

109. Shain AH, Pollack JR. The spectrum of SWI/SNF mutations, ubiquitous in human cancers. PLoS One. 2013;8:e55119.

110. White CD, Brown MD, Sacks DB. IQGAPs in cancer: a family of scaffold proteins underlying tumorigenesis. FEBS Lett. 2009;583:1817-24.

111. Lawrence MS, Stojanov P, Mermel CH, Robinson JT, Garraway LA, Golub TR, et al. Discovery and saturation analysis of cancer genes across 21 tumour types. Nature. 2014;505:495-501.

112. Battiste JL, Pestova TV, Hellen CU, Wagner G. The eIF1A solution structure reveals a large RNA-binding surface important for scanning function. Mol Cell. 2000;5:109-19.

113. Pestova TV, Borukhov SI, Hellen CU. Eukaryotic ribosomes require initiation factors 1 and 1A to locate initiation codons. Nature. 1998;394:854-9.

114. Passmore LA, Schmeing TM, Maag D, Applefield DJ, Acker MG, Algire MA, et al. The eukaryotic translation initiation factors eIF1 and eIF1A induce an open conformation of the 40S ribosome. Mol Cell. 2007;26:41-50.

115. Lomakin IB, Steitz TA. The initiation of mammalian protein synthesis and mRNA scanning mechanism. Nature. 2013;500:307-11.

116. Weisser M, Voigts-Hoffmann F, Rabl J, Leibundgut M, Ban N. The crystal structure of the eukaryotic 40S ribosomal subunit in complex with eIF1 and eIF1A. Nat Struct Mol Biol. 2013;20:1015-7.

117. Fekete CA, Mitchell SF, Cherkasova VA, Applefield D, Algire MA, Maag D, et al. N- and C-terminal residues of eIF1A have opposing effects on the fidelity of start codon selection. EMBO J. 2007;26:1602-14.

118. Olsen DS, Savner EM, Mathew A, Zhang F, Krishnamoorthy T, Phan L, et al. Domains of eIF1A that mediate binding to eIF2, eIF3 and eIF5B and promote ternary complex recruitment in vivo. EMBO J. 2003;22:193-204.

119. Saini AK, Nanda JS, Lorsch JR, Hinnebusch AG. Regulatory elements in eIF1A control the fidelity of start codon selection by modulating tRNA(i)(Met) binding to the ribosome. Genes Dev. 2010;24:97-110.

120. Cowley GS, Weir BA, Vazquez F, Tamayo P, Scott JA, Rusin S, et al. Parallel genome-scale loss of function screens in 216 cancer cell lines for the identification of context-specific genetic dependencies. Nature Scientific Data. 2014;1.

121. Janas MM, Wang E, Love T, Harris AS, Stevenson K, Semmelmann K, et al. Reduced expression of ribosomal proteins relieves microRNA-mediated repression. Mol Cell. 2012;46:171-86.

122. Arava Y, Wang Y, Storey JD, Liu CL, Brown PO, Herschlag D. Genome-wide analysis of mRNA translation profiles in Saccharomyces cerevisiae. Proc Natl Acad Sci U S A. 2003;100:3889-94.

123. Ingolia NT, Ghaemmaghami S, Newman JR, Weissman JS. Genome-wide analysis in vivo of translation with nucleotide resolution using ribosome profiling. Science. 2009;324:218-23.

124. Meyuhas O. Synthesis of the translational apparatus is regulated at the translational level. Eur J Biochem. 2000;267:6321-30.

125. Robinson MD, McCarthy DJ, Smyth GK. edgeR: a Bioconductor package for differential expression analysis of digital gene expression data. Bioinformatics. 2010;26:139-40.

126. Robinson MD, Oshlack A. A scaling normalization method for differential expression analysis of RNA-seq data. Genome Biol. 2010;11:R25.

127. Snyder A, Makarov V, Merghoub T, Yuan J, Zaretsky JM, Desrichard A, et al. Genetic basis for clinical response to CTLA-4 blockade in melanoma. N Engl J Med. 2014;371:2189-99.

128. Zimmer L, Vaubel J, Mohr P, Hauschild A, Utikal J, Simon J, et al. Phase II DeCOG-Study of Ipilimumab in Pretreated and Treatment-Naive Patients with Metastatic Uveal Melanoma. PLoS One. 2015;10:e0118564.

129. Piperno-Neumann S, Kapiteijn E, Larkin J, Carvajal RD, Luke J, Seifert H, et al. Landscape of genetic alterations in patients with metastatic uveal melanoma [abstract]. ASCO Annual Meeting; 2014 30 May - 3 June; Chicago, IL: J Clin Oncol; 2014. p. Abstract 9043.

130. Hoffman GR, Rahal R, Buxton F, Xiang K, McAllister G, Frias E, et al. Functional epigenetics approach identifies BRM/SMARCA2 as a critical synthetic lethal target in BRG1-deficient cancers. Proc Natl Acad Sci U S A. 2014;111:3128-33.

131. Wilson BG, Helming KC, Wang X, Kim Y, Vazquez F, Jagani Z, et al. Residual complexes containing SMARCA2 (BRM) underlie the oncogenic drive of SMARCA4 (BRG1) mutation. Mol Cell Biol. 2014;34:1136-44.

132. Oike T, Ogiwara H, Tominaga Y, Ito K, Ando O, Tsuta K, et al. A synthetic lethality-based strategy to treat cancers harboring a genetic deficiency in the chromatin remodeling factor BRG1. Cancer Res. 2013;73:5508-18.

133. Grzmil M, Hemmings BA. Translation regulation as a therapeutic target in cancer. Cancer Res. 2012;72:3891-900.

134. Silvera D, Formenti SC, Schneider RJ. Translational control in cancer. Nat Rev Cancer. 2010;10:254-66.

135. Thoreen CC, Chantranupong L, Keys HR, Wang T, Gray NS, Sabatini DM. A unifying model for mTORC1-mediated regulation of mRNA translation. Nature. 2012;485:109-13.

136. Hsieh AC, Liu Y, Edlind MP, Ingolia NT, Janes MR, Sher A, et al. The translational landscape of mTOR signalling steers cancer initiation and metastasis. Nature. 2012;485:55-61.

137. Fisher S, Barry A, Abreu J, Minie B, Nolan J, Delorey TM, et al. A scalable, fully automated process for construction of sequence-ready human exome targeted capture libraries. Genome Biol. 2011;12:R1.

138. Wagle N, Berger MF, Davis MJ, Blumenstiel B, Defelice M, Pochanard P, et al. High-throughput detection of actionable genomic alterations in clinical tumor samples by targeted, massively parallel sequencing. Cancer Discov. 2012;2:82-93.

139. Stransky N, Egloff AM, Tward AD, Kostic AD, Cibulskis K, Sivachenko A, et al. The mutational landscape of head and neck squamous cell carcinoma. Science. 2011;333:1157-60.

140. Banerji S, Cibulskis K, Rangel-Escareno C, Brown KK, Carter SL, Frederick AM, et al. Sequence analysis of mutations and translocations across breast cancer subtypes. Nature. 2012;486:405-9.

141. Ojesina AI, Lichtenstein L, Freeman SS, Pedamallu CS, Imaz-Rosshandler I, Pugh TJ, et al. Landscape of genomic alterations in cervical carcinomas. Nature. 2014;506:371-5.

142. Cibulskis K, McKenna A, Fennell T, Banks E, DePristo M, Getz G. ContEst: estimating cross-contamination of human samples in next-generation sequencing data. Bioinformatics. 2011;27:2601-2.

143. Cibulskis K, Lawrence MS, Carter SL, Sivachenko A, Jaffe D, Sougnez C, et al. Sensitive detection of somatic point mutations in impure and heterogeneous cancer samples. Nat Biotechnol. 2013;31:213-9.

144. Costello M, Pugh TJ, Fennell TJ, Stewart C, Lichtenstein L, Meldrim JC, et al. Discovery and characterization of artifactual mutations in deep coverage targeted capture sequencing data due to oxidative DNA damage during sample preparation. Nucleic Acids Res. 2013;41:e67.

145. Robinson JT, Thorvaldsdottir H, Winckler W, Guttman M, Lander ES, Getz G, et al. Integrative genomics viewer. Nat Biotechnol. 2011;29:24-6.

146. Thorvaldsdottir H, Robinson JT, Mesirov JP. Integrative Genomics Viewer (IGV): high-performance genomics data visualization and exploration. Brief Bioinform. 2013;14:178-92.

147. Olshen AB, Venkatraman ES, Lucito R, Wigler M. Circular binary segmentation for the analysis of array-based DNA copy number data. Biostatistics. 2004;5:557-72.

148. Griewank KG, Yu X, Khalili J, Sozen MM, Stempke-Hale K, Bernatchez C, et al. Genetic and molecular characterization of uveal melanoma cell lines. Pigment Cell Melanoma Res. 2012;25:182-7.

149. Trapnell C, Roberts A, Goff L, Pertea G, Kim D, Kelley DR, et al. Differential gene and transcript expression analysis of RNA-seq experiments with TopHat and Cufflinks. Nat Protoc. 2012;7:562-78.

150. DeLuca DS, Levin JZ, Sivachenko A, Fennell T, Nazaire MD, Williams C, et al. RNA-SeQC: RNA-seq metrics for quality control and process optimization. Bioinformatics. 2012;28:1530-2.

151. Radhika V, Dhanasekaran N. Transforming G proteins. Oncogene. 2001;20:1607-14.

152. Whitehurst AW, Bodemann BO, Cardenas J, Ferguson D, Girard L, Peyton M, et al. Synthetic lethal screen identification of chemosensitizer loci in cancer cells. Nature. 2007;446:815-9.

153. Azorsa DO, Gonzales IM, Basu GD, Choudhary A, Arora S, Bisanz KM, et al. Synthetic lethal RNAi screening identifies sensitizing targets for gemcitabine therapy in pancreatic cancer. J Transl Med. 2009;7:43.

154. Aza-Blanc P, Cooper CL, Wagner K, Batalov S, Deveraux QL, Cooke MP. Identification of modulators of TRAIL-induced apoptosis via RNAi-based phenotypic screening. Mol Cell. 2003;12:627-37.

155. Turner NC, Lord CJ, Iorns E, Brough R, Swift S, Elliott R, et al. A synthetic lethal siRNA screen identifying genes mediating sensitivity to a PARP inhibitor. EMBO J. 2008;27:1368-77.

156. Seyhan AA, Varadarajan U, Choe S, Liu Y, McGraw J, Woods M, et al. A genome-wide RNAi screen identifies novel targets of neratinib sensitivity leading to neratinib and paclitaxel combination drug treatments. Mol Biosyst. 2011;7:1974-89.

157. Aarts M, Bajrami I, Herrera-Abreu MT, Elliott R, Brough R, Ashworth A, et al. Functional genetic screen identifies increased sensitivity to WEE1 inhibition in cells with defects in Fanconi Anaemia and HR pathways. Mol Cancer Ther. 2015.

158. Pratilas CA, Taylor BS, Ye Q, Viale A, Sander C, Solit DB, et al. (V600E)BRAF is associated with disabled feedback inhibition of RAF-MEK signaling and elevated transcriptional output of the pathway. Proc Natl Acad Sci U S A. 2009;106:4519-24.

159. Luo B, Cheung HW, Subramanian A, Sharifnia T, Okamoto M, Yang X, et al. Highly parallel identification of essential genes in cancer cells. Proc Natl Acad Sci U S A. 2008;105:20380-5.

160. Lin X, Ruan X, Anderson MG, McDowell JA, Kroeger PE, Fesik SW, et al. siRNA-mediated off-target gene silencing triggered by a 7 nt complementation. Nucleic Acids Res. 2005;33:4527-35.

161. Jackson AL, Burchard J, Schelter J, Chau BN, Cleary M, Lim L, et al. Widespread siRNA "off-target" transcript silencing mediated by seed region sequence complementarity. RNA. 2006;12:1179-87.

162. Jackson AL, Bartz SR, Schelter J, Kobayashi SV, Burchard J, Mao M, et al. Expression profiling reveals off-target gene regulation by RNAi. Nat Biotechnol. 2003;21:635-7.

163. Shimozato O, Waraya M, Nakashima K, Souda H, Takiguchi N, Yamamoto H, et al. Receptor-type protein tyrosine phosphatase kappa directly dephosphorylates CD133 and regulates downstream AKT activation. Oncogene. 2014.

164. Chen YW, Guo T, Shen L, Wong KY, Tao Q, Choi WW, et al. Receptor-type tyrosine-protein phosphatase kappa directly targets STAT3 activation for tumor suppression in nasal NK/T-cell lymphoma. Blood. 2015;125:1589-600.

165. Novellino L, De Filippo A, Deho P, Perrone F, Pilotti S, Parmiani G, et al. PTPRK negatively regulates transcriptional activity of wild type and mutated oncogenic beta-catenin and affects membrane distribution of beta-catenin/E-cadherin complexes in cancer cells. Cell Signal. 2008;20:872-83.

166. Fuchs M, Muller T, Lerch MM, Ullrich A. Association of human protein-tyrosine phosphatase kappa with members of the armadillo family. J Biol Chem. 1996;271:16712-9.

167. Craig SE, Brady-Kalnay SM. Regulation of development and cancer by the R2B subfamily of RPTPs and the implications of proteolysis. Semin Cell Dev Biol. 2015;37C:108-18.

168. Locasale JW. Serine, glycine and one-carbon units: cancer metabolism in full circle. Nat Rev Cancer. 2013;13:572-83.

169. Farber S, Diamond LK. Temporary remissions in acute leukemia in children produced by folic acid antagonist, 4-aminopteroyl-glutamic acid. N Engl J Med. 1948;238:787-93.

170. Tibbetts AS, Appling DR. Compartmentalization of Mammalian folate-mediated one-carbon metabolism. Annu Rev Nutr. 2010;30:57-81.

171. Liu F, Liu Y, He C, Tao L, He X, Song H, et al. Increased MTHFD2 expression is associated with poor prognosis in breast cancer. Tumour Biol. 2014;35:8685-90.

172. Nilsson R, Jain M, Madhusudhan N, Sheppard NG, Strittmatter L, Kampf C, et al. Metabolic enzyme expression highlights a key role for MTHFD2 and the mitochondrial folate pathway in cancer. Nat Commun. 2014;5:3128.

173. Jain M, Nilsson R, Sharma S, Madhusudhan N, Kitami T, Souza AL, et al. Metabolite profiling identifies a key role for glycine in rapid cancer cell proliferation. Science. 2012;336:1040-4.

174. Heidorn SJ, Milagre C, Whittaker S, Nourry A, Niculescu-Duvas I, Dhomen N, et al. Kinase-dead BRAF and oncogenic RAS cooperate to drive tumor progression through CRAF. Cell. 2010;140:209-21.

175. Hatzivassiliou G, Song K, Yen I, Brandhuber BJ, Anderson DJ, Alvarado R, et al. RAF inhibitors prime wild-type RAF to activate the MAPK pathway and enhance growth. Nature. 2010;464:431-5.

176. Poulikakos PI, Zhang C, Bollag G, Shokat KM, Rosen N. RAF inhibitors transactivate RAF dimers and ERK signalling in cells with wild-type BRAF. Nature. 2010;464:427-30.

177. Keith CT, Borisy AA, Stockwell BR. Multicomponent therapeutics for networked systems. Nat Rev Drug Discov. 2005;4:71-8.

178. Emery CM, Vijayendran KG, Zipser MC, Sawyer AM, Niu L, Kim JJ, et al. MEK1 mutations confer resistance to MEK and B-RAF inhibition. Proc Natl Acad Sci U S A. 2009;106:20411-6.

179. Goetz EM, Ghandi M, Treacy DJ, Wagle N, Garraway LA. ERK mutations confer resistance to mitogen-activated protein kinase pathway inhibitors. Cancer Res. 2014;74:7079-89.

180. Ambrosini G, Khanin R, Carvajal RD, Schwartz GK. Overexpression of DDX43 mediates MEK inhibitor resistance through RAS Upregulation in uveal melanoma cells. Mol Cancer Ther. 2014;13:2073-80.

181. Lito P, Saborowski A, Yue J, Solomon M, Joseph E, Gadal S, et al. Disruption of CRAF-mediated MEK activation is required for effective MEK inhibition in KRAS mutant tumors. Cancer Cell. 2014;25:697-710.

182. Lamba S, Russo M, Sun C, Lazzari L, Cancelliere C, Grernrum W, et al. RAF suppression synergizes with MEK inhibition in KRAS mutant cancer cells. Cell Rep. 2014;8:1475-83.

183. Whittaker SR, Theurillat JP, Van Allen E, Wagle N, Hsiao J, Cowley GS, et al. A genome-scale RNA interference screen implicates NF1 loss in resistance to RAF inhibition. Cancer Discov. 2013;3:350-62.

184. Doench JG, Hartenian E, Graham DB, Tothova Z, Hegde M, Smith I, et al. Rational design of highly active sgRNAs for CRISPR-Cas9-mediated gene inactivation. Nat Biotechnol. 2014;32:1262-7.

185. Laurent C, Gentien D, Piperno-Neumann S, Nemati F, Nicolas A, Tesson B, et al. Patient-derived xenografts recapitulate molecular features of human uveal melanomas. Mol Oncol. 2013;7:625-36.

186. Amirouchene-Angelozzi N, Nemati F, Gentien D, Nicolas A, Dumont A, Carita G, et al. Establishment of novel cell lines recapitulating the genetic landscape of uveal melanoma and preclinical validation of mTOR as a therapeutic target. Mol Oncol. 2014;8:1508-20.

187. Dhillon AS, Hagan S, Rath O, Kolch W. MAP kinase signalling pathways in cancer. Oncogene. 2007;26:3279-90.

188. Nair JK, Willoughby JL, Chan A, Charisse K, Alam MR, Wang Q, et al. Multivalent N-acetylgalactosamine-conjugated siRNA localizes in hepatocytes and elicits robust RNAi-mediated gene silencing. J Am Chem Soc. 2014;136:16958-61.

189. Matsuda S, Keiser K, Nair JK, Charisse K, Manoharan RM, Kretschmer P, et al. siRNA Conjugates Carrying Sequentially Assembled Trivalent N-Acetylgalactosamine Linked Through Nucleosides Elicit Robust Gene Silencing In Vivo in Hepatocytes. ACS Chem Biol. 2015.

190. Wolfrum C, Shi S, Jayaprakash KN, Jayaraman M, Wang G, Pandey RK, et al. Mechanisms and optimization of in vivo delivery of lipophilic siRNAs. Nat Biotechnol. 2007;25:1149-57.

191. Xue W, Chen S, Yin H, Tammela T, Papagiannakopoulos T, Joshi NS, et al. CRISPR-mediated direct mutation of cancer genes in the mouse liver. Nature. 2014;514:380-4.

192. Cheng R, Peng J, Yan Y, Cao P, Wang J, Qiu C, et al. Efficient gene editing in adult mouse livers via adenoviral delivery of CRISPR/Cas9. FEBS Lett. 2014;588:3954-8.

193. Yin H, Xue W, Chen S, Bogorad RL, Benedetti E, Grompe M, et al. Genome editing with Cas9 in adult mice corrects a disease mutation and phenotype. Nat Biotechnol. 2014;32:551-3.

194. Johannessen CM, Boehm JS, Kim SY, Thomas SR, Wardwell L, Johnson LA, et al. COT drives resistance to RAF inhibition through MAP kinase pathway reactivation. Nature. 2010;468:968-72.

195. Johannessen CM, Johnson LA, Piccioni F, Townes A, Frederick DT, Donahue MK, et al. A melanocyte lineage program confers resistance to MAP kinase pathway inhibition. Nature. 2013;504:138-42.

196. Konermann S, Brigham MD, Trevino AE, Joung J, Abudayyeh OO, Barcena C, et al. Genome-scale transcriptional activation by an engineered CRISPR-Cas9 complex. Nature. 2015;517:583-8.

197. Shalem O, Sanjana NE, Hartenian E, Shi X, Scott DA, Mikkelsen TS, et al. Genome-scale CRISPR-Cas9 knockout screening in human cells. Science. 2014;343:84-7.

198. Wagle N, Van Allen EM, Treacy DJ, Frederick DT, Cooper ZA, Taylor-Weiner A, et al. MAP kinase pathway alterations in BRAF-mutant melanoma patients with acquired resistance to combined RAF/MEK inhibition. Cancer Discov. 2014;4:61-8.

199. Shi H, Hugo W, Kong X, Hong A, Koya RC, Moriceau G, et al. Acquired resistance and clonal evolution in melanoma during BRAF inhibitor therapy. Cancer Discov. 2014;4:80-93.